Thesis Report for the Design and Qualification of a Modular Scientific Drone

By Mauro Borrageiro

Supervised By Dr. Jane Wyngaard
and Robyn Verrinder

A thesis submitted to the Masters Program in Electrical Engineering in conformity with the requirements for the Degree of Master of Science in Electrical Engineering

University of Cape Town
Cape Town, Western Cape, South Africa
July, 2023

Abstract

Data acquisition using small unmanned aircraft systems (sUAS) or drones for scientific research purposes continues to grow as a new norm across a wide spectrum of disciplines. Consumer sUAS often boast high quality stabilised video capture capabilities and easy-to-use platforms. However, given the need for stringent data provenance and rigour in scientific data capture processes, these platforms are often limiting for academic research purposes due to closed source firmware and communication links, thus requiring sensor and mechanical infrastructure duplication on deployed platforms.

This paper presents the LANDRS open source Modular Science Drone; an open source flexible multirotor design, intended to provide the high quality and easy user experience of consumer platforms in a form that enables advantageous tight integration of custom sensors with full access to necessary data and metadata capture process provenance.

The HexaQuad was designed to operate as either a quadcopter or hexacopter for greater accessibility and versatility, with an operational flight time in the range of 15 to 20 minutes and the ability to lift a 5kg payload. The design used readily available components to configure the powertrain, command and control and power subsystems. The structural frame of the drone was designed and qualified in CAD simulation software with an effort to use simple manufacturing techniques such as 3D printing. The result was a simple to use, easy to replicate, and well documented drone focused on accessibility for research.

The presented design was performance tested and validated in a number of typically expected flight behaviours for scientific research drones to determine the endurance and heavy lift capabilities compared to literature referenced commercial and custom drones.

The dissertation that follows outlines the design decisions and verification methods for the overall multirotor system and associated subsystems. It subsequently, reports the performance results of the quad- and hexacopter configurations in comparison to the set-out requirements before concluding with suggested future work.

Acknowledgments

There is a lot of work that goes into producing a thesis and equally as much support that comes for all parts of one's life, so I would like to use this section to acknowledge those who played a key role in the success and enjoyment of the work presented here.

Firstly I would like to Thank Dr Jane Wyngaard, I had heard horror stories about post-grad experiences being ruined by supervisors but I am so delighted to say I felt nothing but the opposite. Thank you, Jane, for your tireless effort, support and encouragement you provided to me, be it through your guidance and expertise, going out of your way to come flying with me with little Savannah, or just your kind and friendly persona. I could not have asked for a better supervisor, so thank you, Jane, I really appreciate all you did for me and I pity those who didn't get the opportunity to work with you.

Special thanks to the Alfred P. Sloan Foundation for funding this work and to the gentlemen at the University of Notre Dame. Thank you to Robyn Verrinder for stepping in to be my administrative supervisor, I think you're an incredible supervisor and I'm sorry we didn't get to work more together. To my peers in the Lab; Mark, Anicet and Ngoni, I enjoyed your company, conversations and our shenanigans to avoid working. Thank you to the staff at UCT that assisted me to achieve the goals of this project, Brendon Daniels, Justin Pead, Alison Gwynne-Evans and the guys in the workshop, your assistance was appreciated. To the friendly gentlemen at the Dreyersdal Southern Soarers Flying club, thank you for allowing us to use your stunning facilities and for the friendly conversations.

To my parents, Mom and Dad, thank you for all your love, encouragement and for supporting me in achieving my goals. I know Rob and I being away has been difficult but I hope watching us grow, thrive and achieve our goals makes you proud, we love you. To my brother Roberto, I love you unconditionally, thank you for being

my brother and supporting me.

And lastly, to my friends I have made in Cape Town and Ultimate over my time at UCT, you have been my home away from home. I would like to especially thank the Lunch Club, coming back to UCT with most of my close friends having graduated, I was so happy to find people I just naturally clicked with. Tom, James, Jem, Francy, Lyci and John, you guys are amazing and I love spending time with you, you played a huge role in my enjoyment of this post-grad life, from the Ultimate, to the adventures, spikeball and the hours of fun; I can't thank you enough, I love you guys <3

Statement Of Originality

I know the meaning of plagiarism and declare that all the work in the document, save for that which is properly acknowledged, is my own. This dissertation has been submitted to the Turnitin module and I confirm that my supervisor has seen my report and any concerns revealed by such have been resolved with my supervisor.

Signed: Signed by candidate

Glossary

sUAS A sUAS according to the FAA, refers to an unmanned aircraft system with all its associated elements that ensure safe operation without any direct human intervention on or within the aircraft. A sUAS is also categorised by weight and must have an all-up weight less than 55 pounds (25Kg) [1]. 1–7, 11–16, 19–21, 23, 24, 26–30, 33, 35–37, 41–44, 79, 81, 82, 92, 108

Glossary of Abbreviations

AUW All Up Weight. 36, 37, 56, 76

ESC Electronic Speed Controller. 28, 39–41, 55

FAA Federal Aviation Administration. 1

FDM Filament Deposition Modeling. 32, 33

FPV First Person View. 13

GCS Ground Control Station. 23–26, 44, 82

LiDar Light Detection and Ranging. 3

sUAS small Unmanned Aircraft System. 1, 2, 5, 32, 47

UCS Ultimate Compressive Strength. 31, 32

UTS Ultimate Tensile Strength. 31, 32

VTOL Vertical Takeoff and Landing. 14

Contents

Chapter 1

Introduction

This dissertation is intended to demonstrate the design process and performance qualification of an Open Source, Modular Science Drone. The small unmanned aircraft system is specifically designed for scientific research with an emphasis on creating a system suitable for the tight integration of novel or uncommon sensors with full access to all associated metadata to provide context to measurements. The design philosophy revolves around creating an accessible system for studies of varying sizes and drone experience while enabling them to achieve the high temporal and spatial resolution associated with drone data.

The following section is set out to provide context and background on drones, outline the objectives and requirements of the design, and define the scope and limitations before expanding on the structure of the rest of the report.

1.1 small Unmanned Aircraft Systems

Drone is a broad term that can be used to refer to a number of different types of unmanned vehicles. Drones could be used to describe autonomous or remotely controlled land rovers, marine-craft, or air-going vehicles. There are a number of different ways to categorise drones, either according to weight, application, operating range, flight philosophy, etc [1–4]. Drones in this dissertation will be used interchangeably with other terms to describe unmanned aircraft vehicles, specifically a category known as small Unmanned Aircraft System (sUAS).

sUAS is a term defined by the Federal Aviation Administration (FAA) to describe a category of unmanned aircraft with no direct onboard human control and

total weight, including payloads, of less than 25kg (55 pounds) [1]. This category description is still extremely broad as there are a number of different manners in which an sUAS can produce lift and thus fly. sUAS can be further refined into two main configurations to create lift, namely, fixed-wings or rotary-wing aircraft [5] shown in Figure 1.1. Fixed-wings operate like conventional aircraft and require air flow over an aerofoil or wing in order to produce lift, in other words, they require constant forward movement to stay airborne. Rotary-wings utilise propellers in constant motion where the aerodynamic philosophy of the propellers is very similar to a fixed-wing, however, they are capable of hovering in place and do not require forward movement to stay airborne [5]. Other forms of aircraft could fall within the sUAS category, such as air balloons or airships, but these will not be discussed further.

(a) Fixed-wing [6] (b) Rotary-wing [7]

Figure 1.1: Representation of a fixed-wing drone compared to a rotary-wing sUAS.

Each configuration can further be refined by classifying the propulsion design where some sUAS are powered by electric motors, small internal combustion engines or not at all. Fixed-wing drones support all forms of propulsion, including gliders with specifically designed aerofoils for efficient soaring. Notably, fixed wings are commonly used for long-range operations due to the efficient form of flight where forward-directed drive creates lift as a byproduct. Although fixed-wings are suitable for long endurance they have limitations associated with their carrying capacity as well as with their launch and recovery processes. Rotary-wings, on the other hand, require constant propulsion in order to remain airborne, consuming large amounts of energy. However, rotary-wings can produce large amounts of thrust to boost carrying capacity as well as takeoff and land with small space requirements. Depending on the application use case, either configuration has associated benefits and weaknesses.

In a civil context, rotary-wing drones have become increasingly popular as flight systems have developed and simplified remotely piloting an sUAS. Specifically, multirotors have been used in a number of areas due to their improved accessibility with sensor miniaturisation and lowered power demands. Multirotors refer to rotary-wings which have more than 2 rotors producing thrust and assisting with position control, for example, tricopters or quadcopters. Thanks to the miniaturisation of electronics, users are able to fly some drones with a simple radio controller linked to a cell phone giving a live video stream. Previously, an entire setup known as a ground station was required to operate the drone where a laptop was used for telemetry information and a separate monitor provided a live video link. Notably, ground stations have not been completely replaced, however, they are reduced in size aimed at improved portability.

Typical civil multirotors are equipped with high quality cameras for videography and photography, or in higher end models, specialised sensors used for inspections of civil structures and precision agriculture [3, 5]. Arguably one of the biggest commercial producers of civil multirotors is DJI, which caters to a range of applications from hobbyist video and photography to industrial precision agriculture [7, 8]. Furthermore, their application space is growing with an increasing range of miniaturised sensors which were once limited to aircraft and satellite remote sensing. Some additions include Light Detection and Ranging (LiDar) for accurate range estimation and thermal cameras for heat radiation detection [9].

With the increasing efficiency of electric motors, sUAS generally have a flight time between 12 to 40 minutes depending on the size of the drone and the payload attached [5, 7, 10, 11]. It is common for drones to accommodate payloads in the range of 2 to 3kgs, whereas some heavy lift drones are capable of carrying payloads in excess of 5kg [5, 7].

Remote sensing has been highly beneficial to industry and scientific research as it allows for the collection of data from locations with various limitations, be it hazardous or sensitive to disturbance. Previously, remote sensing applications were limited to mainly aircraft and satellites providing varying levels of resolution regarding the field of view and how often samples could be recorded. Satellites offer expansive spatial resolution but are often compromised by cloud cover, limiting successful site revisit. Whereas aircraft can provide detailed spatial resolution but the frequency is dependent on infrastructure, safety and accessibility [8].

The introduction of sUAS to remote sensing allows for both high spatial and temporal resolution at a fraction of the cost. Drones can be rapidly deployed in good weather windows as well as revisit areas with greater ease and repeatability [8, 12].

Commercial companies undoubtedly produce extremely high quality products and

associated sensing systems, allowing research techniques and industries to evolve like that of remote sensing. However, their applications are limited to the sensor systems they cater to. This is especially the case from a scientific research perspective as the use of drones within a study is heavily dependent on the availability of suitable solutions. Considering the study size further perpetuates this issue as it is less likely to find suitable solutions for novel and uncommon sensors.

In some cases, it is possible for a user to connect a non-standard sensor either via collaboration with the manufacturer or, more commonly, through an ad hoc technique. Although it may be possible for a non-standard sensor to be connected to a commercial product, the associated system is typically proprietary preventing users from accessing all flight metadata to contextualise sensor readings [12]. The result is often further ad hoc additions to the drone system, duplicating hardware to recreate the desired flight metadata, all the while altering the initial flight characteristics of the drone. A comparison of a modified commercial drone is depicted in Figure 1.2.

(a) DJI Phantom [13] (b) Modified DJI Phantom [14]

Figure 1.2: A commercially available sUAS, (a), compared to the same model with modifications and duplication of hardware to expand the application range, (b). In Figure (b) there is the clear addition of hardware protruding from the enclosed casing, a communication antenna is suspended out the back and additional batteries are mounted on the left and right of the body.

The alternative to utilising commercially available products is to create purpose-built customs sUAS. Although data limitations can be solved with the selection of open systems, there is now the additional development step to design an effective and, most importantly, reliable drone system to meet the operation requirements. Creating custom-built drones thus requires either prior expertise or third-party consultation

to design and manufacture the system, all before qualifying it according to aviation law to operate under the desired conditions.

Considering the potential data collection power that a sUAS can provide to different industries and especially scientific research fields, there are still significant accessibility gaps allowing for easy integration of custom or novel sensors. Research studies that do not align with industry interests require expertise to perform ad hoc modifications to commercially available products or to create custom purpose-built solutions to access the associated spatial and temporal benefits.

1.2 Motivation and Problem Description

The accessibility of data acquisition through sUAS has improved drastically and has had significant development aimed towards commercial craft for industry use. This has resulted in cheaper high performance, high quality products with simplified flight operations lowering the expertise level required to use an sUAS, and thus broadening accessibility to a larger population. Alongside this, is the increasing use of drones in the scientific communities for applications such as precision agriculture and remote sensing in a number of fields.

A major limitation of commercially available drones is their proprietary nature. Commercial drones are not designed to accommodate the integration of novel or custom sensors. Furthermore, there is a limitation of what flight metadata is provided to the user to contextualise any associated sensor readings. Commercial companies can, understandably, not cater to all potential uses while still providing the same level of quality and reliability, and therefore limit the applications of the products to their sensor range for best application. Thus, commercial drones are mostly suitable for research areas that align with their designed intention or in scenarios where users have the knowledge to modify consumer drones effectively. Although, even if users are able to modify a consumer drone effectively there is then the further question about the repeatability of the process in other studies.

For research studies that fall beyond the use cases of commercial drones, there are few alternatives other than creating custom purpose-built sUAS. The associated benefits of custom drones include an optimal design for the research task where systems are designed to suit the high data provenance associated with scientific data capture. However, in the creation of a custom sUAS there are high development time costs in order to fine-tune the system to achieve a similar level of quality and reliability as seen in commercial products, all before qualifying the sUAS according to local

aviation laws. Beyond time costs, this process requires knowledge of design principles and expertise to create an effective solution. In the absence of design experience within a research group, the alternative is to approach third-party sUAS development companies to create the desired design, often being a costly process.

The scenarios described pose significant barriers to entry for research groups dealing with novel sensors or applications. Additionally, there are limited solutions to overcome these barriers to achieve the data acquisition benefits of drones. Thus it is proposed to create a modular, easy-to-use solution to assist the scientific research community to access the associated benefits of drone data capture.

1.3 Objectives and Requirements

With the problem statement clarified, the overall aim of the project will now be defined within this section. In addition to the aim of the project, specific objectives will be identified to assist in focusing work and to guide the design decisions. And lastly, functional requirements will be defined according to typical science sUAS operations to define the intended flight performance.

The aim of this research dissertation is to design a modular, open source, multipurpose, multirotor drone aimed at enabling the scientific community to integrate novel sensors effectively whilst providing a high level of data provenance to fully contextualise sensor readings. It is intended to be user-friendly and cater to researchers who don't necessarily have prior experience or expertise with the design or operation of sUAS. To improve accessibility, the process will make use of simple manufacturing techniques and have supporting documentation that clearly defines build steps, setup guides, basic automated usage and sensor mounting suggestions.

In order to achieve the aim of the project key objectives were identified to guide the design decisions. These key objectives were as follows:

1. To create a completely open source design, ensuring access to all metadata and design files.
2. The drone should be modular to allow for rapid replacement and reconfiguration of components.
3. Lastly, the drone should be accessible making it simple to use, easy to replicate and well documented.

By designing the sUAS to be open source it ensures that users will be able to integrate into the onboard systems and acquire any necessary flight metadata. Furthermore, making the design files of the drone open source allows users to further develop the system and potentially alter it to suit their operation requirements, especially in the case of experienced drone users.

In order to facilitate the tight integration of non-standard sensors it is imperative for the HexaQuad to be versatile and reconfigurable. Designing various components in the drone to be modular or compartmentalised allows them to be rapidly swapped, either to replace damaged components and reduce downtime or to swap out sensor arrays and alter the function of the sUAS.

Designing the HexaQuad with accessibility in mind refers to both the usage and ease of recreation. Since one of the intended users is research units with limited experience in the operation and construction of drones, it is thus key to ensure the overall systems provide a similar simplified flight experience as commercial drones. For example, the users should not require excessive hours of experience to pilot the sUAS in the desired manner, rather the piloting experience should be easy to learn and improve. Additionally, utilising simple and cost-effective manufacturing techniques will encourage the use of the HexaQuad design.

In addition to the design philosophy objectives to guide the design decisions, functional requirements were created to define the operating range of the drone. The definition of the functional operating range will assist with identifying the potential use cases of the drone.

Evaluation of the literature motivated the design of a sUAS with the capability to carry sensor arrays with varying weight ranges. This focused the project to create a multirotor capable of carrying heavy payloads, with reasonable endurance and good stability. Thus the following operating range was defined:

1. The drone should be able to operate as either a hexacopter or a quadcopter.
2. The drone should have an expected flight time in the range of 15 to 20 minutes whilst carrying the maximum payload, for either configuration.
3. The maximum payload the drone should be able to lift is 5kg as a Hexacopter and 2kg as a Quadcopter.
4. The drone should have a minimum control range of 2km

Allowing the drone to operate as either a hexacopter or quadcopter is intended to make the design more accessible from a practical and budget point of view. The reason is if a user does not require the maximum payload capacity of the hexacopter they can recreate the smaller more cost effective quadcopter instead.

1.4 Scope and Limitations

The main contribution of this dissertation is the presentation of the Nyala HexaQuad science drone design.

This report will discuss in detail the design decisions relating to the creation of the frame of the drone and the selection of suitable components to meet the objectives and requirements of the project. Notably, key components relating to the powertrain, flight control and power distribution were all selected and purchased as ready-made items. The reason again relates to accessibility and to avoid duplicating work and development. Purchasing ready-made components simplifies recreating the HexaQuad as there are fewer custom components.

Sections relating to key design features will be discussed in depth as their selection processes required careful consideration to meet the objectives. However, other sections will simply be a definition of the design with short reasoning.

During performance evaluations, the HexaQuad's payload capacity was tested by carrying dead weight as opposed to operational sensors. The main reason for limited functional sensor testing was limited time and weather windows. Taking realistic sensor readings would have required numerous calibration flights prior to data capture.

Included in the outline of this work is the creation of documentation to guide users through 1) recreating components, 2) assembling the HexaQuad, 3) setting up control and automated flight, and 4) operating the drone. The creation of the documentation is not discussed further than the description of its content, however, access will be provided at the end of the report.

With regards to the HexaQuad being completely open source, it must be noted that proprietary Computer Aided Design (CAD) software was used to design all the components of the drone. The CAD software used was Solidworks 2021 with a number of its tool suits including the finite element modelling and image rendering add-ins. This software was used because the University of Cape Town provides an academic license to students for design purposes. To ensure users without the proprietary

software can still utilise the design, all design files were duplicated as universal part files.

To further clarify the work presented in this dissertation, it should be noted that the creation of the HexaQuad is to assist first time uses intending to implement drone data capture within their research. To cater to this, the design of the drone focuses on three major points, 1) the frame and its structural analysis to meet the weight requirements, 2) the selection of suitable, readily available powertrain components to meet the flight time and lift objectives, and 3) the validation of these processes under practical performance testing. No specific use is set out for the HexaQuad and rather focuses on providing a number of sensor connection methods so as to not limit the potential uses.

1.5 Plan of Development

This dissertation describes the design and performance evaluation of a modular, open source science drone. The report serves as a guide through the several design steps and considerations made to develop the final design and then further goes on to evaluate its performance. A breakdown of each associated section is detailed below:

- **Chapter 2:** Explores the relevant literature associated with drones and their various use cases in scientific research. The section breaks down the components of multirotors, highlighting relevant areas for powertrain design and how control is affected via the autopilot or manually. Lastly, the mechanical design of drones is investigated exploring material considerations and the use of 3D printing as an accessible manufacturing technique.
- **Chapter 3:** In this chapter, the design of the powertrain and flight subsystems is described. The powertrain design explores motor propeller combinations to meet the objectives. Thereafter, the control subsystems are described for the autopilot and flight controller selection before defining the power distribution and auxiliary power design.
- **Chapter 4:** The structural design provides an overview of the iterative design process of the different components included in the frame. Descriptions of simulation techniques are further explained and used to motivate decisions. Lastly, a comparison of 3D printing materials is conducted for part manufacturing before presenting the final HexaQuad design.
- **Chapter 5:** Describes the performance evaluation strategy for the HexaQuad. It outlines regulations about test sites, typical research flight behaviour, how the

performance testing was implemented, the flight procedure and data processing strategies.

- **Chapter 6:** In this chapter the results from the associated performance tests are presented and discussed in relation to the objectives and associated literature. The section is broken down into sections focusing on the specific tests of interest described in Chapter 5.
- **Chapter 7:** Presents the conclusions of the work presented here before describing recommendations of alteration and a definition of a path for future work.

Chapter 2

Literature Review

2.1 Uses of sUAS in Research

sUAS are extremely versatile pieces of equipment and act as a tool for remote sensing or remote deployment. sUAS applications are essentially limited by the sensors attached where the scope can be expanded or narrowed by mounting different sensor arrays. Researchers can now visit study sites and cover large areas in less time due to the nature in which sUAS operate. Due to the rapid deployment of drones, study sites can also be covered more frequently and simultaneously compared to ground based surveys [15].Similar aerial perspectives were previously achieved by using aircraft and satellites, however, these methods are cumbersome and cannot be deployed with short notice due to extensive planning and high costs [3]. Comparatively, sUAS can be used by individual researchers enabling them to capture high quality data with a high frequency and at a reduced cost [15].

The application of the sUAS is mainly dependent on the sensor attached however there are some restrictions which come from the design of the drone. A non-exhaustive list of application determining factors includes flight time and altitude range, payload capacity, temperature and weather conditions, and Manner of auto-piloting, GPS guided or obstacle detection.

The development of electronics has resulted in reduced power consumption and miniaturisation, improving performance and broadening the range of available sensors. Simultaneously, the energy density of battery technology and the efficiency of electric motors continues to improve, increasing the practical operation time of airborne drones.

There are some sensors that have become synonymous with drones either be it for their versatility or industry applications pushing development. Typically sUAS

available can mount RGB cameras; thermal or infrared light cameras; multispectral and hyperspectral cameras which detect wavelengths of light that are outside the visual spectrum and miniaturized Light Detection and Ranging (LiDar) sensors for distance estimation.

There are numerous areas utilizing the benefits of sUAS including commercial, scientific and military. However, this work concerns only the first two domains, with more emphasis on sUAS intended for research. The breadth of sUAS use-cases is too broad to comprehensively review, however, the following serves to provide insight into the diversity of sUAS applications highlighting systems performance and limitations.

2.1.1 Fishery Studies

Harris et al. [15] explored the use of sUAS in fishery studies. Although the sUAS is limited to flying above water bodies they are still capable of providing information on habitat health or census data.

The primary uses of sUAS in marine and freshwater environments are to evaluate critical habitat and for population studies [15]. RGB visual cameras allow fishery studies to map fish nursery grounds, tidal wetlands and coastlines as well as provide insight into species population studies. The sUAS data streams can then be used for management schemes to either remedy habitat stress factors or remove invasive species.

Harris et al. [15] clarify that typical uses of drones in other animal studies do not translate completely to marine and freshwater studies. Currently, sUAS are mainly used for population studies of mega-fauna such as sharks and whales, largely thanks to their ability to cover large areas with a wide field of view and ease of identification. There is the possibility to extend this population study technique to smaller fauna in clear coastal waters and stream habitats however the literature is limited.

Although there has been the successful use of sUAS in fishery science, it does still lag behind the scale of implementation of other disciplines. However, there is room for more adoption of the research technique thanks to accessibility improvements of sUAS technology [15]. The flight assists and autopilots available today make it easy for anyone with no experience to operate. In most cases, automated missions can be created where manual input is not required at all [3, 15].

The challenge appears in the choice of platform to use, be it an off-the-shelf option or purpose built drone, especially if there is limited flight experience. Basic

sUAS systems have limited customisability and are often restricted to the sensor they are delivered with. Perrymen et al. [16] experienced this uncertainty in their selection of a multirotor system to study mega-fauna in the antarctic. They compared three sUAS systems with an expected flight time in the range of 15-45min and small payload ranges for 0.5-1.2kg to carry a high resolution camera. Amongst the options investigated one system was a commercially available quadcopter and the remaining two drones were a custom-built quadcopter and hexacopter for increased payload capacity.

2.1.2 Whale Studies

Pirotta et al. [17] encountered limitations of off-the-shelf drones when attempting to survey the health of humpback whale populations. Their unique sampling method required a custom designed First Person View (FPV) sUAS to accommodate a sampling device to catch the blow from whales. Skilled pilots were required to operate the FPV drone due to its high agility and necessity to react fast to the whales surfacing The sampling device was made up of a container that could be opened remotely and housed a petri dish. Along with the sampling customisation, the sUAS required additional buoyancy devices and waterproofing to prevent the drone and samples from being lost.

In this case, the choice of sUAS required a carefully selected design to meet the requirements of the research task. Pirotta et al. explains the mechanical design decisions that were made to ensure the quadcopter would meet the strength, agility and buoyancy required to perform the research task effectively [17]. A custom design task outlined in [17] is time consuming without experience or consultation with a 3rd party. Such research areas are still less accessible due to the requirement of expertise in either the design of the sUAS or the flight experience to control the drone in a proficient manner.

2.1.3 Civil Applications

With improving reliability and predictability of sUAS the appeal to use drones for civil applications has also grown. Drones have become a feature of precision agriculture, growing to be a multi-million dollar industry [2, 3]. Precision agriculture allows farmers to improve yield estimation, target problem areas for remediation from diseases and abiotic stresses, and act as actuators for pest control or nutrient deposition [18].

There is large industry backing of the agricultural sector and it is not surprising that there are multiple commercial drone applications. Commercially agricultural

drones are capable of being used as crop sprayers or to deposit fertilizer with payload capacities reaching 40kg. In addition, there are multiple sensing drones equipped with miniaturised multispectral cameras to survey crops, orchids and even water bodies. Precision applications require high levels of accuracy, commercial systems accommodate this with the use of centimeter-level accurate positioning systems [19]. These specific intention solutions are exceptional at performing their intended function however are extremely expensive, where small systems can cost upwards of $6000 with limitations in expanding their scope of operation [7, 18].

Beyond agriculture, drones are being investigated as solutions to assist with last mile delivery of goods. Although there are multiple possible obstacles in urban areas, this is less of an issue in rural areas and there are already a number of growing use cases. The South African National Blood Service (SANBS) [20] and Zipline [21] have both developed modular drones for the delivery of blood supplies. Both drones operate in rural areas to transport blood supplies on demand to hospitals within a radius of 80-100km of a blood bank, this increases accessibility to resources and prevents wasted supplies.

Zipline are using a fixed-wing drone and requires specialised equipment to launch and recover the drone during missions. In comparison, SANBS designed a Vertical Takeoff and Landing (VTOL) fixed wing which acts as a multirotor during takeoff and landing and then like a conventional fixed-wing during flight. This is beneficial as there is no requirement for a specialised launch and catchment area while still benefiting from the long endurance of a fixed-wing. However, the system is relatively heavy at 13kg with a wingspan of 3.5m and thus limits the payload capacity to 2kg [20].

2.1.4 Earth Sciences

Earth science studies have long been a user of remote sensing tools. The introduction of sUAS has again introduced a higher resolution to studies with their temporal and spatial advantage over conventional remote sensing techniques.

Rocha et al. [22] made use of sUAS to investigate the interaction of the earth's surface with the close atmosphere known as atmospheric boundary layers. These investigations assist with incites into air quality, weather patterns and climate studies. Using sUAS is beneficial as they are mobile and controllable compared to weather tower and balloon readings. In this case, the drone was used as the sensing platform, where the dynamic control responses were used to interpret the wind speed and direction. The custom drone made use of an open source autopilot, Arducopter, and

Pixhawk flight controller to access the attitude response during flight.

Barbieri et al. [10] also acknowledge the potential of drones for finer resolution readings in atmospheric studies and focused on quantifying how comparable readings are from different sensing platforms. A major difficulty highlighted was quantifying the accuracy of readings from the different sensing systems. The accuracy of readings was found to be influenced by the platform used, mounting and integration strategy, and calibration of the sensors and thus pose potential difficulty to reproduce results [10, 12]. This is where commercial products are convenient as like systems can be used for comparison between studies. However, this can be overcome in studies using custom solutions with the assistance of standardised ground truth measurements and transparent calibration techniques [10].

A number of earth science studies require the investigation of large areas, some more accessible than others. However, a common issue is the labour intensity of surveying a research site by foot and collecting sample data [8, 23, 24]. Jeziorska [23] mentions how sUAS have assisted with mapping hard to reach wetlands for hydrological modelling. The incorporation of sUAS has allowed Jeziorska to access spectral readings for the delineation of wetland areas. Prior to the use of sUAS equipped with spectral sensors, there was a reliance on coarse satellite sensor data. The satellite resolution was sufficient for large scale studies but was not suitable to study smaller sites. There is still concern about the quality of data collected due to the difference in accuracy depending on the platform used. In this case, sUAS based sensor system can be used as a complimentary remote sensor instead of completely replacing the alternatives.

In some cases the issue may not be with the area to cover but the associated dangers posed to humans in the research site. Jordan [24] investigates the use of sUAS for studying volcanic landscapes. sUAS are being used for the deployment of seismic sensors; gas sampling from volcanic plumes; collection of newly formed volcanic rock; magnetometer readings and a host of other applications relating to the different cameras available. Drones can provide immediate data collection from these hazardous environments and transfer the associated risk from people to equipment. Use in harsh and inaccessible environments also motivates for modular systems that can be repaired with minimal tools in a short time [24]. With the increasing accessibility and reduced cost of drones, the thought of losing equipment is also becoming less of a limitation. However challenges that are still prominent are the susceptibility to wind and harsh weather as well as the legal limitations on where and when drones can be flown.

On the opposite side of the spectrum, Gaffey et al. [8] consolidated the different research applications of drones in the Cryospheric regions. Cryospheric regions generally refer to areas where water is present in a solid form and thus require sUAS systems to operate in temperatures below freezing. sUAS are used for snow depth estimation however struggle with surface contrast, thus sometimes rely upon ground readings. They have also been used for monitoring glacial movement and carving. The fine temporal and spatial resolution of sUAS is again recognised as frequent visits to a glacier provide high resolution velocity fields. High temporal resolution assists with the development of digital surface models (DSM), especially with glaciers as the face and structure can change drastically during carving making recognition of points difficult [8]. Due to the difficulty associated with accessing glaciers on the ground and taking readings, sUAS based monitoring systems have become the preferred method and effective ground truth for satellite data.

2.2 Design of Drones

Multirotors are inherently simple machines to understand from a broad perspective. However, there are a number of components that require careful consideration during design in order to achieve an efficient and effective flying drone. This section will be a brief explanation of how multirotors fly and some key considerations for their design. Also included in this section will be an outline of the essential components required for a research sUAS and their purpose.

2.2.1 Multirotor and Fixed Wing Flight

The major distinction between fixed wing and mutlirotor sUAS is the manner in which they produce lift. Fixed-wings rely on a motor for thrust however they also have a carefully designed aerofoil or wing to provide lift and keep the sUAS airborne. It is key to understand that the motor propels the fixed wing forward and keeps air flowing over the wing, it is the flow over the wing that creates lift [5]. The control of a fixed-wing comes from adjustable surfaces which provide pitch, roll and yaw control.

In comparison, multirotors are reliant on their rotors to provide thrust, lift and control. It is the act of rotating the propellers that creates a low pressure area above the multirotor and a high pressure area below the multirotor, resulting in lift. The attitude control of a multirotor comes from manipulating the speeds and torques of the rotors relative to one another. Relative increases or decreases in rotor speed and torque allow mutlirotors to achieve a desired roll, pitch and yaw angle. In most multirotor configurations the rotation direction of adjacent rotors will alternate between clockwise (CW) and counter-clockwise (CCW), this is to balance motor

torques and maintain a single yaw heading.

There are associated tradeoffs for fixed-wings and multirotors due to their mechanisms of flight and ultimately these influence the applications. Fixed-wings are more efficient and have longer flight times compared to multirotors due to the fixed aerofoil creating lift with forward thrust [5]. Extended flight times mean fixed wings are able to cover larger areas of interest compared to mutlirotors, lending themselves to a different application set. However, multirotors unique ability to create lift without forward movement creates its own advantages. Multirotors are capable of vertical takeoff and landing making them more suitable in situations with limited space. In addition, they have higher payload capacities as well as better manoeuvrability compared to fixed wings [5].

Due to this versatile control mechanism, multirotors can have multiple configurations. The configurations are defined by the number of rotors: quad-(4), hex-(6) or octocopter(8) to name a few. Additionally, within each configuration category, there are a number of configurations which vary in symmetry and shape. Figure 2.1 illustrates four different quadcopter motor arrangements with varying lines of symmetry. The variations in symmetry in the quadcopter arrangements influence the attitude control output by the flight controller, thus each set of outputs will be unique.

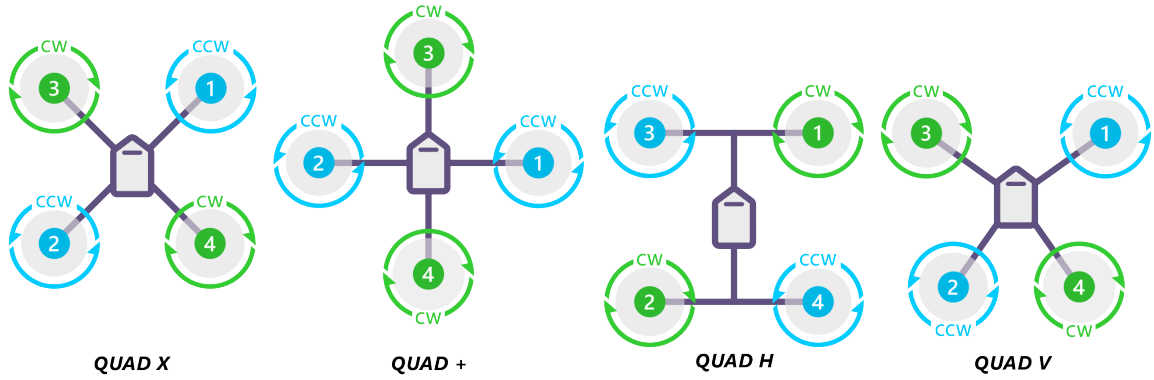

Figure 2.1: Four unique Quadcopter configurations, each requiring slightly different control actions to fly [25]

There are alternative rotor configurations with fewer than 4 rotors that require additional servo motors to ensure full control of the system. The tricopter shown in Figure 2.2 is an example motor arrangement that requires an additional servo motor for full attitude control.

Some specialised rotor configurations are used to improve the performance of the

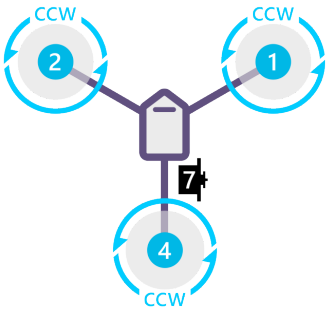

Figure 2.2: A tricopter drone requires an additional servo motor on the tail to achieve full control action. The servo will tilt the tail rotor to the left or right to assist with yaw and roll [25]

common configurations. An approach to increase the thrust of a multirotor while maintaining a large propeller diameter is to utilise a configuration known as coaxial rotors. Coaxial rotors refer to identical motor and propeller sets being installed one above another to increase the amount of thrust produced without additional rotorbooms [26]. While this approach will increase the overall thrust, the increase is less than the total of two individual propellers due to one propeller operating in the wake of the other, reducing efficiency.

An alternative rotor configuration approach to increase efficient thrust delivery is to increase the distance between two adjacent rotors as Lei et al. performed [27, 28]. Theoretically, the minimum spacing between adjacent rotors should be equal to the diameter of the propeller used but is usually slightly larger for safety. However, if the rotor spacing of adjacent propellers is increased then there is less interference between the propeller wakes, thus improving efficiency [27,28], an illustration is shown in Figure 2.3. Lei et al. [27, 28] performed this in both a hexacopter and octocopter drone and determined there was potential to improve hover efficiency when there was less interference between adjacent propellers wakes.

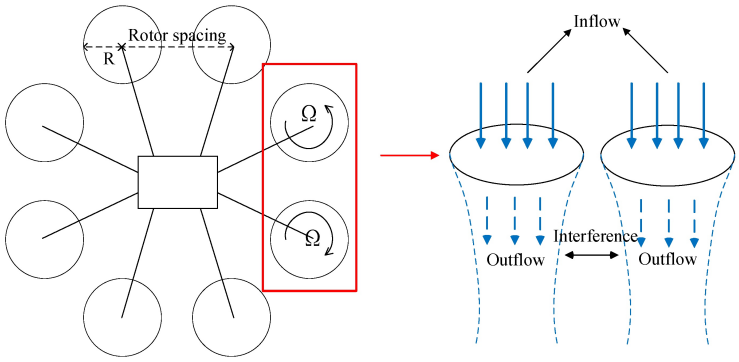

Figure 2.3: Relationship of rotor spacing and rotor diameter in an octocopter and the associated interference between propeller wakes [28].

2.2.2 Key Components of a Multirotor

Multirotors are simple to understand the basics of how they operate and fly but the associated systems can become complex. There are a number of different subsystems that make up a multirotor and ultimately allow it to fly. This section intends to highlight all the key components that require consideration in research related drone design and will briefly explain their functioning.

Figures 2.4 and 2.5 highlight the necessary components required in order for a sUAS to take flight. It further names certain parts of the drone that will be referred to throughout this dissertation.

Fundamentally for an sUAS to fly there is a requirement for a structural frame to connect and mount all the subsystems. A Frame can be further broken down into subareas, in Figure 2.4 these areas are identified as rotorbooms, central plates, landing gear and sensor mount spaces such as gimbal rails. In designing a frame there is careful consideration of the intended purpose which leads to considerations of weight and strength that ultimately influence the material choice. Beyond functional design decisions, there are further practicality decisions such as portability and compactness, modularity and how easy it is to integrate external systems.

Having briefly discussed the structural considerations, the thrust delivery system can be investigated; this will be referred to as the *powertrain*. Generally, an sUAS powertrain is made up of motors, propellers and a fuel source. Specifically, electric sUAS require a charge source like batteries and electric speed controllers to control the motors. Each choice of component in the thrust system has a heavy dependence on the other components in the train, requiring careful matching of components to

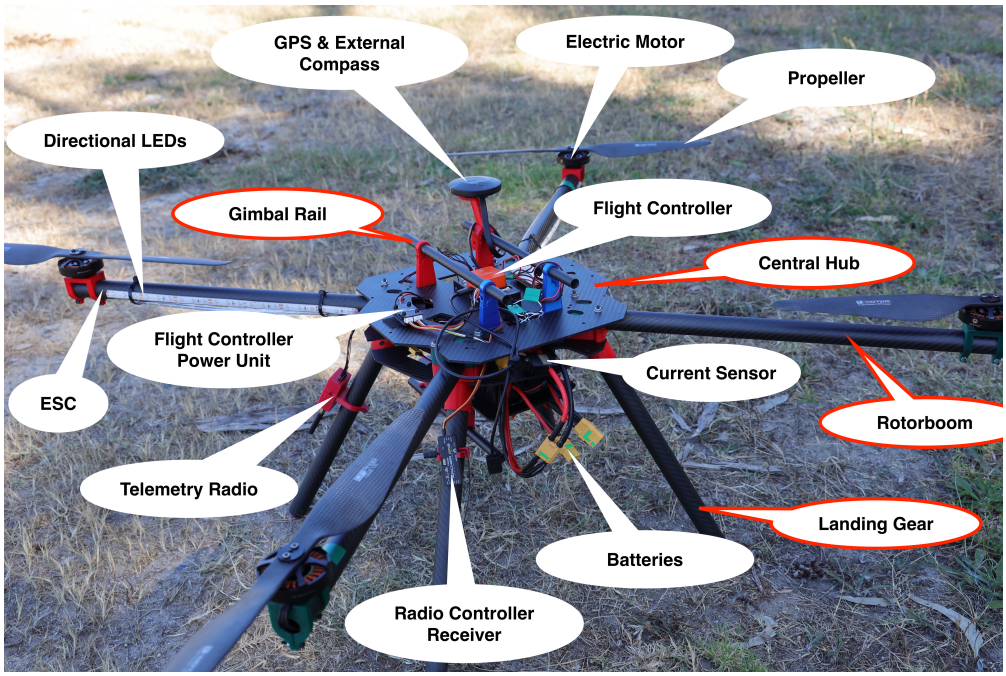

Figure 2.4: An overview of the main components found on a sUAS, identifying their typical look and general mounting location. White captions highlight electrical components and red captions identify parts of the frame.

achieve an efficient and effective system. Additionally, within powertrain design are considerations for power distribution to the thrust system and periphery connections such as directional lights and the autopilot.

With the structure and powertrain considered there is then the last necessity of command and control of the sUAS. On most drones today, there is a flight controller with varying levels of autopilot system. The systems range from fully autonomous with no user input, to completely dependent on manual user input. The choice of flight controller and level of autopilot will depend on the application, racing drones have very minimal stabilizing systems, whereas research drones could require GPS signal, compass heading and gyroscope input for automated flights.

Regardless of the level of autopilot, all sUAS under regulations require a radio control link for either primary control or as a fail-safe system to recover control of a drone [1]. In some cases, additional telemetry radios are attached to the drone in order to live stream data to a connected ground station or laptop, the streamed data could be anything from airspeed to pitch and roll angles. Figure 2.5 below gives a general mounting location of the above discussed components.

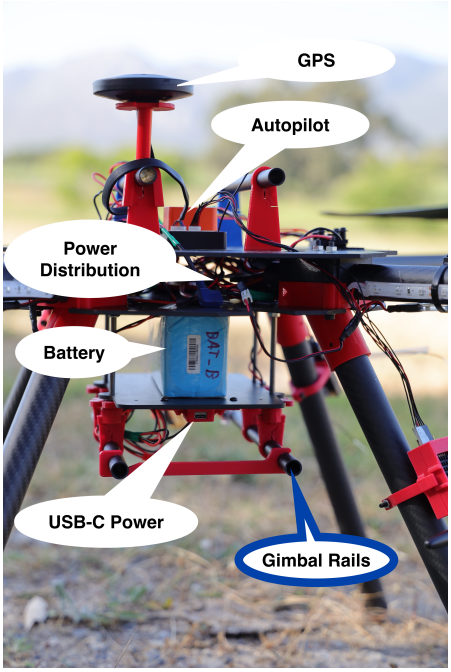

Figure 2.5: Identifying key electronics for the command, control and powering of a typical sUAS. White captions highlight electrical components and blue captions identify parts of the frame.

2.3 Command and Control

This section will detail the command and control elements of and sUAS system. The section will describe the manner in which an autopilot and flight controller operate before exploring common open source solutions. Thereafter, communications systems on and off the drone will be discussed.

2.3.1 Flight Controllers and Autopilots

The flight controller and autopilot are a combination of two systems which assist with the command and control of a drone. The *flight controller* is the physical hardware used to perform the computations. Whereas, an *autopilot* is the firmware which is run on the flight controller to interpret and act on input information.

Together, the flight systems fuse data from multiple onboard sensors along with GPS readings to determine drone orientation and position. User inputs from control links allow for manual manipulation of the drone [29]. The collection of input information is interpreted and then converted to a motor signal which is sent to the ESCs

to control the motor speeds and torques.

There are certain sensors incorporated into the hardware of a flight controller however, non-standard sensors can be integrated through external UART and I2C ports [29–31]. Inertial measurement units (IMUs) are found on drones which require guided navigation and movement through 3D space. An IMU consists of accelerometers which detect linear accelerations and gyroscopes to measure rotation rates, the readings allow for accurate estimation of the relative attitude of the drone in 3D space. In other words, an IMU provides estimates of the roll, pitch and yaw relative to the starting position. A magnetometer can be included in the IMU sensor set to supplement accelerometer and gyroscope readings for heading or the yaw angle and assist with magnetic field readings surrounding the drone [30]. Altitude estimations come from barometric readings that use instantaneous atmospheric pressure relative to the pressure at takeoff to determine altitude.

All the sensors mentioned thus far operate in a reference frame relative to an initial estimate. The concern with this is that some sensor readings can 'drift' due to external interference, thus introducing error. A solution is to incorporate external sensors which can provide a reference frame relative to the external 3D world. These systems serve as redundancy fail-safes for guided systems, especially since aircraft interact in environments where people may be present. Global Navigation Satellite Systems (GNSS) can help determine the location of a drone by measuring the distance between the receiver on the drone and satellites at predefined locations [30]. The accuracy of GNSS systems varies depending on the quality, low cost units have an accuracy of approximately five meters however precision units can provide cm accuracy in real time. Furthermore, GNSS systems are slower compared to the on board IMU sensors simply because of the transmission latency. Regardless of the accuracy and time delay, the introduction of GNSS systems provides an absolute position estimate to accompany the relative readings of the IMU sensors. External compasses are also packaged with GNSS systems to serve as additional references for heading. Having multiple compasses allows for instantaneous comparison as they are susceptible to electromagnetic interference, thus improving heading estimates and serving as an additional fail-safe.

2.3.2 Available Flight Controllers and Autopilots

The massive development boom surrounding flying drones has led to a large range of available flight controllers, some open source and some proprietary, each with varying capabilities. Ebeid et al. [30, 31] perform a thorough comparison of the available

flight controllers and autopilots whilst specifically highlighting the open source options. This section will highlight some well known autopilots and flight controllers that are available and suitable for research focused sUAS.

Well known open source flight controllers included the Pixhawk series and the derivative Cubepilot. There are a number of different Pixhawk hardware boards each catering to different requirements. The mRo Pixracer is optimised for small racing drones with minimal casing and cannot integrate a GPS. The Pixhawk 4 is intended for research and commercial use, it has external ports to integrate GNSS systems as well as additional IO ports to control servo motors or for further sensor integration. The Pixhawk 5 is the latest flight controller from Pixhawk featuring redundant sensors, a modular flight control unit, and sensor and vibration isolation for reliable research and commercial use [32].

The Cubepilot flight controllers are modular and can be 'hot-swapped' between carrier boards. Cubepilot has a variety of carrier boards: the standard carrier board provides connections for all the functions of the flight controller, a mini board to reduce form factor and weight and a carrier board with power distribution built-in along with the standard features. There are a number of different variations of the Cube with slightly different performance parameters. The main variations come from the clock frequency, onboard RAM and level of Redundancy. The Orange Cube is the latest in the range with the best specifications, it has triple redundant IMUs, temperature isolation and 1Mb of RAM [33].

Both flight controllers are compatible with Ardupilot and PX4, too large open source, community backed autopilots. Both autopilots can be configured to operate as planes, copters, rovers, boats, submarines and VTOLs. [25, 32, 33]. Ardupilot has different firmware versions depending on the application of the flight controller, Arducopter is the firmware used for helicopters and multirotors in a number of configurations. The Ardupilot and PX4 firmware are configured from a Ground Control Station (GCS) software, QGroundControl [34] and Mission Planner [35] can both be used to configure the parameters and then further serve as a communication link between the drone and GCS. There are other open source autopilots available such as Cleanflight, BetaFlight and INAV, all of which are inherently based on Baseflight [31]. Notably, these autopilots can be configured and display sensor readings from a browser based tools and don't require an additional GCS software.

2.3.3 Communication Systems

There are two main types of communication link that can be found transmitting to and from a sUAS as displayed in Figure 2.6. The first, is a communication link transmitting to and from a GCS. The second is a standard remote control link used mainly to control the attitude and minor parameter changes [31]

Figure 2.6: Distinction between a remote control transmitter for manual operation of an sUAS and a GCS for telemetry data viewing and mission control.

Ground Control Stations

A GCS is application software that runs on a computing device and communicates wirelessly with a target vehicle over a radio signal, or more recently, mobile networks. The GCS is used to monitor the target vehicle by streaming telemetry data like position but can also be used for control by transmitting waypoints or commands. As with flight controllers and autopilots there are open source and proprietary options, common ones are Mission Planner, QGroundControl and DJI GS Pro. For firmware like Ardupilot and PX4, a GCS is also required to configure parameters and calibrate sensors before any operation can take place.

As mentioned, the GCS can connect to the drone over a radio telemetry link, the operating frequency depends on the legislation in the geographical area of use.

Some telemetry radios have a transmission range of up to 40Km, this range is influenced by the antennas connected to the transmitters, the transmission power and the landscape.

More recently, mobile networks have also been used to transmit data between a drone and a GCS. Burke [29] describes a network stack where a mobile modem is connected to the companion computer on the drone to provide internet connection. The drone connects to a cloud hosted Linux server and the GCS does the same, allowing for transmission of telemetry data and video streaming over a secure link. A limitation of this network setup is the requirement of a mobile network with an internet connection, something that is not readily available in remote areas. An alternative for remote areas would be to generate a private mobile network at the site of interest that both the GCS and drone can connect to.

As mentioned, GCS applications can also be used to control a drone with commands and predefined waypoints missions. Waypoint automated missions can be created in GCS software and uploaded to a drone to perform when an automated mode is invoked. Automated missions require guidance and thus accurate position and orientation estimations which are provided by GPS signal and IMU readings. Mission Planner defines three types of command: *Navigation* commands to control the movement of the drone, *Do* commands that operate servos or signals to take pictures but do not affect movement and *Conditional* commands which must be met before a Do command can occur [25]. Beyond waypoints and commands, joystick controllers can also be connected to GCS applications for manual control through the GCS telemetry link.

In order to transmit data between the GCS and drone there is a requirement for a transmission protocol. Ardupilot and QGroundControl make use of the MAVLink protocol to transmit data between the GCS and drone. MAVLink is a lightweight messaging protocol and is suitable for applications with limited bandwidth and thus makes it perfect for telemetry connection over radio to drones, limited bandwidth would not be an issue for mobile networks [36].

Remote Control Transmitters

In the absence of a GCS, the alternative to control a drone is via a remote transmitter and receiver for radio control. A remote controller is mainly used for attitude and throttle adjustments and minor parameter changes like setting flight modes. The controller takes the inputs from the user, converts them to either Pulse Width Modulation (PWM) or Pulse Position Modulation (PPM) signals and transmits them to

a receiver on the drone. The receiver is connected to the flight controller which interprets the signals and converts them to an associated motor signal [30]. If a GCS is in use, the remote controller is mainly used as an emergency backup to regain control of a drone. However, if no GCS is in use then the remote controller is sufficient for manual control but requires more expertise for fine control.

Off-the-shelf (OTS) transmitters and receivers operate at either 900MHz or 2.4GHz. There are some benefits to each RF band: the lower 900MHz band has higher object penetration and range whereas the higher 2.4GHz band consumes less power and operates in a larger band allowing for a higher density of users before interference. The choice of radio frequency is dependent on the application requirements, if a longer range is important then the 900MHz band is more suitable. However, if the research project concerns drone swarms then it would be better to operate in the 2.4GHz band for its greater density possibilities.

2.4 Powertrain Components

This section will describe the key components associated with the design of an electric powertrain. Each section will outline a number of key elements related to the selection of the components and emphasise the close relationship between them in order to create an efficient system.

2.4.1 Motors

The motors allow drones to convert energy from one form to another, specifically from potential stored energy to mechanical energy. There are different types of motors that could be used to construct a sUAS, namely electric and combustion motors. Electric motors, specifically brushless motors, dominate the drone industry for their fine control, efficiency and almost immediate torque response. There are two types of brushless motors known as inrunners and outrunners, this refers to which part of the motor body rotates and is connected to the output axle. Inrunners have a ring of magnets enclosed by an array of windings, outrunners are the reverse with an array of windings enclosed by magnets. Inrunners are generally used on smaller mutirotors as they have a smaller form factor however outrunners can produce more torque and are used more often on larger scales [37].

A key parameter to consider when selecting a motor is the Speed Constant, KV. This is a parameter provided by the manufacturer that is used to estimate the unloaded speed of a motor given an applied voltage, RPM/V [37]. The speed constant serves as a guide for propeller matching and meeting thrust requirements. Speed

constant values range from as low as 40KV to in excess of 1000KV and there are optimal ranges for different applications. High KV values, over 1000KV, are associated with smaller propellers with high pitch angles. Small propellers are generally easier to rotate compared to larger ones due to their lower mechanical and torque demands and thus rotate at high RPMs. This is suitable for applications where agility and speed are important instead of efficiency and endurance [37] Larger propellers are more difficult to spin due to their high torque demands and thus make them less agile, however, they are generally more efficient due to their large surface area making them ideal for endurance and carrying payloads.

Essentially the speed constant limits the range of propellers that a motor can accommodate and propellers outside of the optimal range will either be ineffective or damage the motor through high demand. With this in mind during design, the KV value can be a good indicator of the applications of a motor but should be accompanied by thrust testing or simulation of different motor propeller combinations.

2.4.2 Propellers

Propellers used in sUAS come in varying diameter sizes, pitch angles, number of blades and different materials. Each parameter has a varying effect on the performance of the propeller and in turn, also influences the possible applications.

Increasing the number of blades and pitch angle are associated with increased thrust but at a cost of decreased efficiency and higher torque demands from the motor [37]. Typical racing drones can be seen with small diameter propellers with 2 or more blades at high pitch angles for their 'punchy' high thrust-to-weight ratios. The efficiency costs of increased blades results from more blades operating in the wake of others. As a propeller blade moves through the air it creates a disturbance wake, however, propellers have higher performance and efficiency in undisturbed air compared to turbulent air. The efficiency difference can be understood from observing a 2 and 4 blade propeller. The 2 blade propeller has each blade spaced 180°apart, however, the 4 blade propeller has a blade spaced twice as often, meaning the more blades present the closer they are to the previous blade and its respective disturbance wake.

As mentioned in the previous section, propellers with larger diameters are generally more efficient compared to small diameter propellers as they can generate the same lift whilst spinning at lower speeds [37]. Another consideration of propeller diameter is the associated noise, larger diameters tend to output a low pitched sound vs the high pitch of a small diameter prop.

Lastly, the material and quality of the finish can also have an effect on the performance. Stiffness and well balanced propellers assist in reducing any unwanted oscillations in the system as a propeller spins. Stiffness, weight, strength and quality of the finish are all influenced by the material and production process. It is common to find propellers made from wood, carbon fiber or a thermoplastic each with its own set of advantages and disadvantages.

2.4.3 Electronic Speed Controllers

Electronic Speed Controller (ESC), assist with the fine control of electric motors. A PWM control signal is sent from a flight controller or radio control link to the ESC, the PWM value is interpreted and then a DC input is converted to an AC output for the motor. When considering ESCs for the design of a sUAS, the main parameter of interest is the maximum current throughput. This relates to the maximum load that can be expected from the propeller and motor pair. Most ESCs come with a maximum continuous current draw rating and a burst current draw rating which can be sustained for a brief time.

2.4.4 Battery Chemistry

Most sUAS are battery powered however it is not the only solution to power a sUAS. Internal Combustion Engines (ICE) are also an option along with hybrid solutions which make use of an ICE and electric propulsion system. ICE fuel energy and power density is greater than the battery technology currently in production, however, the multistage processing of fuel results in poor efficiency. Electric motors are preferred for sUAS due to their low thermal and acoustic signatures, well developed electric control, efficiency, fast response time and simplicity [38]. This section is going to focus on battery technology as the source of power for its simplicity and ease to replicate in a self-build.

There are a number of battery chemistries, each having certain application benefits. When comparing battery chemistries the three main parameters of interest: the *specific energy*, *specific density* and *specific power* which translates to the available energy per kilogram, (Wh/kg), available energy per litre, (Wh/l), and the available power per kilogram, (W/kg) [39, 40]. Higher values of specific energy and power translate to a battery which can discharge more power for longer. Beyond chemistry composition, there must also be consideration of current demand, required voltage and capacity for battery selection.

Batteries are built up of individual cells either connected in series (S) or in parallel (P). To achieve different battery voltages and capacities, individual cells are connected

together either in series to increase the voltage or in parallel to increase the capacity and discharge capabilities [37]. For example, a 6S1P battery has six cells in series and one in parallel, the voltage of the battery would be six times the nominal voltage. The current discharge capabilities of a battery are specified as 'C' ratings, with a continuous and burst rating. The continuous rating describes the maximum current a battery can discharge continuously without damaging the cells. The burst rating is the absolute maximum current value that a battery can discharge, however, this can only occur for a short duration, usually 60 to 180 seconds. The C rating is defined by the capacity of the battery, where a battery with a capacity of 8000mAh will have a 1C rating of 8A. The continuous and burst C ratings are then specified as multiples of the 1C rating, for example, a continuous rating of 30C equates to 240A.

Having defined some key parameters to distinguish different batteries, the available technologies can now be compared. Lithium Ion (LiIon) and Lithium Polymer (LiPo) batteries are the current choices of chemistries for sUAS use. Lithium batteries have replaced Nickel based cells due to their improved specific energy and thus weight reduction. Table 2.1 compares typical specific energy and power values for different battery chemistries.

Table 2.1: A comparison of battery chemistries and their specific energy and power [2, 39, 40].

Parameter	LiIon	LiPo	NiCd	NiMh
Specific Energy (Wh/kg)	50-260	180	45-80	80-120
Energy Density (Wh/l)	250-670	300	100	300
Specific Power (W/kg)	245-430	2800	300	900

From Table 2.1, it is clear that LiPo and LiIon batteries outperform the older Nickel based batteries with reduced weight and higher discharge capabilities.

The comparison can now focus on LiIons and LiPos as both have different application benefits based on their construction. LiPo batteries are regarded for their high specific power capabilities which translates into high discharge currents reaching in excess of 100A for sustained periods. LiPo batteries can have continuous C discharge ratings reaching 50C allowing for extremely high discharge capabilities. The result is a battery which is suitable for agile manoeuvring and heavy payloads. This extreme current capability comes at a weight cost and thus poorer endurance.

Alternatively, LiIon batteries are the opposite and are better suited to endurance applications with higher specific energy but lower specific power [37, 40]. Although

LiIons have lower specific power they are still capable of reasonably high current discharge with ratings reaching 25C. This means that LiIons are still suitable for sUAS designed for research, however, the system should be efficient with a focus on endurance over agility.

The choice of battery chemistry is influenced by the field of research and thus the application of the sUAS. As with Pirotta et al. [17], a LiPo battery is more suitable as the sUAS must be extremely agile to respond to whale blows to collect samples. However, in the case of Galle et al. [11] and Jordan [24], LiIon batteries prove more suitable for extended flight times at high altitudes to sample volcanic gas plumes.

Fortunately, it is relatively easy to switch between LiIon and LiPo on the same sUAS. The benefit is the power source can be chosen to suit the application requirements depending on the conditions at hand. The main requirements to revise are if the battery voltages are similar and if the propulsion system can accommodate the current supply of the chosen battery chemistry.

2.5 Mechanical Considerations

This section will discuss the mechanical design aspects relating to the drones. It will firstly describe theory relating to the mechanical properties of material and their influence in the design of drones. The section move to defining 3D printing and the growing use in drone building. Thereafter, a description of the frame and motor placement will be covered and the potential efficiency gains of rotor spacing.

2.5.1 Understanding Material Properties

In order to effectively design the structural parts of an sUAS requires an understanding of material properties. When comparing materials, there is often a consideration of a number of specific parameters which influence the performance of a material under operating conditions [41]. Parameters that are useful for comparing materials intended for drone design are:

1. Young's Modulus: E
2. Yield Strength: σ_{yield}
3. Ultimate Tensile Strength: σ_{uts}
4. Ultimate Compressive Strength: σ_{ucs}
5. Ultimate Strain

6. Density

A number of these properties can be determined from a curve known as the stress and strain curve, an example is shown in Figure 2.7.

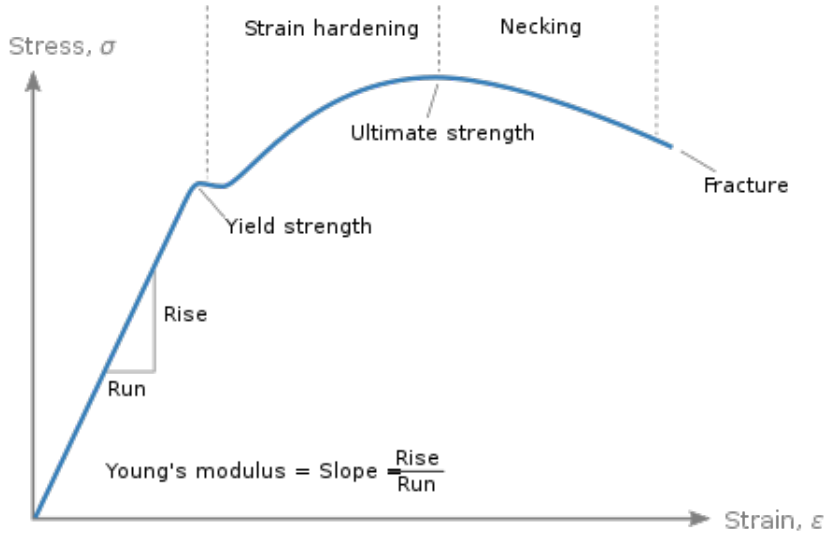

Figure 2.7: A typical stress strain curve for a ductile material. The curve highlights the major points of interest relating to the material. The Elastic region is to the left of the yield strength and the plastic region is located on the right side.

Young's modulus relates to the stiffness of a material or in other words, how much the material is likely to bend. Stiffness is not solely influenced by this parameter as increasing the cross-sectional area of an object will also improve the stiffness performance. The stiffness of a material is key in load transferring areas of a drone, this can be described in two ways. The first relates to extremely stiff materials, this is beneficial to efficiently transfer energy. With regards to thrust transfer, it is undesirable for a rotorboom to absorb potential energy as it bends under loading as this will require more thrust. In the second case, a flexible material can be used to absorb energy from a crash or hard landing.

The Ultimate Compressive Strength (UCS) and Ultimate Tensile Strength (UTS) refer to the maximum stresses a material can withstand in compression or tension respectively, some materials will have a higher tensile strength or a higher compressive strength.

The elastic region is the area of the stress and strain curve with a linear gradient, it defines how much stress a material can withstand before being permanently deformed.

If a material is stressed beyond the elastic region it enters the plastic region where the material may continue to deform before fracture.

The yield strength is the point of transition between the elastic and plastic region and thus is the point a material will be permanently deformed. In the case of a brittle material, the UCS or UTS is usually the same as the yield strength as there is no deformation before fracture. Ductile materials are the opposite and will undergo plastic deformation before fracturing, thus the ultimate strengths and yield points will likely not be the same.

Understanding the relationship between the yield and ultimate strengths provides guidance into the behaviour of a material and whether a material will deform before failure or not. In the design of load bearing components it can prove beneficial for a material to show signs of plastic deformation before failure as this can serve as an early warning system.

The ultimate strain of material relates to how much a material will elongate relative to its original length before fracture. Materials that are ductile in nature have longer strain capabilities relative to brittle materials. High strain capabilities can be useful indicators that a component has been stressed beyond yield and may fracture under increased load.

Lastly and one of the most critical material properties in drone design is density as it provides insight into the weight. In the design of a multirotor which requires constant propulsion, it is beneficial to have a light weight system as it increases thrust overhead which can contribute to payload capacity or manoeuvrability of the small Unmanned Aircraft System (sUAS).

2.5.2 3D Printing as a Manufacturing Technique

3D printing is an additive manufacturing process whereby a material is heated from solid form and deposited in layers to build up a complete object. Specifically, 3D plastic printing has become increasingly accessible as a tool to rapidly iterate designs and create functional parts [41, 42]. This section will describe the use of 3D printing, specifically Filament Deposition Modeling (FDM), to create load bearing parts in the design of drones and discuss key aspects to consider in the printing process.

The 3D printing process has become extremely accessible with entry models costing a few thousand Rands with simple to use interfaces. The creation of printed

components begins with the design of a 3D model in CAD software. During the design, careful consideration is given to the orientation a component will be printed as it is influential in the mechanical performance, especially regarding strength. Post design, the 3D model is exported in a universal file format to a slicing program. The slicing program is used to partition the component into a number of layers and create an associated path for the printer head to follow and deposit material. During this process, additional settings are configured such as infill percentage and layer height.

In designing load bearing components it's especially important to understand the strength of the material to ensure a component can sustain its intended operation. Although the strength of 3D printed components has been previously studied on industrial scale machines, Johnson et al. [42] conducted studies on the ASTM international D638 [43] standard specimens to evaluate the performance of 3D printed components on consumer level printers. The use of global standards allows for comparison between different materials as well as different printing devices. A major influential factor, apart from the material used, in the strength of a component was found to relate to the infill percentage of the specimen [42]. The infill describes what percentage of the internal volume of a printed part is filled with material.

In addition to the infill percentage, the orientation of a part is also influential in the strength and strain performance. During the printing process, a single layer is commonly a continuous single deposition where as each layer simply adheres to the previous layer. There is a significant difference in strength between layer adhesion and the continuous unified strand of material [41, 44]. The orientation can be affected in two ways, either by the orientation of the component on the print bed as shown in Figure 2.8. Alternatively, the orientation of the infill material can vary in angle relative to the direction of loading. For example, the infill material under standard settings is at 45 °to the loading direction but can be altered to be parallel to increase strength [44].

Due to the rapid nature of 3D print iteration and the associated material performance in weight and strength, printed components are suitable for use in drones [2]. Nvss et al. [45] used additive manufacturing and optimisation techniques to redesign the load bearing central hub of the frame into a single printed monocoque. The work was driven to reduce weight and improve assembly time all the while ensuring the monocoque could sustain the stress, vibrations and fatigue requirements of the central hub.

Kotarski et al. [46] also used FDM components to create a modular sUAS for education purposes where students could reconfigure the drone and develop associated control algorithms. In the educational drone, FDM and other additive manufacturing

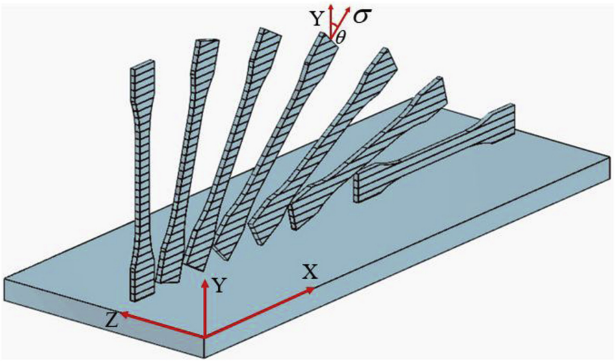

Figure 2.8: A standardised material testing specimen showing the different print orientations from 0°through to 90°, including indications of the layer separations [41].

processes were used to iterate parts and manufacture items such as the central frame and motor mounts.

Additionally, Ragib et al. [47] utilised 3D printing to create a number of custom components to secure peripheries of a drone mounted water sampling system for sample collection and in situ measurements.

Chapter 3

Powertrain and Flight Subsystems Design

3.1 Powertrain Design

The powertrain design combines the key components required to provide thrust and drive to the sUAS. There are large levels of dependency in the powertrain design, where each choice of component restricts other component choices. In order to guide the design, a set of requirements were formulated to describe the desired performance of the HexaQuad. The two most influential requirements for the powertrain were the flight time and payload capacity as these give an indication of thrust requirement and endurance.

The section will start with the motor and propeller selection and the techniques used in the associated process before investigating the associated power distribution requirements.

3.1.1 Motor and Propeller Combination

The motors were the chosen starting point for the design of the HexaQuad as it was the point with the most resources and data to make informed decisions. This section will be broken down into two main parts, the first, giving insight into how manufacturers data assisted with narrowing the scope of options, and the second will explain the use of a simulation tool to create expected flight performance under controlled conditions.

Two key parameters were required to aid the selection of powertrain components, the first being a payload capacity of 2kg and 5kg for the Quad and Hex respectively. The second was a flight time range of 15-20 minutes for either configuration. The payload and flight time requirements gave insight into the thrust requirements of the sUAS. In order for the drone to fly it would need to provide sufficient thrust to carry the payload, the weight of the drone itself and still have overhead thrust to

manoeuvre. A simple estimate as a starting figure is to have twice as much thrust required to lift the All Up Weight (AUW) of the drone and the additional payload

$$Maximum\ Thrust = 2 \times (Payload + All\ Up\ Weight)$$
$$or$$
$$Hover\ Thrust = Payload + All\ Up\ Weight$$

Depending on the use case of the sUAS, this estimation of thrust can be adjusted. For example, if a more agile sUAS is required then there should be more overhead thrust to assist with fast manoeuvres. However, for the HexaQuad, the main flight requirements were stability and endurance thus the thrust overhead can be lower for steady controlled manoeuvring.

In order to determine a thrust value, weight estimates of the HexaQuad had to be created as a starting point for the design. The estimated weight ranges are shown in Table 3.1. The estimates were determined by researching typical components included in heavy lift drones as well as frame size and materials. The weight ranges were also affected by the number of rotors in the configuration.

Table 3.1: Weight ranges of the subsystems in heavy lift drones used to estimate the thrust requirements of the HexaQuad.

Subsystem	Estimated Weight(g)	Description
Frame	2500 - 3000g	The frame and all structural components
Powertrain	3000 - 4000g	Motors, propellers, ESCs and batteries
AUW	5500 - 7000g	All Up Weight, excluding payload

With the weights in Table 3.1 an estimated maximum thrust can be calculated:

$$Maximum\ Thrust = 2 \times (5kg + [5.5; 7]kg) = 2 \times [10.5; 12]kg \tag{3.0.1}$$

Guided by the maximum thrust and thus hover thrust, different motors could be considered based on manufacturers' specifications. Some reputable manufacturers provide detailed test data of motor and propeller pairs, reporting thrust, current draw, power, RPM and operating temperature at incremental throttle percentages. Motor options from a number of manufacturers were reviewed through specifications to create a short list that met the thrust requirements. Parameters of interest were maximum thrust, weight, compatible propellers and price. Price was of interest to limit the motor selection to suitable options which were not grossly over designed.

A short list of motor options can be seen in Table 3.2. Any considered motors were required to be able to lift the AUW and the payload with a throttle value of 65% or less.

Table 3.2: Short list of motor options to consider in simulations based on manufacturers' specifications.

Motor Name	Max Thrust (g)	KV	Mass (g)	Voltage	Propellers (in)	Price ($)
SunnySky V4014	3900g	330	166g	6S	12-18"	$80.00
Tarot 4008	3050g	330	85g	6S	17-19"	$46.00
Tarot 5008	3500g	340	168g	6S	17-18"	$57.00
T-Motor MN501-S	5200g	360	170g	6S	17-18"	$100.00
T-Motor MN5008	4200g	340	135g	6S	14-18"	$90.00
KDE 4215XF	5860g	465	250g	6S	12-18"	$154.00

Additionally, a short list of propellers was drafted to reduce the number of varying parameters in the simulations. A diameter range was selected based on the propellers recommended by the motor manufacturers and their expected thrust performance. Table 3.3 defines the details of the propellers used in the simulations.

Table 3.3: Reduced range of propellers to compare in simulations. * marks an alternative eighteen inch propeller.

Name	Diameter (in.)	Pitch (in.)	Material	Price ($)
T-Motor P17x5.8	17"	5.8"	Carbon Fiber	$72.00
T-Motor P18x6.1	18"	6.1"	Carbon Fiber	$83.00
*Quanum T-Style	18"	5.5"	Carbon Fiber	$24.00

With a shortlist of motors and potential propeller sizes, simulations could begin. eCalc [48] is an electric drive simulation tool with a large database of motor and propeller performance metrics. eCalc prompts the user to enter or select a number of specific details such as a motor and flight conditions, these inputs are used to simulate performance and return metrics such as flight time and current demand. It is beneficial to use a simulation tool such as eCalc as it defines some boundary conditions for the expected performance of an sUAS without going through a practical trial and error method.

During the simulations there were three variables that were varied: 1) the motor and propeller combination; 2) single or double battery capacity; and 3) the payload from 0 to 2.0kg or 5kg depending on the configuration. Other parameters were initially held as fixed during simulations and are shown in Table 3.4.

Table 3.4: Fixed values entered into eCalc for the motor comparison simulations.

Parameter	Value
Battery Voltage	6S
Battery Discharge	85%
Frame Weight	2500g
Number of Rotors	4 or 6

The results of interest returned from the simulations were flight time, efficiency and throttle level at hover. The results from the first set of simulations can be seen in Table 3.5, it is these values that guided the selection of two final motor and propeller combinations. The flight time and throttle percentages presented in Table 3.5 represent a range of expected performance for the motor propeller combinations with varying payload capacity.

Table 3.5: eCalc motor and propeller simulation results used to reduce the number of considered combinations.

Motor	Propeller	Efficiency (g/W)	Flight Time (min)	Throttle (%)
SunnySky V4014	P17x5.8	6.85	[9.3 - 21.6]	56 - 78%
	P18x6.1	7.18	[9.7 - 22.7]	53 - 73%
Tarot 4008	P17x5.8	7.01	[9.6 - 24]	56 - 80%
	P18x6.1	7.31	[10 - 25]	53 - 76%
Tarot 5008	P17x5.8	6.78	[9.2 - 21.3]	55 - 76%
	P18x6.1	7.10	[9.6 - 22.4]	51 - 72%
T-Motor MN5008	P17x5.8	7.38	[10.3 - 24]	51 - 69%
	P18x6.1	7.77	[10.9 - 25.3]	47 - 65%
T-Motor MN501-S	P17x5.8	7.14	[9.9 - 22.5]	48 - 66%
	P18x6.1	7.53	[10.4 - 23.7]	45 - 62%
KDE 4215XF	P17x5.8	6.81	[9 - 20.4]	41 - 56%
	P18x6.1	7.14	[9.4 - 21.4]	38 - 53%

The *T-Motor MN5008* was selected as the preferred choice with the highest efficiency and flight times. The throttle percentage at hover was a minor concern with a possible 65-69% when carrying the maximum payload of 5kg.

Out of the two propellers compared in Table 3.5, the eighteen inch propeller displayed the best performance with higher efficiency, flight time and thrust. However, due to the high cost of the $P18 \times 6.1$, an alternative eighteen inch propeller was also considered and compared in a second round of simulations. The specification of the alternative eighteen inch propeller can be seen in Table 3.3 depicted with an

asterisk(*), the *Quanum T-Style* 18×5.5.

The two eighteen inch propellers were compared in further eCalc simulations to interpret the expected performance and aid in design decisions. The simulation results are presented in Table 3.6 and showed similar performance between the two propellers.

Table 3.6: Simulation comparison of the 18 inch propellers to investigate any performance gains or benefits associated.

Motor	Propeller	Efficiency(g/W)	Flight Time(min)	Throttle(%)
Hex Configuration				
T-Motor MN5008	T-Style 18x5.5	8.42	[10.6 - 23.7]	49 - 67%
	P18x6.1	7.77	[10.9 - 25.3]	47 - 65%
Quad Configuration				
T-Motor MN5008	T-Style 18x5.5	7.09	[14.5 - 21.8]	59 - 69%
	P18x6.1	6.44	[14.4 - 21.7]	58 - 67%

Interestingly, it is estimated that the *Quanum* propellers would have a higher efficiency compared to the *T-Motor* propellers. It is assumed that this behaviour is related to the *Quanum* propellers being simulated as generic propellers with the entered diameter and pitch instead of relying on test data as in the case of the *T-Motor* propellers. However, there is a significant cost difference of $59.00 between the two propellers, which according to simulations seems unjustified. Due to the close similarity between the eighteen inch propellers and the large cost difference, it was decided to test both models in the experimental tests to investigate any cost benefit that exists.

Thus, the final motor and propeller combination that the HexaQuad would make use of is as follows:

1. T-Motor MN5008 340KV 6S electric motor
2. T-Motor P18x6.1 or the Quanum T-Style 18x5.5 propellers

3.1.2 Electronic Speed Controller Selection

Within the powertrain design, the selection of the Battery and Electronic Speed Controller (ESC) is more flexible compared to the motor and propeller combination. Once the motor and propeller combination has been confirmed an ESC and battery can be matched to the requirements of the systems to achieve the desired performance. This section will outline the specifications of the motor and propeller combination that guided the selection of the ESC.

The selection of the ESC is a trivial process and depends mainly on the maximum current demand of the motor and propeller combination. From the simulations and manufacturer specifications, it was found that an ESC capable of operating at 40A continuous demand should be used. With this specification, a short list was created comparing the weight, price and operating ranges of available ESCs, the short list is shown in Table 3.7.

Table 3.7: Short list of ESCs suitable for use on the HexaQuad.

ESC	**Max Amps(A)**	**Voltage**	**Weight(g)**	**Price**
Air 40A 6S	60	2-6S	26	$40.00
XRotor Pro 40A	60	2-6S	50	$25.00
Turnigy Plush-32	60	2-6S	46	$22.00

All the ESCs presented in Table 3.7 would be suitable for the HexaQuad and the selection process was based on preference for the intended design with reasonable cost. The *XRotor Pro 40A* and *Turnigy Plush-32* had similar specifications and price, the main distinction was the form factor of the two units shown in Figure 3.1.

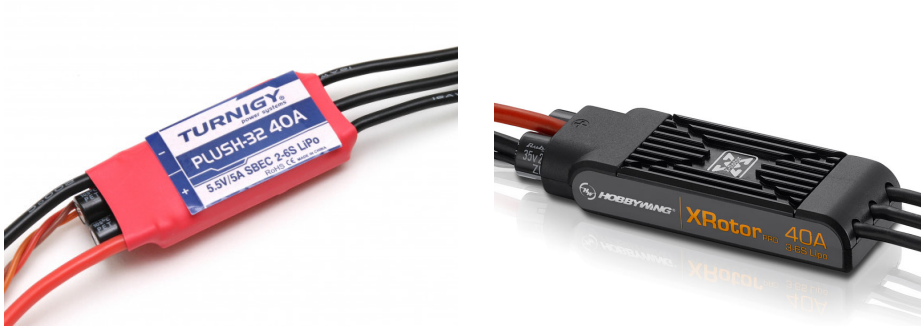

(a) Turnigy Plush-32 [49] (b) XRotor Pro 40A [50]

Figure 3.1: Comparison of the Turnigy and Xrotor form factors highlighting the inclusion of a heat-sink on the Xrotor for cooling and instillation within a rotorboom.

The *XRotor* had a built in heat sink to assist with cooling and is designed to be installed inside a rotorboom whereas the *Turnigy* had to be placed under the propeller in the rotor-wash for cooling. The *Air 40A 6S* was the lightest of the three ESCs, however, it was double the cost of the other two options and also had to be mounted in the rotor-wash for cooling.

Based on these considerations the *XRotor Pro 40A* was selected for its versatility of mounting locations, reasonable cost and weight.

3.1.3 Battery Selection

The selection of the battery followed a similar process to that of the ESC and was guided by certain parameters derived from the motor and propeller combination.

Influential parameters were the motor voltage and the expected current. The motors require a maximum input of a 6S voltage and 40A of current each, resulting in a total maximum demand of 240A. The maximum current demand would be a burst value and could only occur for a short time before any damage would occur, this is quoted as three minutes by the manufacturer. From the simulations, typical hover operating currents ranged between $[6.94 - 11.61]A$ per motor, for a range of payload weights. The identification of the current demand at burst and continuous rates assists with determining the associated discharge rates of the battery, in other words, the C-ratings. The expected current demand of the battery is summarised in Table 3.8.

Table 3.8: Expected operating current ranges of the HexaQuad from eCalc simulations.

Discharge Rate	Current per Motor	Total Current
Continuous	[4.68 - 15.2]A	[28.1 - 91.2]A
Burst	40A	240A

The other major parameter of an sUAS battery is the capacity. The capacity of the battery is extremely influential in the endurance of a flight, however, any increase in capacity also increases the weight. The relationship of weight to capacity is also affected by the chemistry of the battery, where LiIon based batteries have a higher specific energy compared to LiPos. Given these key parameters, a short list of battery options could be considered and are represented in Table 3.9.

Table 3.9: Short list of 6S batteries considered for use with the HexaQuad. C-Ratings are presented as burst/continuous.

Name	Chemistry	C-Ratings	Capacity	Weight	Specific Energy(Ah/kg)
Glacier	LiPo	50C/30C	8000mAh	1049g	7.63
Dark Lithium	LiIon	25C/10C	8400mAh	849g	9.89
Tattu	LiPo	60C/30C	10000mAh	1357g	7.37
Tattu	Lipo	30C/15C	12000mAh	1532g	7.83
Tattu	LiPo	50C/25C	22000mAh	2544g	8.84

During the initial design and simulations of the motor and propeller combinations, a 10000mAh LiPo was used as a starting point to meet the endurance targets.

However, upon review of the different available technologies it was decided that the 10000mAh was the least efficient battery available with the lowest specific energy. Other than the LiIon battery, the 22000mAh LiPo displayed a reasonably high specific energy of 8.64 Ah/kg, outperforming all the other LiPo options.

Although the high capacity LiPo was a competitive option it was also extremely expensive and difficult to source. Beyond these reasons, it was deemed beneficial to utilise the 8400mAh LiIon and 8000mAh LiPo so as to compare the performance between the chemistry types.

The selected batteries for use in performance testing were:

1. Dark Lithium 8400mAh 6S 25C LiIon, and
2. Glacier 8000mAh 6S 30C LiPo

3.2 Flight and Power Electronics Design

The flight and power electronics assist with the control and power distribution of an sUAS. The flight electronics section will present the components associated with command and control of the sUAS. Thereafter, the power distribution design will be covered expanding on distribution design and monitoring.

3.2.1 Command and Control Design

The command and control of and sUAS is dependent on a flight controller operating an autopilot to interpret sensor readings and create a resulting action. Additionally under aviation laws, there is a requirement for control via a remote control connection. The combination of these three aspects allows a user to command and control an sUAS effectively in a number of different scenarios. This section will outline the design of the command and control units used in the HexaQuad and give reasoning for their selection. The section will cover the flight controller and autopilot before moving to remote control connections in the form of radio receivers and the associated ground station.

Flight Controller and Autopilot

For the selection of a flight controller and autopilot pair, a major requirement was for the entire system to be open source and accessible to allow users to integrate external systems into the HexaQuad and access any desired data. There are a number of available open source units such as the Pixhawk board series however the selected flight controller system was part of the Cubepilot ecosystem.

The selected flight controller was the Cubepilot Orange cube mounted on a standard carrier board. The carrier board has a number of I/O ports for connection of external peripheries such as sensors and GNSS units, PWM ports for control of motors or gimbals, and a number of communication ports supporting SPI, I2C and CAN for different devices. The Cube is equipped with numerous sensing systems which assist with different flight modes, especially automated flight. The Orange Cube is equipped with triple redundancy IMU sensing systems which assist with providing stabilized flight and, with the addition of an external GPS unit and correct calibration, the entire system can run automated flights.

The Cubepilot flight controller was paired with ArduPilot's autopilot firmware, an open source and community driven software. ArduPilot has a number of autopilots for different use cases ranging from submarines to fixed-wing planes, all of which are compatible with the Orange Cube. The specific instance of ArduPilot used was ArduCopter 4.3.1 firmware for multirotors or helicopters. ArduCopter is versatile and can be configured to work with a number of multirotor configurations, ranging from a simple quadcopter to coaxial Y-shaped hexacopters.

Radio Remote Control

According to aviation law there is a requirement for a user to have direct control of the sUAS at all times. The direct control link is usually fulfilled via a radio remote control link between a transmitter on the ground and a receiver on the sUAS. There are a number of different transmitters and receivers available with varying ranges of capabilities and costs. The choice of transmitter is based on user preference and requirements where certain transmitters are compatible with a range of supported receivers. When considering compatible transmitter and receiver pairs, the major consideration is if both support the same communication protocol.

The selected transmitter was a FrSky Taranis Q X7S Access enabled Radio device. The Taranis Q X7S utilises the open source operating system Open TX and is compatible with new generation receivers running the ACCESS protocol and is backwards compatible with old generation receivers running ACCST D16. Open TX allows users to create custom profiles for each drone configuration and stream telemetry data to directly to the transmitter for a user to view.

The paired receiver was the FrSky's Archer GR8 which operates at 2.4GHz and uses the ACCESS protocol with reduced latency. The receiver is capable of operating over a range greater than 2km and offers 8 high precision PWM channels for universal

servos as well as a configurable 16 channel serial BUS to control multiple servos with a single line. A benefit of the Archer GR8 was that it could be connected to multiple units in a slave and master configuration to introduce receiver redundancy. A 2.4GHz receiver was selected for its wide bandwidth and ability to deal with possible interference experienced at the public testing area, which was also used by private hobbyists.

Telemetry and Ground Control Station

Accompanying the radio remote control link was a telemetry link between the sUAS and a Ground Control Station (GCS). The telemetry link allows for a live stream of flight parameters such as fail-safe states and battery status to the open source GCS. In addition, to live streamed telemetry data a GCS can be used to send commands like waypoints and actions to the drone. Mission Planner [35] was the selected GCS used for configuration, initial calibration, mission planning and all test flights. Mission Planner is an Open Source GCS and is mainly used on Windows based machines however it can operate on android and Linux machines. Mission Planner version 1.3.77 was run on a Windows based Lenovo Thinkpad with an Intel i5 and 8Gb of RAM.

To facilitate the telemetry communications the GCS is connected to a radio transmitter with a paired unit mounted on the sUAS. The radio transmitters used were the RFD900+ radios operating between 902-928MHz with a range of over 40km and a data transfer rate of 256 kbit/s.

3.2.2 Power Distribution and Auxiliary Power

The power distribution and auxiliary power relate to ensuring each system within the sUAS is provided with the correct operating current and voltage. The design was broken down into subsystems based on the various power requirements. The subsystems were identified as 1) high power such as motors and ESCs, and 2) low power for devices that accept a voltage stepped down from the input 6S such as directional LEDs and the flight controller. Included in the power distribution design were monitoring devices to report the battery status to the ground station. This section will give a design overview of each subsystem reporting the key components and operating ranges.

The high power subsystem design was influenced by the maximum power requirements of the motor and propeller combination. The maximum operating conditions required by the motor and propellers pair was a burst current of 240A at a 6S voltage.

The Matek PDB-HEX power distribution board was used for its 264A burst current rating and ability to accept voltages in the range of 2-12S The PDB-HEX is displayed in Figure 3.2, the PDB can split the input power into six individual routes for the Hex configuration. In the case of the Quad, two sets of wires would be secured and left disconnected.

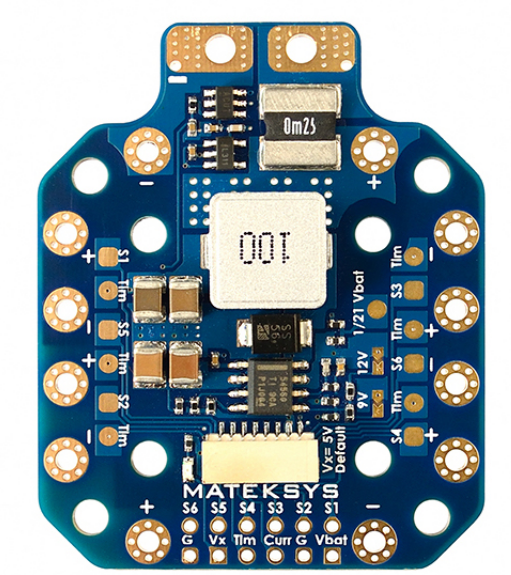

Figure 3.2: Matek PDB-HEX suitable to accommodate both a Hex and Quad configuration. Unused wires are left disconnected and secured during flight [51].

The PDB also had a current and voltage sensor built in as well as a configurable Battery Eliminator Circuit (BEC) which could be set to output either 5V, 9V or 12V at a maximum of 4A continuously. The on board PDB was set to 12V to power green and red directional LED strips. The current and voltage sensor was not utilised as alternative devices integrated into the autopilot were preferred.

Within the higher power subsystem, an external current and voltage sensor was installed on the main input line and reported the values directly to the flight controller. The unit used was a Mauch003 PL200A current sensor which can be setup and calibrated within Mission Planner. The current sensor would be used to detect and report current and voltage readings to trigger fail-safes or evaluate performance from logged data.

The low power subsystem included any device which required power at a voltage lower than the input 6S. There were three BECs included in the low power design, two BECs were installed with the intention to power external sensors or companion

computers and the third was a dedicated BEC for the flight controller. The BEC dedicated to the flight controller was a Mauch015 PL2-6S providing power redundancy and connections for communication with the Mauch PL200A current sensor. The two additional BECs were Matek UBEC DUOs, with efficient buck voltage regulators allowing for the configuration of one output to either 5V,6V,7.2V or 12V at 4A maximum continuous output. The secondary output was fixed at 5V with a 4A maximum continuous demand. The multipurpose BECs were installed with the intention of providing power to external sensors via USB Type-C ports and to power a Raspberry Pi Companion computer with a 5G telemetry communication module as part of a different project.

All other lower power devices such as the telemetry radio and radio control receiver were all powered via the flight controller and its periphery connections.

Chapter 4

Structural Design

The structural design section will discuss most of the components relating to the frame of the science drone. The section will be broken down to focus on major components and the design processes associated with them. Major considerations for all frame components were to minimise weight and maximise strength, additionally, there was the intention to make parts easy to replace and reproduce. The considerations were met by means of accessible manufacturing processes, careful material choice and selection of readily available standard parts. The design of each component was modelled in SOLIDWORKS computer aided design software [52] and utilised the associated iterative optimisation and finite element model tool suits. Each part underwent a number of iterations, some were modelled a number of times during the design and others were improved after practical testing.

4.1 Landing Gear Design

The landing gear is intended to stabilise the small Unmanned Aircraft System (sUAS) on the ground and provide vertical clearance from any obstacles immediately below the multi-rotor. Usually, the landing gear is of a simple design to land on flat surfaces but can be more complex for specialised use cases, such as perching on lamp posts or retracting landing gear from a camera's field of view. The landing gear of the HexaQuad had simple requirements which ultimately guided the selection of the design. The key requirements were 1) providing clearance to attach sensors below the drone, 2) add minimal weight with enough strength to withstand a hard landing, 3) suitable for both a hexacopter and quadcopter and 4) easy to replace if damaged during a crash. The following section will describe the benefits of the chosen design over alternatives, highlighting the material choice and the use of 3D printing to meet design requirements.

During the evaluation of different landing gear designs three main options stood

out as most likely to meet the requirements and are representing in Figure 4.1 as (a) a simple rod design, (b) a standard T-shape, and (c) an S-bend.

(a) Simple Rod Leg (b) Standard T-Shaped Leg (c) S-bend Leg

Figure 4.1: Illustration of the 3 considered landing gear designs.

The T-shaped landing gear is commonly found on commercial drones likely because it only requires two legs to provide stability, meaning less weight and there is a 180°undisturbed field of view for cameras mounted below the drone. However, early in the design phase the standard T-shape was no longer considered because it was deemed fragile. From practical experience, it was found that the top of the T commonly broke in crashes or during hard landings often meaning an expensive carbon fiber part had to be replaced.

This left two designs which were further considered where material choice and accessibility influenced the design decision. The simple rod design consisted of a standard carbon fiber tube which would be paired with 3D printed parts such as a foot for stability and a mount to connect the landing gear to the frame. The S-bend was intended to be made from an aluminium alloy flat bar with a bend at the bottom to act as a foot and a bend at the opposite end to secure it to the frame. These two designs prompted a material comparison between aluminium alloy and carbon fiber.

When comparing the two material choices there were ultimately 3 properties of interest, the stiffness, density and yield point of each material. Stiffness was of interest as it would influence how much the material would flex whilst under load. Ideally, the material would flex in the event of a crash to absorb impact energy and protect more fragile or expensive components. However, if the landing gear were too flexible it

would mean that a heavy payload mounted below the drone would bend the landing gear excessively and possibly be pushed into the floor. The yield strength and density were obvious considerations as strength was desired to be maximised and weight minimised. A summary of material properties for typical aluminium and carbon fiber are compared in Table 4.1.

Material:	Carbon Fiber	Aluminium
Young's Modulus	$234GPa$	$68GPa$
Tensile Strength	$4.14GPa$	$75MPa$
Compressive Strength	$1,738GPa$	$30MPa$
Density	$1.85g/cm^3$	$2.57g/cm^3$

Table 4.1: Typical material properties for carbon fiber and aluminium used within Solidworks for simulation element analysis.

From Table 4.1 carbon fiber distinctly stands out as lighter and stronger in both compression and tension making it favourable, however, it is extremely stiff and offers little flexibility which translates to the material being brittle. The favourable trait of aluminium is the ductile nature and flexibility it would introduce to the landing gear allowing for shock absorption during landings. The compromise of aluminium is apparent in the associated weight and accessibility to replace the parts if they are damaged. The aluminium S-bend landing gear requires specialised equipment to prepare the alloy and then bend it to the desired orientation. With the combination of increased manufacturing complexity, poorer strength compared to carbon fiber and the high probability that the landing gear would be damaged during testing, it was decided that the aluminium S-bend would not be suitable for the HexaQuad.

The selected simple rod landing gear design can be seen in Figure 4.1 (a). As indicated the simple rod design made use of 3D printed parts to incorporate the carbon fiber tube into the frame and make it suitably stable. Some advantages of the simple design were that it made use of standard and readily available carbon fiber tubes as well as 3D printed parts that could be complex but manufactured easily and on demand. The addition of 3D printed parts also meant that in the case of a crash, the 3D printed parts could be designed to break instead of the carbon fiber tubes, further preserving the resources of the HexaQuad. A downfall to the simple rod design was the requirement to have a minimum of three legs in order to stabilise the drone which results in an increase in the weight of the landing gear. As mentioned above, since the 3D printed components are intended to break in the event of a crash, they will clearly be the failure point of the landing gear. Thus, in order to ensure the 3D printed connections points can sustain the weight of the drone and any potential

sensors, a material analysis was performed and will be presented in a later chapter.

With the landing gear style confirmed, there were some additional design decisions such as the placement of the landing gear. In the initial idea, the simple rod design had the potential to be placed anywhere along the rotorboom between the motor and the central hub of the frame. A simple bending moment investigation motivated for the landing gear to be mounted at the same location as the rotorboom. Using the same mounting point meant the landing gear would not apply a moment about the rotorboom mount point, and therefore reduce the chance of snapping the rotorboom, this was especially preferential in the event of a crash. Figure 4.2 is an illustrative free body diagram used in the bending moment analysis and showcases the original idea where the landing gear could be re-positioned along the rotorboom.

The finalised landing gear made use of a carbon fiber twill weave cylinder, with an outer diameter of 25mm and a wall thickness of 1mm. The length of the cylinder was 350mm and connected to the frame at an angle of 30°off the vertical giving an effective ground clearance of 313mm. The length of 313mm allowed for 75mm beneath the central hub to mount batteries and 198.5mm of clearance to suspend payload between the bottom gimbal rails and the floor. Notably, the landing gear and rotorbooms made use of carbon fiber tubes with the same diameter, reducing the number of distinct components used in the HexaQuad design.

4.2 Rotorbooms Design

The rotorbooms or arms of the drone are a means of connecting the motors to the frame and thus providing thrust to the drone and its associated payload. During flight, the entire weight of the frame and payload is exerted across the rotorbooms and is increased when there is acceleration that is opposite to the weight direction. The rotorbooms thus require careful consideration in their design to ensure they can support the expected weight of the frame and payload requirements. Beyond meeting strength requirements there is further consideration of the influence between adjacent propellers and their effect on efficiency. This section will outline the design considerations of the rotorbooms guided by strength simulations and work done by Lei [27, 28] on rotor spacing's influence on system efficiency.

4.2.1 Material selection

As with the landing gear design, there were material considerations for the rotorbooms to ensure the design would meet the flight requirements. Key parameters, as

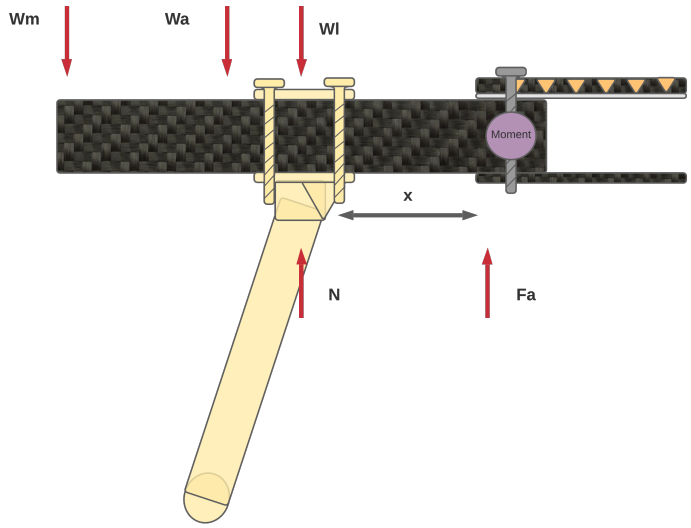

Figure 4.2: Illustrative bending moment diagram used to evaluate landing gear mount location. *Wm* is motor weight, *Wa* is arm or rotorboom weight, *Wl* is the landing gear weight, *N* is the normal force, *Fa* is a reaction force at the cantilever and x is the distance from the cantilever.

was for the landing gear, were the density, strength and stiffness. In the case of the rotorbooms, it is desirable for the material to be extremely stiff to ensure the thrust is transferred efficiently from the motors to the rest of the frame. If the rotorbooms are flexible and too ductile, then the rotorbooms would first bend before transferring thrust to the rest of the frame, thus requiring additional energy. As alluded to, the rotorbooms are required to support the entire weight of the drone and thus must be able to deal with the induced stress from supporting the frame and payload. With regards to density, if the rotorbooms have a high density they will increase the overall weight of the frame and thus reduce the payload capacity. Therefore from these considerations and those performed within the landing gear section, carbon fiber tubing became a favourable choice for the design.

4.2.2 Adjacent Propeller Spacing

Within the rotorboom design extra consideration was given to the length of the rotorbooms due to work presented by Lei [27, 28]. Lei found that the efficiency of a multirotor can be increased when adjacent motors interacted less with each other. The rotor interference was reduced when the distance between adjacent rotors was more than the minimum required. Rotors should theoretically have a minimum of

one propeller diameter spacing between the centers of two adjacent rotors. Practically this distance would be slightly more than a single propeller diameter to increase the safety of the system and guarantee adjacent propellers do not collide if rotorbooms shift during flight.

Lei proposed a spacing between motors based on a ratio of the propeller diameter, where 1.0 would be the minimum required distance between adjacent rotors. With regards to the HexaQuad, the spacing between the rotor centers would be equal to the distance from the center of the frame to the center of the rotor due to the nature of the geometry, this is illustrated in Figure 4.3

$$\frac{Spacing}{Diameter} = Spacing\ Ratio$$
$$Spacing = Rotorboom\ Length + Mount\ Distance$$

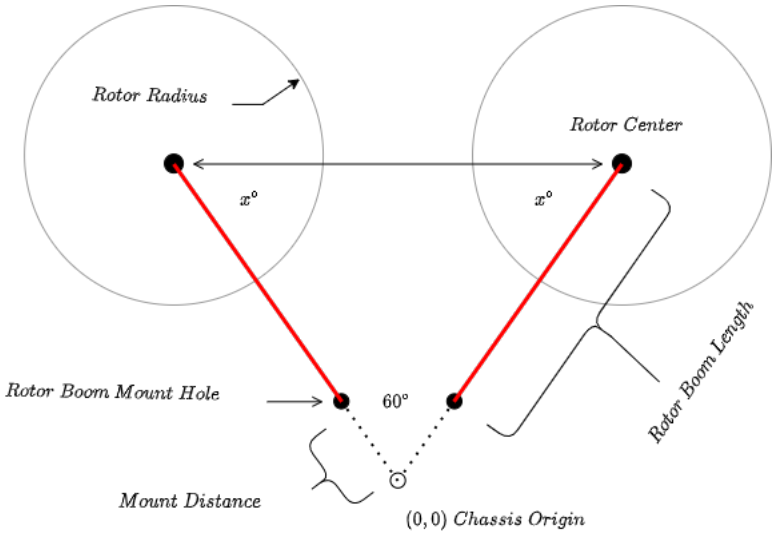

Figure 4.3: Relation of rotorboom length to the spacing between adjacent rotors for a symmetrical Hexacopter, $x = 60°$ for an equilateral triangle.

It was decided the spacing between rotors for the HexaQuad should be larger than the minimum to benefit from any efficiency that could be gained. The work by Lei thus guided investigations into rotorboom length and influenced the range of lengths tested during simulation. The range used spanned spacing ratios of 1.05 - 1.6, which translated to lengths of 420-675mm when using an 18 inch (458mm) propeller.

4.2.3 Iterative Design Modeling

With a material choice and spacing information identified, there was then a strength comparison performed between two profiles of carbon fiber tubing, one with a round cross-section and the other with a square cross-section. A square cross-section was proposed for its increased stiffness and its accessibility for users to create simple square-based sensor mounting solutions.

With the proposed cross-sections and materials, simulation software was then used to aid the design choice. The two cross-section profiles were modelled in Solidworks with the same material properties to investigate the associated benefits. Solidworks provides investigation tools to optimise over a number of given parameters and thus compare different designs.

The process begins with an initial dimensioned part, the user can then define parameters such as length and diameter to be varied to create iterations of a design. With a fully defined model, constraints can be applied to simulate a desired operation of the component. For example, constraints would be applied to the rotorboom to allow it to move in a certain way, such as fixing it at one end like a cantilever. The rotoboom for these simulations was constrained to act like a cantilever at one end simulating being fixed to the central hub. While at the opposite end, a force was applied in the vertical direction perpendicular to the rotorboom to mimic the thrust from a motor, an illustration can be seen in Figure 4.4.

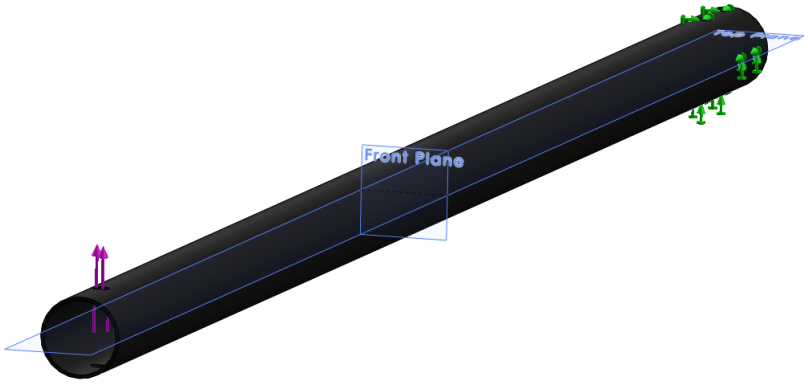

Figure 4.4: Cylindrical carbon fiber tube represented in Solidworks simulation tool as a cantilevered beam where the fixed end is shown with green markers and an applied force is acting at the opposite end shown as purple arrows.

Thus the objectives of the simulations were to investigate 1) the weight to strength

benefit of the two profiles, 2) an optimal accessible tube diameter, and 3) a practical length with a spacing ratio greater than 1.0. The two profiles were simulated over a range of diameters and lengths to investigate the objectives, the length varied between 420 - 675mm and the outer diameter was tested between 15 - 30mm with a wall thickness of 1mm.

4.2.4 Rotorboom Simulation Results

Three parameters were investigated in the simulation, the displacement, weight and stress under applied load. All three parameters were graphed against rotorboom length for a number of diameters.

In a comparison of the different tube diameters and the two cross-sections, it was decided to compare tubes with similar weights instead of similar diameters. From review of the mass curve in Figure 4.5 it becomes clear that the larger round tubes have a similar weight to the smaller square tubes. For example, the 25mm round tube is almost identical in weight to the 20mm square tube for all lengths.

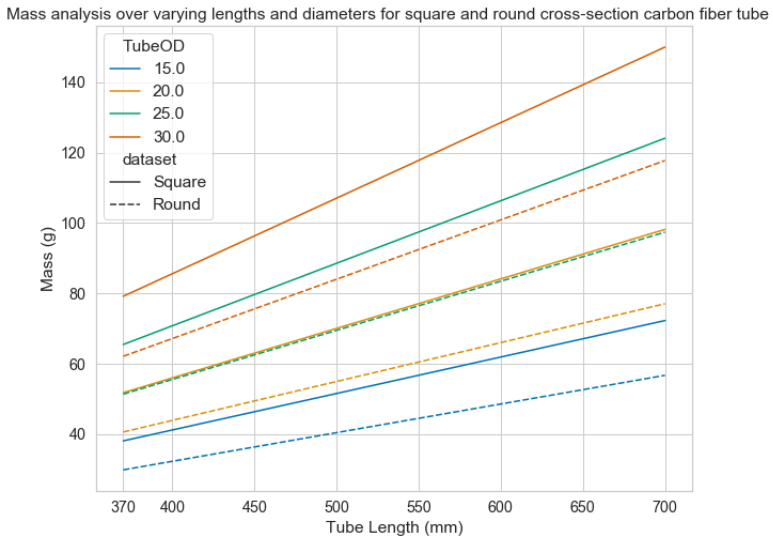

Figure 4.5: Solidworks simulation results displaying similar weight performance between larger round profiles and smaller square profiles. The dataset relates to two tested profiles.

This characteristic resulted in the similarly weighted round tubes outperforming the square tubes by having lower induced stress values, shown in Figure 4.6.

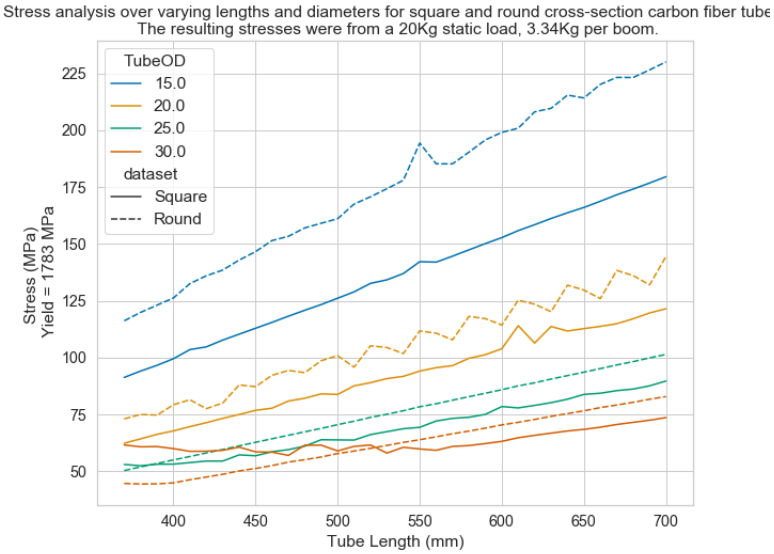

Figure 4.6: Soldiworks simulations displaying the estimated induced stress in the various rotorboom configurations. In the cases where there are seemingly arbitrary spikes, the general slope of the line was considered.

Similarly so for the displacement evaluation in Figure 4.7, it can be seen that the round profiles either have the same or lower displacement when comparing similarly weighted tubes.

For this reason, it was decided that the round profile should be chosen over the square one. Beyond the improved weight to strength and displacement performance of the round profile tubes, they were also more accessible and readily available compared to the square profiles. This was beneficial in the potential circumstance that the drone crashes during testing and requires a number of replacement rotorbooms. With regards to the diameter, it was decided to select the 25mm for its similar strength performance to the 30mm, while having a reduced weight. In comparison to the 20mm round tube, the 25mm was preferred for the flexibility to install the selected Electronic Speed Controller (ESC) inside the rotorboom and for its superior minimised displacement.

With the diameter and profile selected the design phase then moved to select a length that would reduce interference between adjacent rotors and improve efficiency. Due to the nature of Lei's [27, 28] works, there was no suggested model to estimate the performance of a multirotor given a propeller diameter and frame size. Therefore,

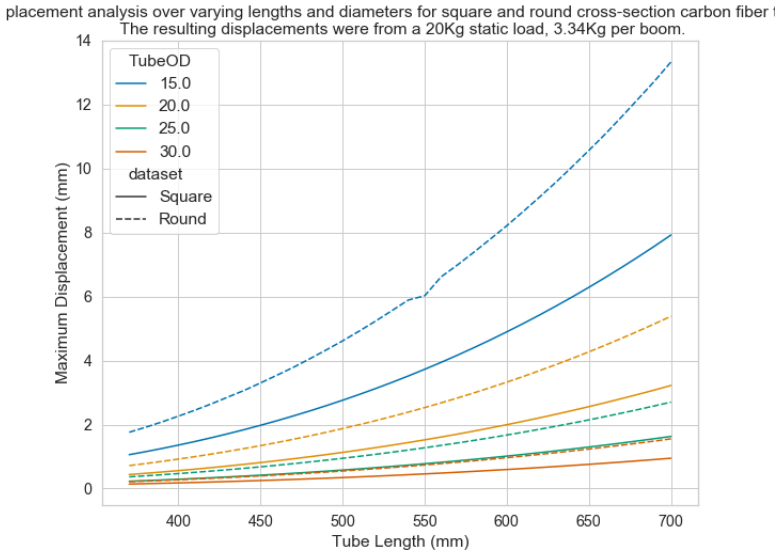

Figure 4.7: Solidworks simulation of the estimated displacement of the end of the rotorboom where the load was applied.

performance improvement had to be inferred from Lei's results and applied to the HexaQuad.

Performance was inferred by assuming each spacing ratio within Lei's studies would relate to an estimated efficiency gain. For example, a spacing ratio of 1.2 would equate to 10% efficiency improvement. A limitation of this assumption was that only the spacing ratios mentioned in the studies could be used to estimate performance. Along with this assumption, two additional investigations were performed, 1) a weight cost was calculated for each spacing ratio to investigate the contribution to the All Up Weight (AUW) of the drone, and 2) the practicality of transporting a drone with extremely long rotorbooms.

From the investigations and assumed performance improvement it was decided the rotoroboom should relate to the spacing ratio of 1.2. The ratio of 1.2 was beneficial as it could improve efficiency by 10% and translated to a practical length that was reasonable to transport. The spacing between adjacent rotors equated to 560mm, this translated to a 500mm long rotorboom with 60mm of additional space between the end of the rotorboom and the center of the frame for mounting.

4.3 Central Hub Design

The Central Hub refers to the central structural part of the frame that connects all other parts together. Furthermore, it houses most of the flight electronics such as the flight controller, power distribution and payloads of varying sizes. During design there were a number of iterations from configuration ideas to simulated designs, all guided by functional requirements. Designs were inspired by pre-existing products that were then tailored to the specific use case of the HexaQuad. A number of designs were tested with Solidworks simulation tools to investigate their suitability under operating conditions and to optimise the final configuration. This section will present the design of the Central Hub focusing on the final form.

4.3.1 Central Hub Iterations

The central hub underwent a number of iterations, some of which drew inspiration from existing models and others from basic ideas of drones. All of the design iterations attempted to meet a set of operational and practical requirements, most of which related to supporting different payloads and keeping the design simple. Two major requirements of the central hub were to be modular and support both a hexacopter and quadcopter configuration, and to utilise manufacturing techniques that are reasonably accessible. There were other requirements to meet strength demands but the practical applications were the main influence in the design of the central hub. Through iteration and inspiration from other modular drones, the design progressed to the final design which will be discussed later in the section. Figure 4.8, represents a chronological representation of the design iterations until the final design was achieved.

Figure 4.8 (a), was an initial design that required sheet metal bending but was abandoned due to weight concerns. Figures 4.8 (b) and (c), highlight a key design point known as the Modular Chassis Unit, where each part that would make up the frame could be removed individually and reconfigured. The difference between Figures (b) and (c) was a change of material consideration and the general shape of the central plate. Carbon Fiber became the focus material for its strength, stiffness and low weight. The central plate was based on octagons and dodecagons until Figure (c) was reached, thereafter, an oblong polygon and a dodecagon were compared to see which shape had optimal surface area for a given weight. It was concluded that both shapes performed similarly however the oblong shape was preferred as it was more suitable to mount sensors which were housed in cases with rectangular-based footprints. Through simulations and design optimisation studies the final multi-plate design was reached in Figure 4.8 (d), the Central Hub.

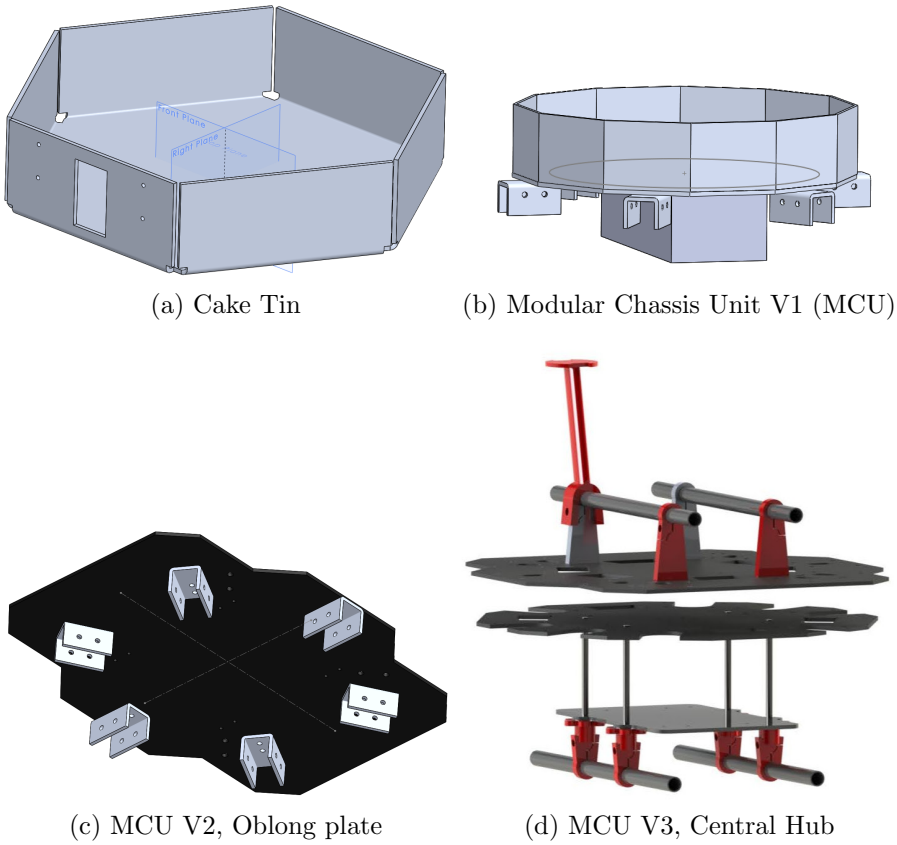

(a) Cake Tin

(b) Modular Chassis Unit V1 (MCU)

(c) MCU V2, Oblong plate

(d) MCU V3, Central Hub

Figure 4.8: A chronological evolution of the central hub design at major iterations which defined the path to the final three plate design.

4.3.2 Development of the Central Hub

The iteration process assisted with arriving at a final starting point for the central hub design. The Oblong plate shown Figure 4.8 (c) was the first design to undergo a number of simulations to investigate the suitability of the design and material choice of Carbon Fiber. This section will present a summary of the development of the central hub and the key simulations that influenced the design.

From version two of the MCU shown in Figure 4.8 (c), a major concern was allocating room to suspend a battery in the center of the plate. The placement of the battery thus had a large influence on the size of the central main plate and of course the mounting location of the rotorbooms. However, it was soon discovered that creating a separate mounting location for the battery would allow more flexibility with regard to the central hub size and designing plates that can be reconfigured to

suit either a hexacopter or quadcopter configuration. This directed the design to a three-plate-based central hub, 1) the top plate to connect the flight controller and lightweight sensors, 2) the bottom plate to install power distribution equipment, and 3) the battery plate to support and secure the battery.

The top and bottom plates were secured together by means of M4 bolts and 3D printed rotorboom mounts. The rotorboom mounts provided clearance between the plates to house the PDB and relevant wiring for the powertrain system. The battery plate was housed below the bottom plate and was connected to the rest of the central hub by means of four threaded rods secured to the bottom plates. The threaded rods allowed for the battery plate to be moved up and down to secure the battery in place with frictional forces during flight.

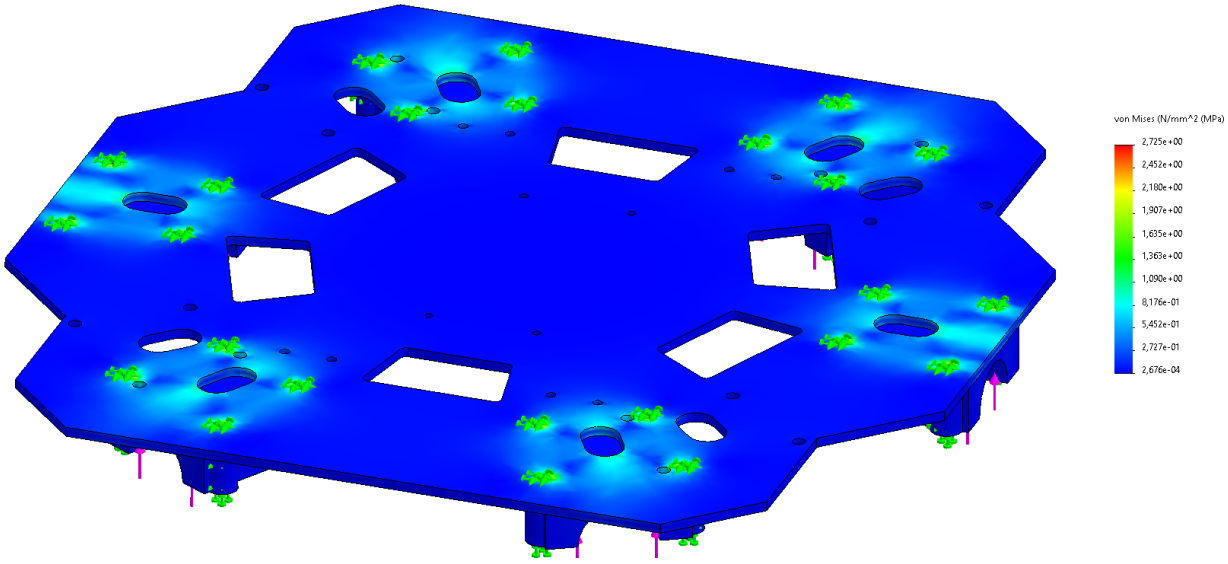

Figure 4.9: Solidworks finite element model of the stress induced in the top plate of the central hub. This simulation was to investigate the effect of the cutouts on the strength of the plate.

The three plate central hub was subject to stress and displacement simulations in Solidworks to determine optimal locations for rotorboom mounts and battery plate mounting rods, as well as to determine a suitable thickness for the carbon fiber plates. Within the simulations, an applied load is defined and used to estimate the mechanical performance. Within the design simulations a hover load of 300N was applied to the top and bottom plates, which equates to twice the expected hover load while carrying a 5kg payload, this was imposed as a safety factor. A stress simulation for the top

plate during a hover can be seen in Figure 4.9, the plate had a thickness of 3mm and was estimated to weigh 388g with dimensions of 300mm by 190mm.

The maximum stress experienced during a hover was 2.73MPa and this was mainly focused on the rotorboom mount holes as can be seen in Figure 4.10, the maximum stress areas are displayed as a shade of red. The hover stress of 2.73MPa was significantly below the simulated carbon fiber yield point of 1738MPa. Similarly for the bottom plate under hover load, the high stress areas were located around the battery mount holes and the rotorboom mount holes, similar to those seen in the top plate Figure 4.10. However, the induced stress was still significantly below the yield point of the material causing no concern in the operation.

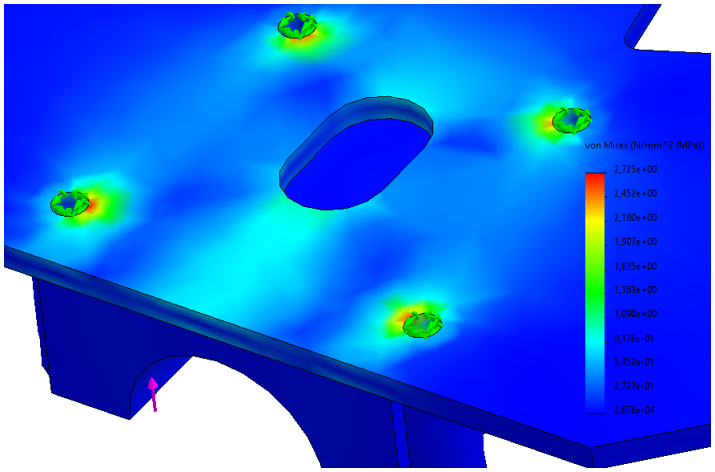

Figure 4.10: Zoomed in view of the rotorboom mounting holes of the top plate where the maximum stresses were located. The maximum stresses are shown in shades of red and reached 2.73MPa, where the yield strength of the simulated carbon fiber was 1738MPa.

The displacement of the edges of the central plates was extremely low for both the top and bottom plates, where the bottom plate is represented in Figure 4.11. For the same applied hover load, the displacements were 0.218mm and 0.273mm for the top and bottom plates respectively. These values were from individual simulations and are expected to be lower due to the nature in which the two plates are connected to each other.

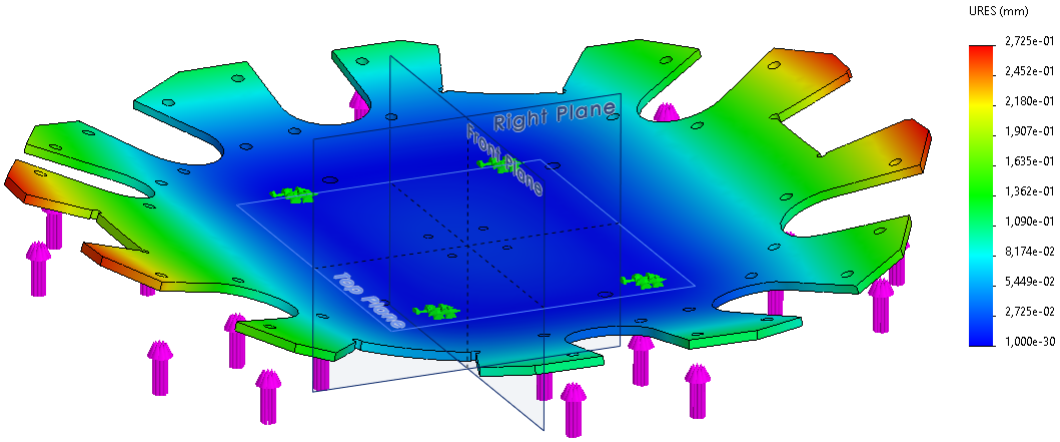

Figure 4.11: Displacement simulation of the bottom dodecagon plate under hover loading where the maximum displacement is 0.273mm shaded in red. Note the displacement is scaled up for visual representation.

The bottom plate was based on a dodecagon shape with twelve sides as opposed to the oblong shape of the top plate. This was the case to introduce more symmetry to allow for easy reconfiguration of the plates to suit either a hexacopter or a quadcopter. With the increased symmetry it meant only the bottom plate had to rotate to accommodate the reconfiguration while the top plate would maintain its orientation and use alternative mounting holes. An illustration of the bottom plate symmetry can be seen in Figure 4.12 where the red markers represent the forward direction and mount holes for the hexacopter configuration and the blue for the quadcopter.

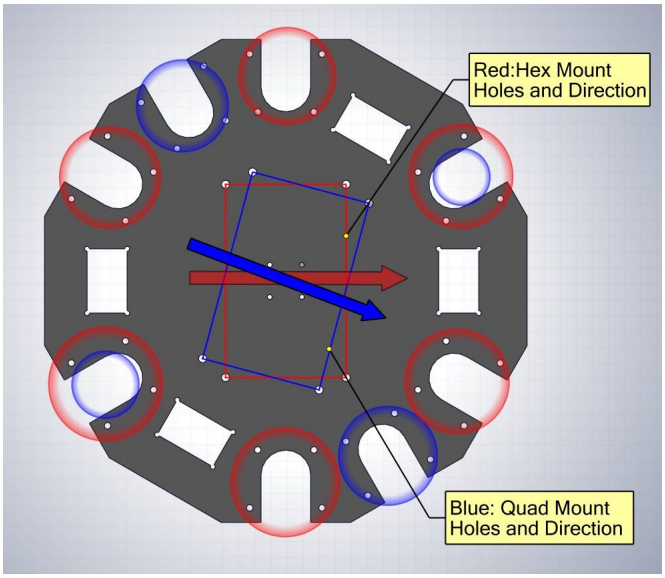

Figure 4.12: Illustration of the bottom plate symmetry where the plate can be rotated to reconfigure the HexaQuad between a hexacopter and quadcopter. The red markers indicate the hexacopter's mount locations for the rotorbooms, landing gear and battery plate mount holes. The arrows indicate the direction of flight.

Solidworks optimisation tools were used on the bottom plate to evaluate the optimal location to place weight saving and accessibility cutouts. The optimisation was constrained to minimize stress and ensure the cutouts were outside the battery area to prevent covering up the openings with the battery. A similar process was followed on the battery plate to determine the optimal mounting hole and thus threaded bar size to secure the batteries to the central hub. These design optimisations are run in an iterative way exploring the numerous combinations and selecting the most suitable combination within the constraints.

Throughout the design process of the central hub, all the plates and mount locations had to be considered with regard to a manufacturing technique and its limitations. Two processes were explored, the first being traditional computerised numerical controlled (CNC) routing, and the second was laser cutting with specialised C02 based lasers. The laser cutting was beneficial as it had no limitations on the design of internal cuts, whereas, with a more traditional CNC router, internal cuts will always have a radius at a corner due to the use of a rotating bit to create the cuts. However, the CNC routing was preferential to cut 3mm thick carbon fiber and was considered more accessible to most individual users through university campuses or small commercial companies. The laser alternative required a powerful system

to cut 3mm carbon fiber effectively to ensure no damage was done to the material. Although CNC routing is a relatively complicated process which requires expertise it was deemed that the process was unlikely to be performed more than once in the construction of the HexaQuad and had the sufficient necessity to create the central plates with good performance.

4.4 3D Printed Frame Components and Design

3D printing has revolutionised the manufacturing industry allowing for rapid iteration and the creation of complex parts. The versatility of 3D printing caters to the creation of complicated functional parts to mount simple devices or can be used to design load bearing parts. Early in the design phase of the HexaQuad, it was concluded that 3D printing a variety of frame components would assist with the accessibility and reproducibility of the drone due to the increased availability of consumer printers. A benefit of the 3D printed components is the reduced downtime when parts are damaged as complex parts can be reproduced within hours as opposed to the extended wait times for replacements from skilled workshops. Furthermore, 3D printed parts promote the development and use of the HexaQuad through the open source community, encouraging users to modify parts to suit their use case. This section will detail the use of 3D printed parts in the HexaQuad and present test data which assisted with the material selection before discussing the design of key printed components.

4.4.1 Material Filament Selection

There are a number of materials available that can be used on 3D printers each with different mechanical characteristics and varying levels of difficulty to use. Since components in the HexaQuad were going to be designed as load bearing, there was a necessity to select a suitably strong and easy-to-use material. There are a number of materials which are known for their strength such as polycarbonate blends, some of which are combined with carbon fiber to create new blends. However, these materials are expensive and either require specialist setups to utilise or are difficult to print effectively. The two thermoplastics which were readily available and relatively easy to use were Polylactic Acid (PLA) and Polyethylene Terephthalate Glycol (PETG). PLA was selected for its reasonable strength and stiffness whereas PETG was selected for its elasticity and relatively high strength, typical characteristics of both materials are in Table 4.2. Although there are a number of alternative filaments such as Acrylonitrile Butadiene Styrene (ABS), PLA and PETG were selected for their superior strength performance and associated ease of use in the printing process.

Given the two materials, it was decided to conduct tensile tests to investigate their

Table 4.2: Typical material properties for the two thermoplastics tested in the tensile tests [53]

Material	PLA	PETG
Density	$1.24 g/cm^3$	$1.27 g/cm^3$
Tensile Strength	57.4 ± 0.4 MPa	46 ± 1 MPa
Young's Modulus	2.2 ± 0.1 GPa	1.5 ± 0.1 GPa
Cost/kg	$30.24	$36.24

stress and strain performance to infer the performance of the printed components, especially to infer the performance of the motor mounts and landing gear connection points. Furthermore, there was a concern that the melting temperature of PLA was close to the estimated operating temperature of the motors calculated in the eCalc simulations. The transition temperature of PLA is 58°C and the estimated operating temperatures of the motors were 46°C at hover and 76°C at maximum throttle. Therefore, the two materials were compared in case PLA would not work in the operating window of the motors.

4.4.2 Tensil Testing and Results

Tensile Test Description

A number tensile tests were conducted in accordance with a global standard for reinforced and unreinforced plastics. The standard used was ASTM International's D638 which describes the process to follow and defines the properties of the specimen to use in the tests. The specimen used was a typically shaped bone specimen with dimensions that can be seen in Figure 4.13.

A total of 16 specimens were used in the tensile test, half were PLA and the remaining were PETG. There were two distinct printing orientations used to test the materials as the orientation is extremely influential in the performance. Thus half of the specimens for each material were printed in a horizontal orientation where the largest surface area was in contact with the print bed. The remaining specimens were printed in a vertical position which can be described as the horizontal orientation rotated 90°about the long axis. All specimens were printed on an Original Prusa Mini with a maximum infill of 100%, individual print settings can be seen in Table 4.3.

The specimens were tested in a tensile rig, specifically the Zwick 1454 universal tester to investigate the stress and strain performance of the specimens. The movement speed was set according to the D638 standard of 50mm/s and a maximum

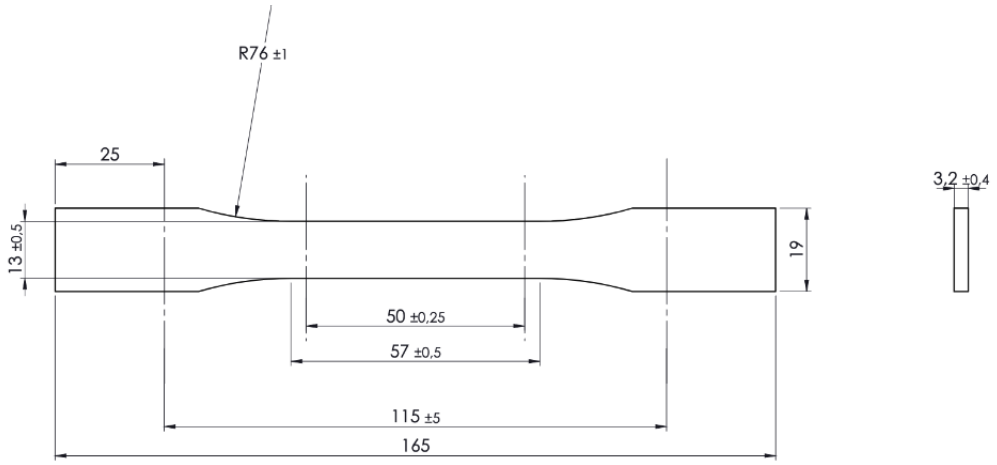

Figure 4.13: D638 standard bone specimen used for tensile testing of reinforced and unreinforced plastics [43].

Table 4.3: Slicer setting information defining the print conditions for PLA and PETG tensile specimens.

Material	Prusament PLA	RSPro PETG
Layer Height	0.2mm	0.2mm
Bed Temp.	60°C	70°C
Nossile Temp.	215°C	220°C
Print Speed	200mm/s	80mm/s

strain of 7% was set as the limit to avoid specimens extending out of view of the extensometer.

Material Performance Results

The stress and strain curves for both materials and orientations can be seen in Figure 4.14 where PLA is the stronger of the two materials when comparing like orientations.

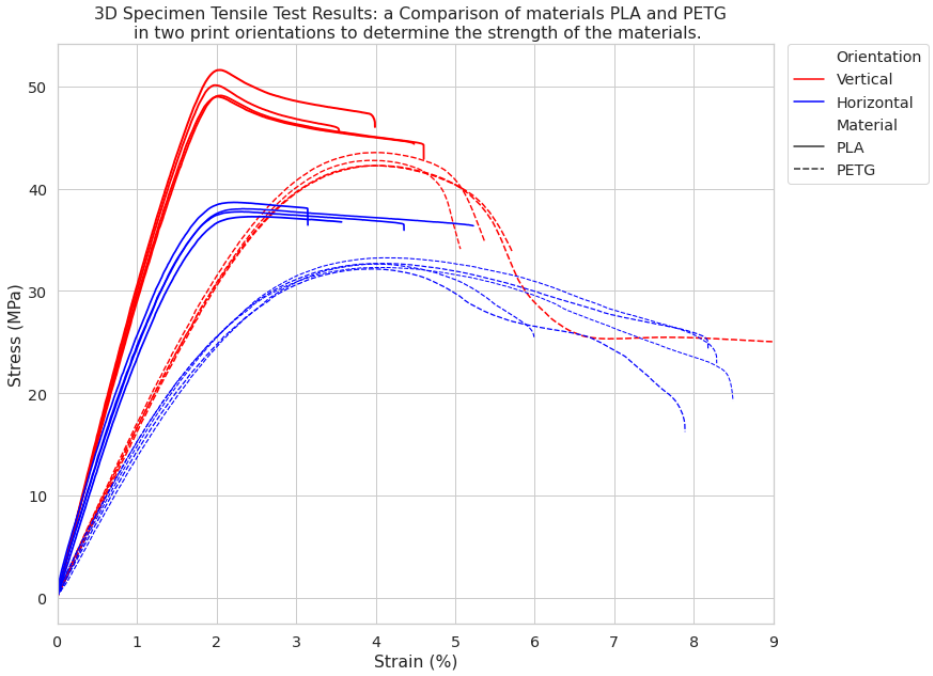

Figure 4.14: Comparison of stress and strain for PLA and PETG under tensile testing to determine mechanical material properties.

PETG in the vertical orientation is more elastic and ductile in nature with the capability to reach high strain values of 36% without failure. However, the vertical PETG tests were stopped early as seen in Figure 4.14 between strain values 5 - 6% to avoid the specimen exiting the extensometer's view and corrupting results. The horizontal PETG specimens failed at a much lower strain value, averaging 7.8% and thus displayed a more brittle nature. The brittle nature of PLA is confirmed with the low average strain values of 4% as they fail abruptly with a sharp drop off. The average maximum stress values can be seen in Figures 4.15 for the two materials and orientations.

PLA clearly outperformed PETG with regard to strength but PETG was identified for its potential usefulness to detect fatigue in parts through extensive elongation before failure. Due to temperature concerns, PETG was initially used for the motor mounts but later reverted to PLA upon practical evaluation of the motor operating temperature. Furthermore, the potential strain capabilities of PETG were limited to parts operating in the tensile direction which only occurred in a limited number of functional parts such as the gimbal rail mounts.

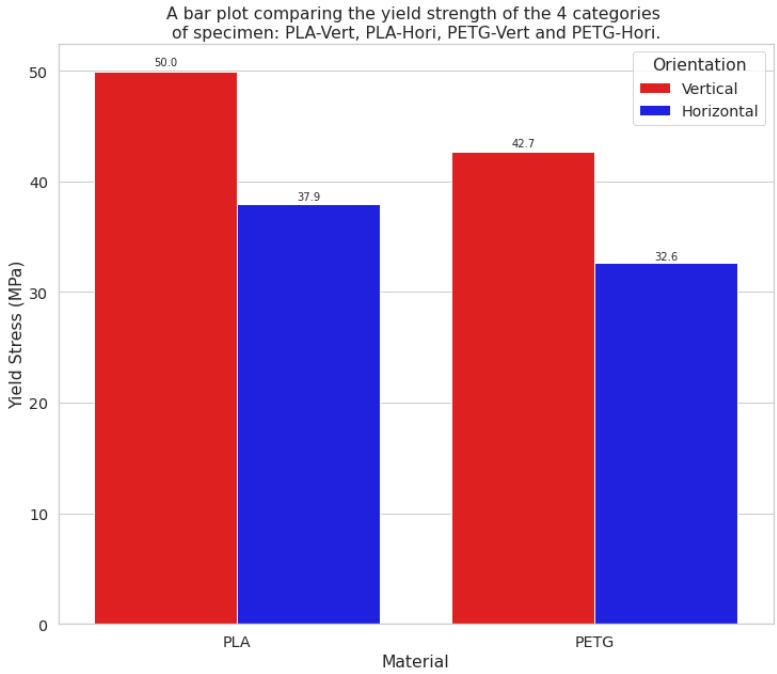

Figure 4.15: Average stress values for both PLA and PETG in both orientations.

4.4.3 Load Bearing Printed Components

The tensile testing was used to forecast the performance of the load bearing components of the frame, two such components were the rotorboom and motor mounts shown in Figures 4.16 (a) and (b). The rotorboom mounts were secured between the top and bottom plate of the central hub and further allowed the rotorbooms to be clamped into place. The motor mounts were located at the ends of the rotorbooms and functioned as a fixture point for the motors.

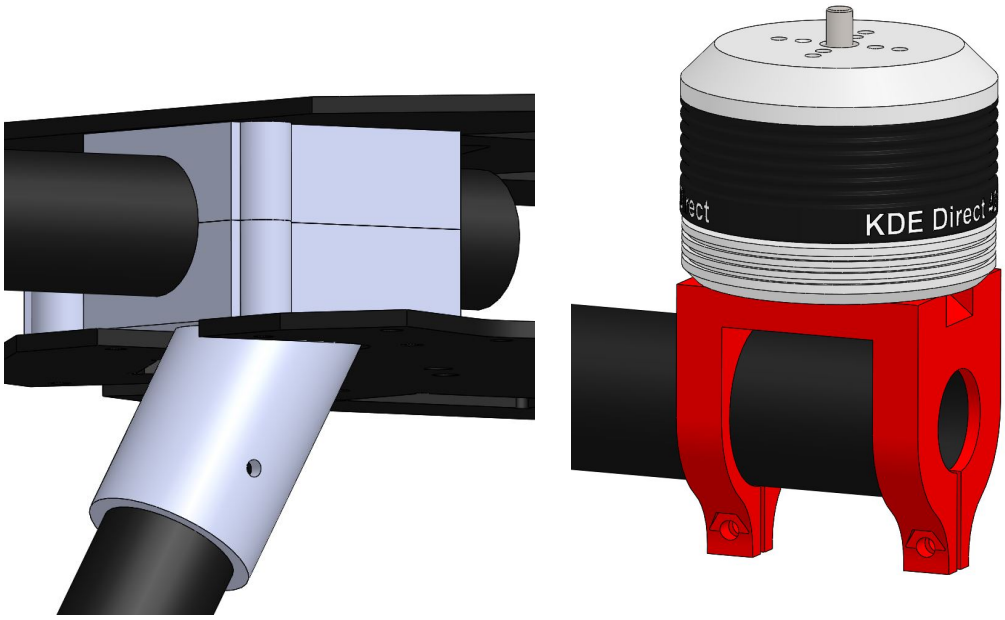

(a) Rotorboom mount with landing gear (b) Motor mount

Figure 4.16: Solidworks CAD representation of the rotorboom mount with landing gear connection and a motor mount.

Both components operating conditions were simulated in Solidworks with the material mechanical properties recorded during the tensile tests. The simulations assisted with iterative designs to ensure both components would only fail in desired circumstances and not under regular operation.

The rotorboom mount with a landing gear connection was specifically designed with the intention to break in the case of a hard landing or crash. It was intended to support the load of the HexaQuad with any additional payload, however, in the case of a crash the lower end of the mount connecting to the landing gear would shear off preventing the transfer of large stresses into the central hub. A comparison of a sheared landing gear section and an undamaged one can be seen in Figure 4.17.

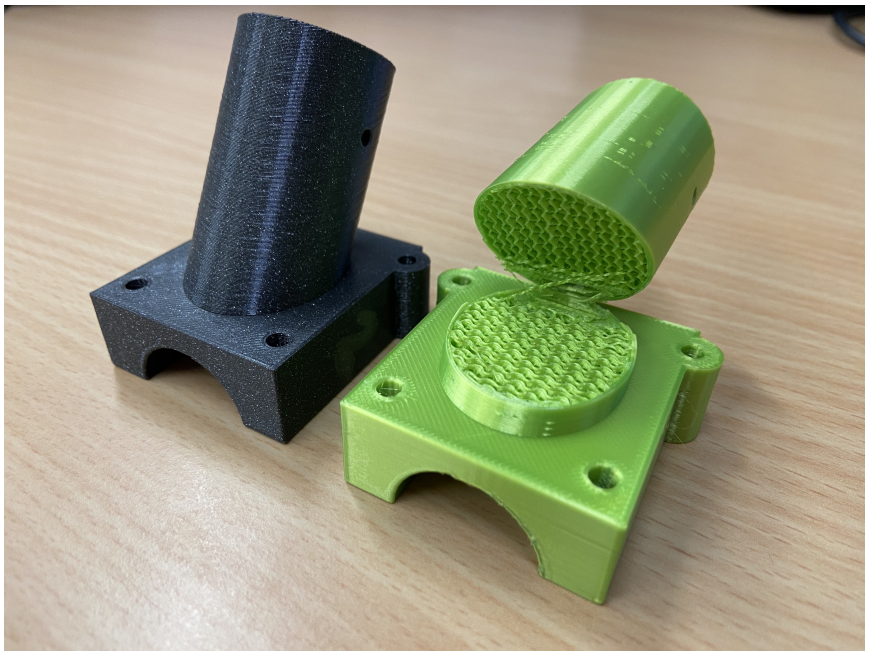

Figure 4.17: Landing gear section of a rotorboom mounted sheared during a hard landing compared to a new mount.

The design of this component behaviour was performed mostly during the print process of the rotorboom mount by adjusting the infill percentages at different layers. The print layers surrounding the rotorboom tube had an infill percentage of 100% and the landing gear section designed to shear had an infill percentage of 50%. The infill percentages were adjusted in an iterative manner through experience to achieve a combination that operated suitably.

The motor mount design also followed an iterative design process but more in a practical sense from experiments during the initial build of the drone and during flight testing. The first iteration of motor mount had weak points that secured the mount to the rotorboom and when placed under tension for extended periods of time the part would fatigue and break. Figure 4.18 highlights the weak area of version 1 in the red circle where the two surfaces meet at a corner, this is the focal point of stress, and the green circle presents where the connection point broke.

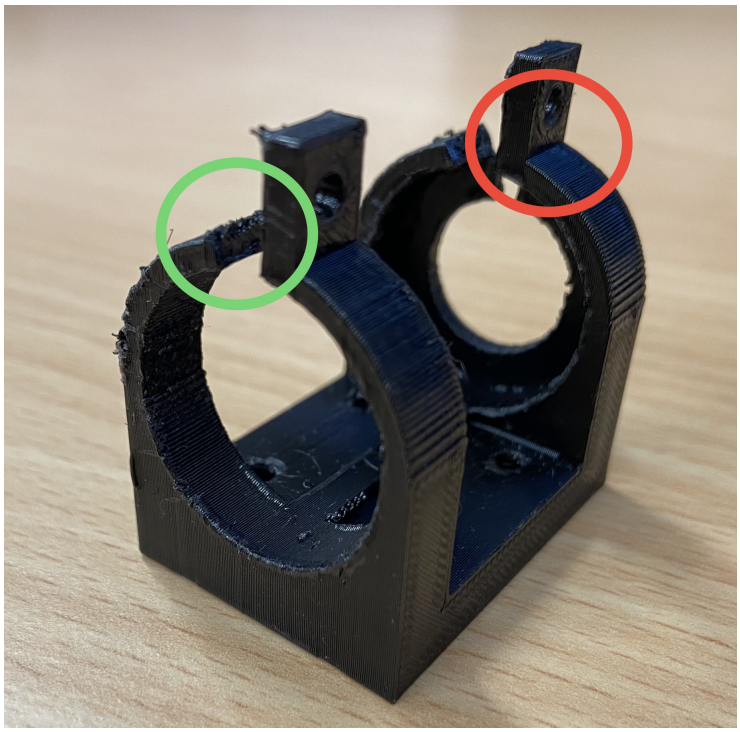

Figure 4.18: Failure point of the version 1 motor mount due to high stress, highlighting the focal point of the stress in red and result in green.

The weak point was fixed with the addition of a gentler slope from the rounded surface to the securing area of the mount, the variation can be seen in Figures 4.19 (a) and (b). The print orientation was also changed between iterations 1 and 2 to improve the strength of the part used to secure the mount in place. The motor mount had an additional 3 iterations to achieve the final design used on the HexaQuad. In most cases, there were small variations between the versions such as including spacing for the motor wires to run or a clearance cut to avoid the rotor shaft of the motor rubbing on the mount, seen in Figure 4.19 (c). Additionally, as with the rotorboom mount, the print infill percentages varied between the iterations and settled on 80%.

A major variation was introduced in the final iteration to improve the strength of the overall part and longevity of the component by creating a larger contact area with the rotorboom, a comparative view can be seen in Figure 4.19 (d)

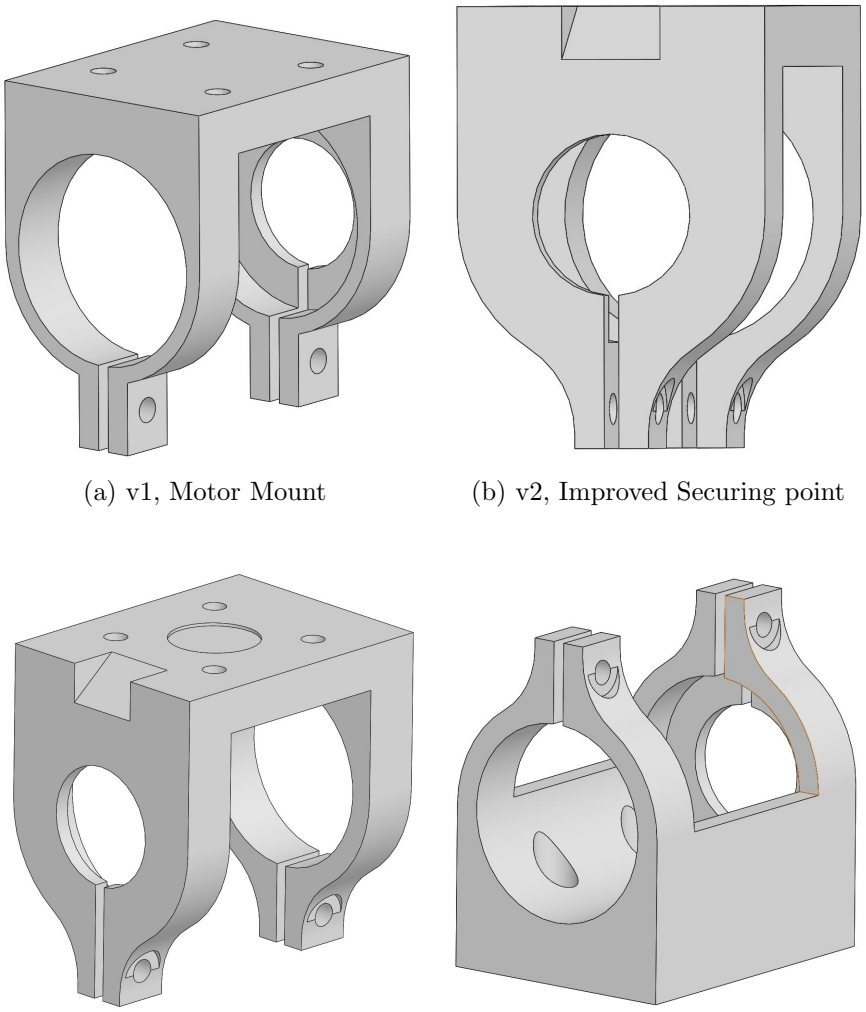

(a) v1, Motor Mount

(b) v2, Improved Securing point

(c) v3, Shaft Space

(d) v4, Increased Surface area on Rotorboom

Figure 4.19: Motor mount evolution defining the iterations in chronological order.

4.4.4 Identification of All Printed Components

Attributed to the fast iteration and ease of manufacturing of 3D printing, a number of components on the HexaQuad were designed with the intention to be printed. In total there were 47 parts that made up the frame, where 32 of those were 3D printed. A number of custom and complex parts were created with a single intention such as mounting a GPS or housing a telemetry radio, parts that would otherwise have been difficult to mount consistently. In components that required improved mechanical

capabilities inserts were used to improve the strength and longevity of the part. An example insert used in the HexaQuad was embedding steel nuts in prints to create reusable threads. This section simply serves as an overview and identification of all the 3D printed components on the HexaQuad.

All the 3D printed components are presented in Figure 4.20 with descriptions in Table 4.4, the references between the table and figure correspond.

Table 4.4: Description of all the 3D printed components used in the HexaQuad.

Image ID	**Part Name**	**Desctiption**
a)	Wing Nut	Used to secure battery plate
b)	Landing Gear Foot	Provide a stable footing for the landing gear
c)	Top Rotorboom Mount	Top half of the rotorboom mount
d)	Bot Rotorboom Mount	Bottom half of the rotorboom mount with landing gear extension
e)	Motor Mount	Secure motor to the rotor
f)	Top Rail Mount	Secure the top gimbal rail to the top plate
g)	Bot Rail Mount	Secure the bottom gimbal rail to the threaded rods
h)	GPS Mount	Mount GPS on the top gimbal rails
i)	PDB Mount	Secure the PDB to the bottom plate
j)	Sensor Mount	Universal sensor mount used for the RC and Telemetry radio
k)	RC Radio Mount	Radio mount for the FrSky Archer GR8
l)	Telemetry Radio Mount	Mount for the RFD900+ telemetry radio

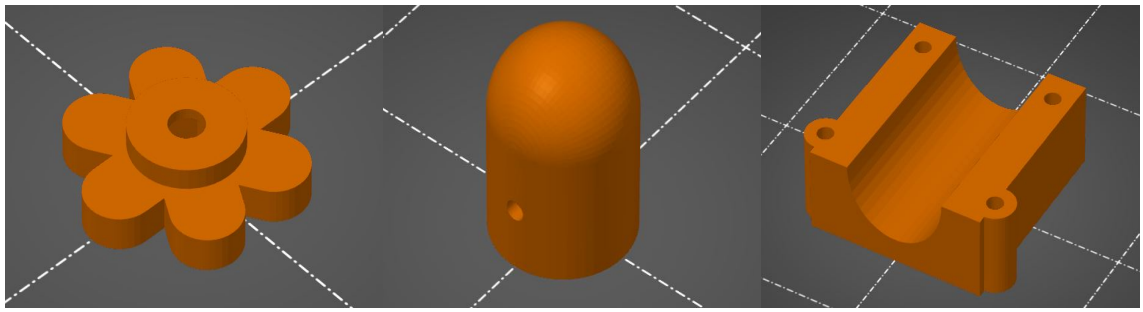

(a) Wing Nut (b) Landing Gear Foot (c) Top of Rotormount

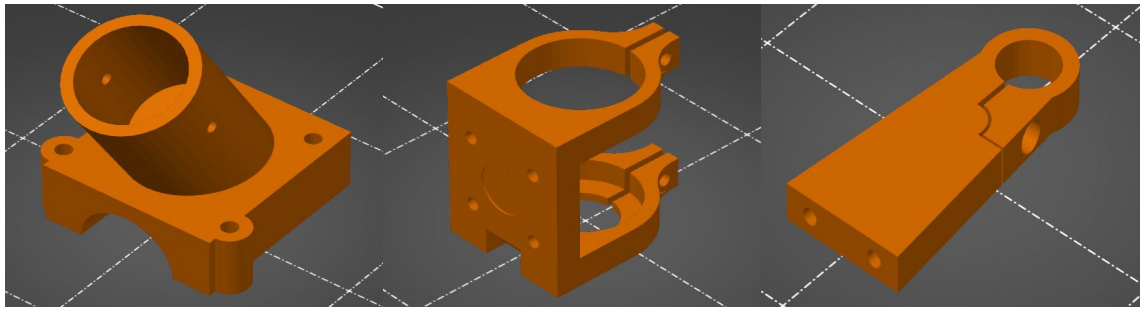

(d) Bot of Rotormount (e) Motor Mount (f) Top Rail Mount

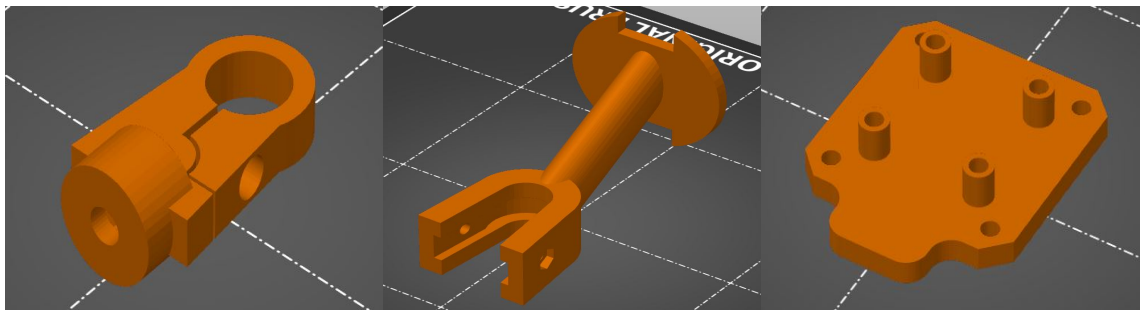

(g) Bot Rail Mount (h) GPS Mount (i) PDB mount

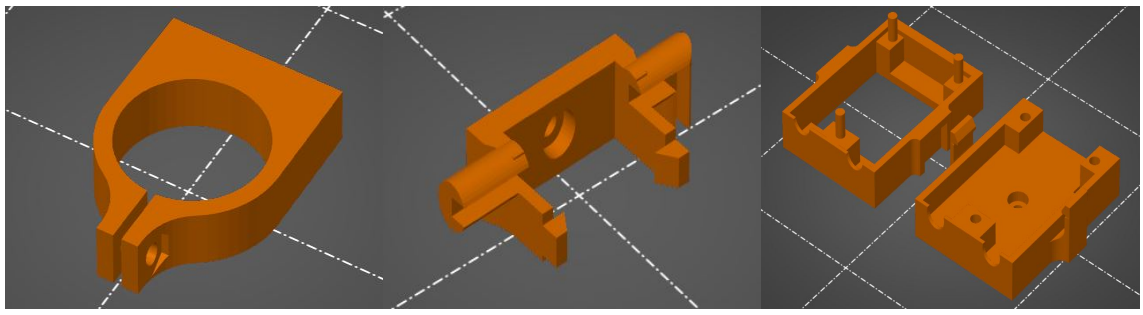

(j) Sensor Mount (k) RC Radio Mount (l) Telemetry Mount

Figure 4.20: All 3D printed components on the HexaQuad

4.5 Final Nyala HexaQuad Design

The final design of the HexaQuad is simple to replicate and easy to assemble catering to drone experts and novices alike. The construction of the design presented here requires access to standard shipping, a consumer level 3D printer and once off access to CNC routing facilities to create the central hubs. Incorporating all the components discussed within the sections above the final design for the Nyala HexaQuad was reached and is presented here in Figures 4.21 to 4.23.

Along with the Figures of the final design, a set of the specifications for the HexaQuad and individual parameters is presented in Table 4.5.

Furthermore, the associated documentation and source files are presented, showing the landing page of the Git Hub repository that houses all the design files, flight parameters and documentation. The documentation focuses on tutorials to assist with manufacturing each part of the drone and includes a step-by-step guide for assembling the HexaQuad in either configuration.

Figure 4.21 is a Solidwork render of the Final design of the Hex configuration, focusing on the frame and all designed components.

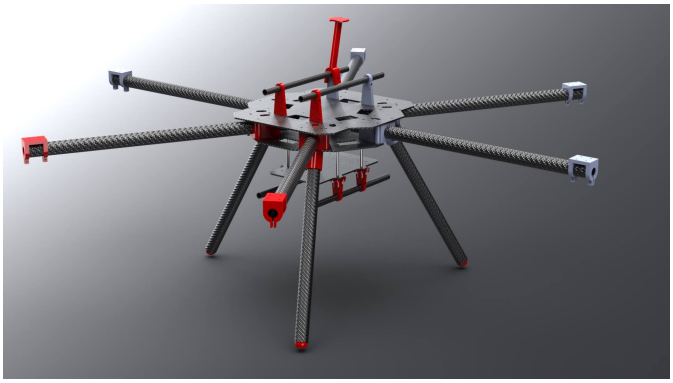

Figure 4.21: HexaQuad final Frame, Hex configuration rendered image.

Figure 4.22 displays the HexaQuad in the Hex configuration during one of the testing sessions.

Figure 4.22: HexaQuad in Hex configuration at test field.

Figure 4.23 displays the HexaQuad in the Quad configuration during one of the testing sessions.

Figure 4.23: HexaQuad in Quad configuration at test field.

Table 4.5: Specifications of the HexaQuad with specific details of each configuration.

Model	**General**
Flight Controller	Cubepilot Orange Cube
Autopilot	Arducopter 4.3.1
Navigation	Here 2 GPS
Remote Control	FrSky Archer GR8 ACCESS (Receiver), Taranis Q X7S (Transmitter)
Telemetry Radio	RFD900+ 900MHz radios
Operating Range (km)	2
Battery Voltage (V)	22.2 (3.7×6)
Battery Capacity (Ah)	8.4 - 16.8
	Hexacopter
Configuration	Hex-X
Wingspan (mm)	1120 (no props), 1578 (props on)
Dimensions ($W \times L \times Hmm$)	$1120 \times 970 \times 450$
Frame Weight (kg)	2.7
AUW, No battery (kg)	3.7
AUW(kg)	4.6 - 5.5
Max Thrust (N)	246
Max Payload (kg)	5
Typical Flight Time (1kg, min)	28.8
Maximum Flight Time (min)	19.2 - 30.6
	Quadcopter
Configuration	Quad-X
Wingspan (mm)	1120 (no props), 1578 (props on)
Dimensions ($W \times L \times Hmm$)	$792 \times 792 \times 450$
Frame Weight (kg)	2.2
AUW, No battery (kg)	2.9
AUW(kg)	3.8 - 4.6
Max Thrust (N)	165
Max Payload (kg)	2
Maximum Flight Time, single battery (min)	23

Nyala HexaQuad

Version: Release 1.0

Welcome to the primary source for all the design materials and users guides for the LANDRS Nyala HexaQuad.

The HexaQuad is an open source, modular multirotor designed with stringent academic research data provenance in mind. It is a simple to replicate and user friendly design for drone novices and experts alike, all you need are some basic tools, 3D printer and access to CNC routing.

Status:

- Drone is undergoing performance testing, see provisional flight performance here
- This repo contains CAD files for the Nyala HexaQuad, associate documentation and ardupilot parameter files
- This repo intends to release version 1 before the end of 2022

Documentation

The documentation can be found at https://www.landrs.org/LANDRs-Science-Drone/. This will house the build instructions, assistance guides and all information relating to the HexaQuad.

Presentation at Linux Open Source Summit Europe 2022

We were invited to present our work at the Linux Open Source Summit that took place in Dublin, 2022. The Linux foundation flew us out to present our work to the open source community.

The full presentation given at the summit can be found on YouTube here.

In the presentation we explore the motivation for the HexaQuad and how it can benefit researchers compared to drones available off the shelf. There is further exploration of the design considerations and performance.

License

Licensed under CERN-OHL-P v2 permissive variant or later.

Citation

Figure 4.24: Home repository of the HexaQuad project housing the design files, flight parameters, documentation and video footage. LANDRS-Science-Drone Repo

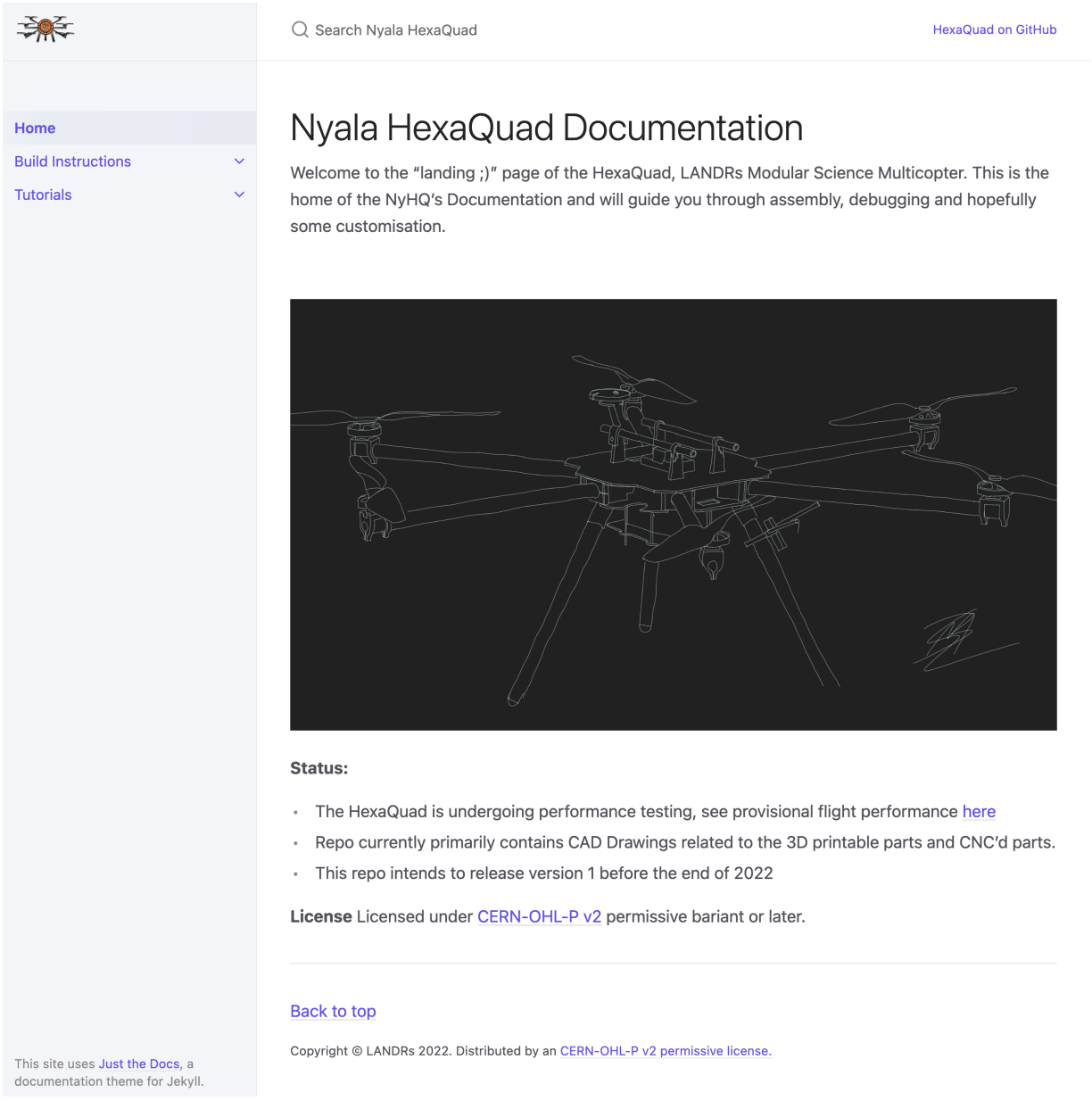

Figure 4.25: HexaQuad Documentation site with the associated build instructions and tutorials, this is still under development. LANDRS-Science-Drone Docs

Chapter 5

Performance Testing The HexaQuad

During the synthesis of the performance tests for the HexaQuad it was decided that the tests should try to mimic expected applications. The literature on research sUAS applications was used to determine common flight patterns that could be automated for repeatability. Beyond the flight patterns, certain flight time parameters were identified to vary between tests to investigate their effect on performance. Additional considerations of flight testing include reviewing regulations from governing bodies to ensure compliance and responsible operation. The following section is broken down into four subsections, the identification of the flight patterns and parameters to vary, the description and implementation of the performance tests, regulations surrounding operation of sUAS for private use and the typical procedures followed during testing for accurate reporting of contextual information.

5.1 Regulations for Test Flights

There are a number of regulations to revise and adhere to for safe and responsible use of sUAS. The Federal Aviation Authority (FAA) drafted an advisory circular for the operation for sUAS and the many variations [1]. Governing bodies such as the South African Civil Aviation Authority (SACAA) have drawn from the FAA legislation to create guidelines specific to South Africa. The legislation of interest here is with regard to flying locations and line-of-sight rules.

Before any testing could be performed, an approved flying location had to be found. With regards to flight regulations under SACAA, a user cannot fly a sUAS within 50m of any group of persons or any property without the permission of the owner [54]. When flying the sUAS, the pilot in control must maintain a visual line-of-sight without any assistance and any flying should take place during daylight hours with clear conditions. Furthermore, any flying of an sUAS should be for private use or a commercial license is required. There are further regulations which require direct

approval from SACAA, such as flying within 10km of an airfield, however, there was no need to apply in the circumstances of this project as the anticipated operation did not breach any special requirements.

In order to comply with the regulations highlighted here and other regulations stipulated by SACAA, all test flying was performed at a registered hobby flying club located in Bergvliet, Cape Town, South Africa. All personnel operating the HexaQuad were required to be registered with the South African Model Aeronautic Association (SAMAA) [55] as well as be registered members of the SAMAA registered club, The Southern Soaring Club. During test flying, it was ensured that the HexaQuad stayed within a visual line of sight and did not approach too closely any people or structures within the vicinity of the test flying area designated by the Southern Soaring Club.

5.2 Flight Test Identification

The performance tests of the HexaQuad were influenced by the design requirements to be versatile and easy to integrate with different sensor sets. This meant exploring the different use cases of multirotors for research and the possible scenarios that it could be applied to. From reviewing the literature, there were typical flight behaviours that could be replicated into standardised and repeatable tests [10, 11]. Three distinct flight behaviours were identified:

1. Flying in a horizontal grid, such as those used in site surveys
2. Hovering at predefined altitudes
3. Ascending and descending in vertical grids, i.e. a vertical survey grid

With clarification of the type of flights to test performance, additional parameters were highlighted to vary between the flights. The parameters were identified as key components that are easy to change and could influence the flight time of the HexaQuad.

The components that varied were as follows:

1. A comparison of two different propellers, one slightly cheaper with a lower quality finish and a more expensive one with a high quality finish
2. Flight time comparison of LiIon and LiPo Batteries

The propeller comparison served as a cost benefit analysis with the intention to investigate whether the efficiency gain of the expensive propellers had a material effect on flight time performance. The battery chemistry variation was to verify if the higher specific energy of LiIon batteries did translate to improved endurance.

Table 5.1 explicitly identifies the difference between the components that were varied between flights. Note, the different components will be referred to by their short hand names as defined in Table 5.1 for the remainder of this dissertation.

Table 5.1: Components that varied during flight tests to investigate their influence on performance.

Parameter	Description	Short Hand
Propellers	Quanum Carbon Fiber Props, 18x5.5	Cheap Prop
	T-Motor Carbon Fiber Props, 18x6.1	Expensive Prop
Batteries	Glacier 8000mAh, 6S, 30C LiPo	LiPo
	Dark Lithium 8400mAh, 6S, 25C LiIon	LiIon

Having clarified the type of flights and parameters that changed during flight testing, Table 5.2 shows a consolidated overview of the repeatable tests for both the Hex and Quad configuration of the sUAS.

Table 5.2: A description of the flight performance tests and their varying parameters. The table also details the expected number of tests.

Flight Mission	Propellers	Chemistry	No. of Batteries	No. of Tests
Static Hover	Cheap	LiIon	Single	4
	Cheap	LiPo	Single	4
Vertical Grid	Cheap	LiIon	Single	4
	Cheap	LiPo	Single	4
Horizontal Grid	Cheap / Expensive	LiIon	Single	8
	Cheap	LiPo	Single	4

Beyond these standard repeatable tests there were some specialised tests for specific interests, this included:

1. Investigating the HexaQuads ability to lift 5kg
2. The peak performance flight time of the HexaQuad
3. The maximum wind tolerance of the HexaQuad.

The details of these specialised tests are outlined in Table 5.3:

From closer inspection of Table 5.3, there is simple reasoning for the chosen configurations in the specialised tests. For the payload test, the cheap propellers were chosen to reduce cost risk in the case of a crash and the LiPo battery was used for its ability to operate at higher continuous current levels over the LiIons. The peak flight time is conducted for both configurations due to the different power requirements,

Table 5.3: Overview and descriptions of the specialised tests for performance evaluation of the HexaQuad.

Flight Mission	Propellers	Chemistry	No. of Batteries	No. of Tests
Payload Capacity	Cheap	LiPo	Single	5
Peak Flight Time	Expensive	LiIon	Double	2 Hex, 2 Quad
Wind Resistance	Cheap	LiPo	Single	1 Hex, 1 Quad

the best components are selected to identify the peak performance. The wind resistance test is intended to determine the maximum wind speed that the HexaQuad can takeoff safely in. The cheap propellers are used in case of a crash and the LiPo was chosen for its higher current performance which will assist with control and thrust in strong winds.

5.3 Test Mission Implementation

Having identified the required tests to perform, a strategy to implement the tests in a standardised and repeatable fashion had to be defined. The repeatable missions were implemented through automated missions designed in the Ground Control Station (GCS), Mission Planner. A detailed guide on how to create different types of automated missions can be found in the Ardupilot documentation [35].

For the specialised missions, other than the peak flight time performance, were conducted in a semi-manual control mode. Semi-manual refers to flight modes where there is assistance from the autopilot to hold a position and stabilize the sUAS only and the user inputs the desired attitude and thrust commands. The payload capacity and wind resistance test required the use of *stabilise mode* for a user controlled takeoff and once the drone was at an altitude of three metres *loiter mode* was activated to hold the drone in a static Hover.

The automated missions created for testing the HexaQuad were made up of navigation waypoints and do commands to perform procedures such as a takeoff. To conclude the missions in a consistent manner conditional commands were implemented, these took the form of battery fail-safes. The fail-safes were configured to ensure the HexaQuad would suspend the mission and return to the launch location when a low battery voltage and remaining capacity were reached. The battery fail-safe parameters are defined in Table 5.4, the *low* values are used as an indicator that the battery is almost depleted and a fail-safe action will soon trigger. When the *critical* values are reached then a fail-safe action is triggered. The set fail-safe action was a Return To Launch (RTL) that automatically guided the sUAS back to the takeoff location.

Table 5.4: Arducopter fail-safe parameters that would be adjusted in Mission Planner to indicate when the HexaQuad should trigger the fail-safe operations.

Parameter Name	LiIon	LiPo	2 x LiIon
BATT_CAPCITY (100%)	8400mAh	8000mAh	16800mAh
BATT_LOW_VOLT	20V	21.6V	20V
BATT_LOW_MAH (32.5%)	2730mAh	2600mAh	5460mAh
BATT_CRT_VOLT	19.4V	21V	19.4V
BATT_CRT_MAH (30%)	2520mAh	2400mAh	5040mAh

Having clarified the manner in which the automated tests would were executed, the specific missions can now be described.

The *Static Hover Mission* was the simplest of the automated missions and is represented in Figure 5.1(a) The mission was initiated by an automated takeoff to an altitude of 15m. Upon reaching the desired altitude, the HexaQuad then navigates to a single waypoint defined by GPS co-ordinates and holds position. The HexaQuad will hold position at the defined co-ordinates until the fail-safe values in Table 5.4 are reached and an RTL is triggered. The mission was concluded once the HexaQuad had landed and disarmed.

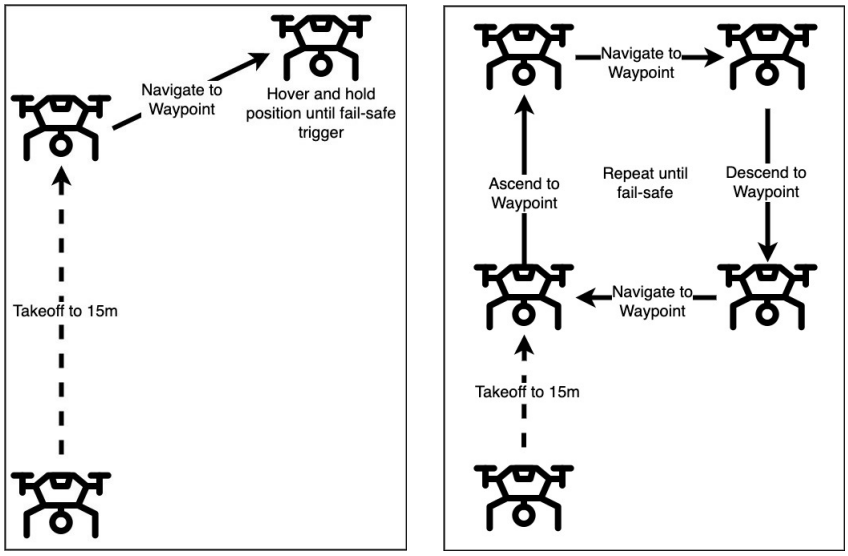

(a) Static Hover Mission (b) Vertical Grid Mission

Figure 5.1: Visual representation of the static hover and vertical grid mission. The mission planner view is a simple birds eye view and does not show the change in altitude.

The *Horizontal Grid Mission* consisted of 25 waypoints. The mission was initiated by an automated takeoff and ascended to an altitude of 20m. The HexaQuad then flew to the first waypoint guided by compass and GPS co-ordinates before continuing onto the other predefined co-ordinates in a sequential manner. Once the HexaQuad reached the final waypoint, a conditional command was invoked and instructed the HexaQuad to return to the first waypoint to repeat the mission. The mission was repeated until the fail-safe conditions were met and an RTL was triggered. Figure 5.2 illustrates how the horizontal grid mission is represented on Mission Planner with waypoints being numbered in sequential order.

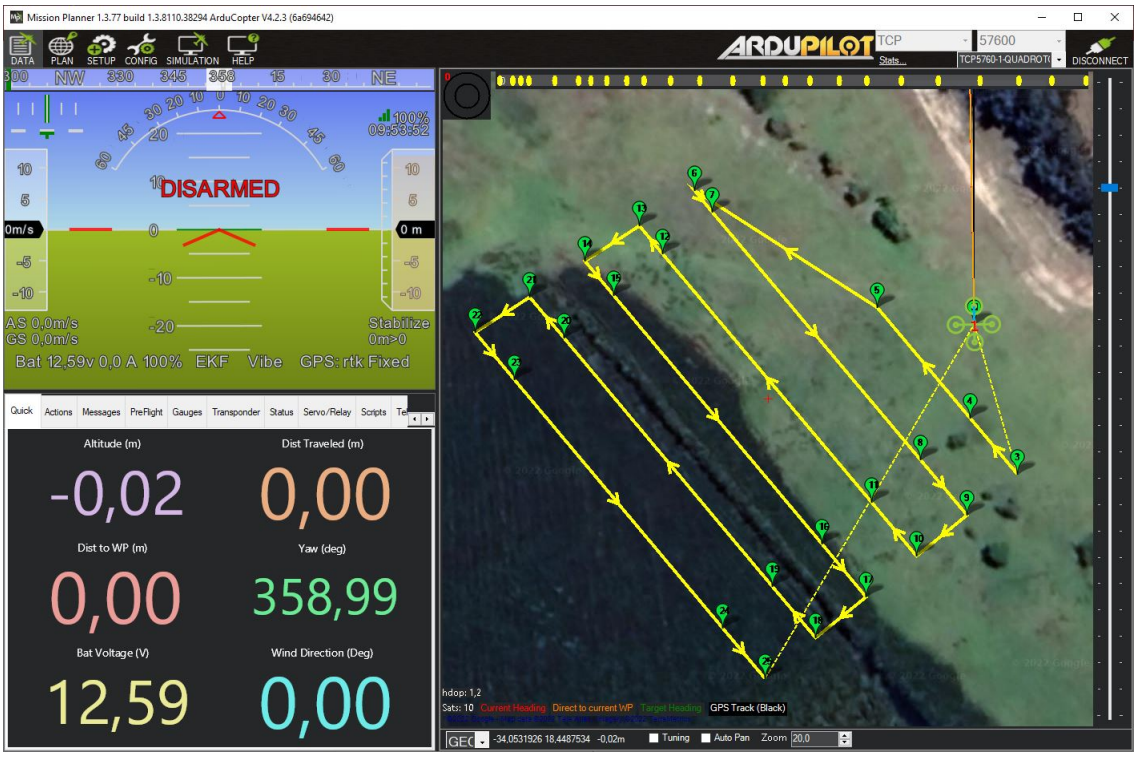

Figure 5.2: Horizontal Grid Mission as represented in Mission Planner

Designing a *Vertical Grid Mission* was slightly more complicated and required manual adjustment of commands to reach the desired operation. However, the order of operations was as follows: the mission was initiated by an automated takeoff and ascended to an altitude of 15m. The HexaQuad then navigated to the first waypoint before ascending to 40m without any intended horizontal displacement to reach the second waypoint. There was then a small horizontal displacement to waypoint three before descending in a straight line to waypoint four. This operation would repeat in

a similar manner to that described for the horizontal grid mission until the fail-safe values were reached and an RTL was triggered. A simplified illustration of the vertical mission can be seen in Figure 5.1(b).

5.4 Test Flying Procedure

Due to the large number of test flights planned for the HexaQuad, a testing procedure was created with the intention of making tests consistent. The testing procedure included a checklist of tasks to complete before, during and after each flight. This section will provide some detail about the captured data and preparation steps.

There were two types of data captured during the test flights: the logged data from the flight controller which records values such as IMU readings and battery related readings; and manually captured data about external conditions like wind speed or which propellers were used in the test fight. The logged data was simple to setup and access, however, it did require parameter configuration on the arducopter autopilot firmware in order to record. The manually captured data was recorded via a Google form with information such as the flight name, wind speed at the start of the test, location and battery ID as a few examples. The google form assisted with uniquely identifying each flight and subsequently each data log stored on the flight controller as well as providing contextual information.

Beyond capturing information about the flight and related conditions, there were procedural steps taken to ensure the proper functioning of the HexaQuad and the planned mission. A typical flight procedure would be as follows:

1. Upload correct mission to flight controller
2. Ensure fail-safe parameters are set for corresponding battery
3. Propellers are secure, correctly oriented and level
4. Battery/Batteries connect and securely mounted
5. Connect the GCS and radio control transmitter to the HexaQuad for control and observation
6. Clear any fail-safes or errors for the autopilot prior to arming
7. Set flight mode to stabilize mode for arming

8. Arm the HexaQuad and start stopwatch
9. Change flight mode to auto mode and set throttle to 50% to begin mission
10. Observe the HexaQuad during flight for odd behaviour and monitor key parameters on the GCS in case of manual intervention
11. Upon an RTL in the closing of a mission, ensure landing area is clear and prepare to stop the time when the HexaQuad disarms
12. After disarm, record battery voltage and capacity state and submit in Google form

5.5 Data Processing for Performance Review

During the testing of the HexaQuad it was vital to acquire data and performance metrics in order to review the test and evaluate it. Fortunately, the open source flight controller and autopilot provide access to all data captured by the sensors and can be recorded to data and telemetry log for review post flight. The logging systems assisted not only with performance evaluation but problem solving strange behaviour or identifying the cause of crashes. This section will give a brief explanation of the tools that were used during data evaluation and the sources of data for performance review.

There are a number of parameters monitored and logged by ArduCopter including attitude, motor PWM signals and IMU readings. In the case where additional external sensors such as battery monitors are connected these parameters are also added to the log. During the design of the performance tests, battery data was highlighted as a key parameter to evaluate performance. The battery data included information about the power demand and energy consumption which could be used to evaluate the difference in performance between batteries, propellers and mission types. With regards to the payload test, throttle readings were also identified as useful to investigate the weight lifting capabilities of the HexaQuad.

With the key log data identified a data processing method had to be created to interpret and present the results from the performance testing. The log files were extracted from the autopilot SD card as large binary files and had to be reduced to smaller manageable data sets. This was made possible with functions within MavLogDump.py which were part of the pymavlink packages. The desired data was extracted using MavLogDump.py to smaller .CSV files which could then be evaluated with other tools. The chosen method of processing took the form of a python notebook

which made use of typical data science packages such as Seaborn and Pandas to order and plot the desired data into a presentable form.

The data processing notebooks and log extract batch tools are available on GitHub.

- Log Extraction: https://github.com/MBorrageiro/HexaQuad-bin-analysis
- Data Processor: https://colab.research.google.com/drive/1PSyf1fBYvkvbS$_h$$IFxK1_xDN9UVmF5zJ?usp=sharing$

Chapter 6

Experimental Results and Discussion

This section will present the results captured during the performance testing of the HexaQuad as well as discuss them in relation to the expected performance and relevant literature. For ease of reading, reference to the HexaQuad in either of the two configurations will simply be referred to as either the *Hex* or *Quad*. The results and discussions have been broken down into sections relating to the tests described in the Testing chapter. Thus, the layout will first discuss the mission type influence, then the battery and propeller design comparison, followed by the specialised test performances of the payload and peak flight time performance. The section is concluded with a results summary.

6.1 Mission Type Influence on Results

This section will present and analyse the results of the HexQuad in both configurations, focusing on the influence of the mission type on the flight time performance.

There were three different automated missions designed to mimic typical applications of research drones. These tests were: 1) a static hover mission, 2) a vertical grid mission, and 3) a horizontal grid mission. Overall, there was a total of 20 performance tests for the Quad and 18 performance tests for the Hex. Seven of the test flights were excluded from the combined data set, however, this only occurred if the test resulted in a crash or if the behaviour was uncharacteristic due to incorrect parameters or arbitrary fail-safe occurrences.

The Hex did not undergo the same number of repetitions as the Quad due to time and weather constraints. It was decided that flight time should be allocated to a peak performance test so as to compare the results to the desired specifications and simulated values. The vertical grid and peak wind performance tests were also abandoned and removed from the testing schedule due to the restricted time and weather windows.

Figure 6.1 represents the current draw density distribution of all the Quad test flights. In other words, it showcases the range and frequency of occurrence of the current drawn by the Quad during the automated missions. The distributions of current draw for the static hover missions are shown on the left and the horizontal grid missions on the right of Figure 6.1.

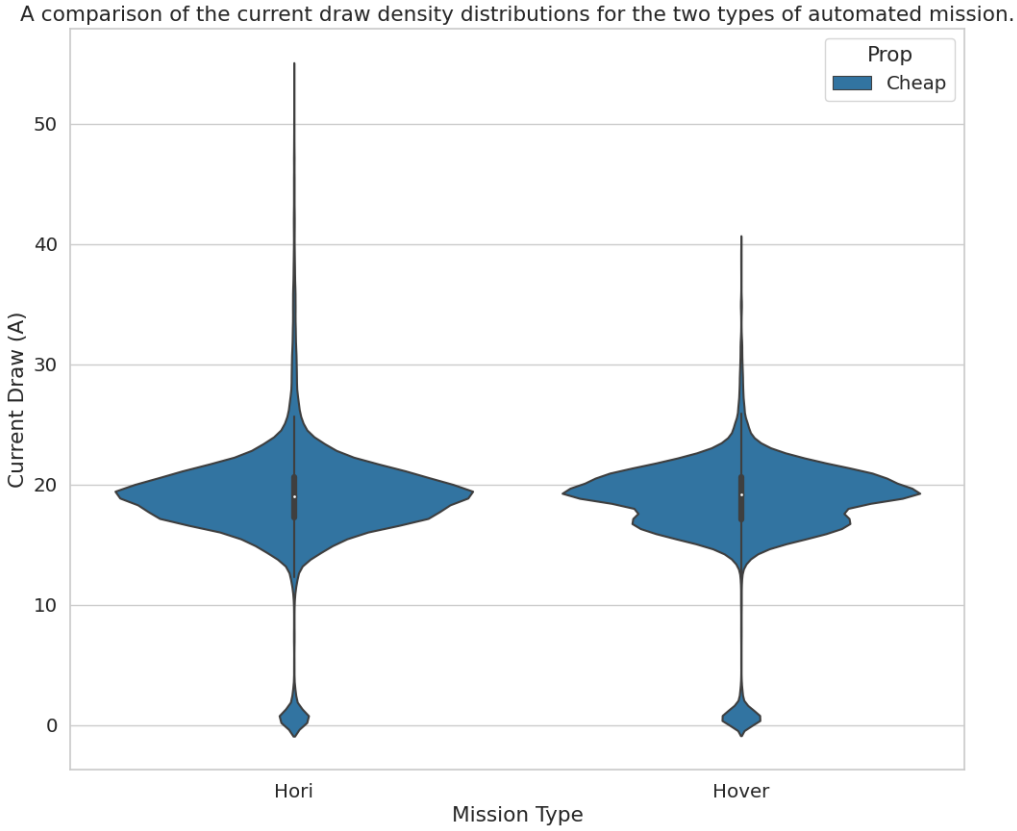

Figure 6.1: Comparison of the current draw densities for the two types of automated missions. This figure also highlights the influence of the propeller on the current draw of the Quad.

The violin plots extend to current values of 40A and 50A for the static hover and horizontal grid missions respectively. These are instantaneous peak current values likely from external disturbances such as responses to wind gusts or to reach a desired travelling speed when accelerating with or against the wind. Additionally, there are small density clusters found near the 0A mark for both missions in Figure 6.1. These values are from the draw of low current when the motors are armed and start to spin slowly before ascending in the automated takeoff. The orange density curve is centered on a lower current value because of the type of propeller used. The propeller

used was the expensive set and resulted in a lower operating current during the flight, however, this will be discussed later in a section below.

Comparing the current densities for the two mission types, Figure 6.1 shows that the current ranges for the two missions were similar when using the same cheap propeller. There was a difference of 660mA between the mean values of the two missions, where the static hover was the lower of the two. Although the static hover had a lower mean value, the operating current ranges of the two missions significantly overlap. The operating current ranges are defined to be within one standard deviation of the mean, these ranges are presented in Table 6.1.

Table 6.1: Operating current ranges within one standard deviation of the mean for the two test types. The configuration used was a Quad with Cheap propellers.

Mission	No. Flights	Average Current	Standard Deviation	Current Range
Static Hover	7	18.19A	3.74A	[14.45, 21.93]A
Horizontal Grid	7	18.84A	4.39A	[14.46, 23.93]A

The horizontal mission's range extends 2A higher than that of the hover, this is attributed to accelerating against the wind multiple times during a mission and explains the higher standard deviation. Although the horizontal mission had a slightly higher operating range, there is still a significant overlap of the two operating ranges and this can be translated to similar performance between the mission types.

The similar current draw values for the Static Hover and Horizontal Grid missions in Figure 6.1 are translated to similar flight times for the two missions when considering the same propeller. It is to be expected that lower current and hence lower power usage over the flight will result in extended flight time. Figure 6.2 shows the typical flight times for the two mission types and is further split by the type of propeller used.

The respective mean flight times for the static hover and horizontal grid were 18.3 and 18.2 with standard deviations of 3 and 3.3 minutes

Within Figure 6.2, there are some outlier values distinguished by diamond shaped dots. These were flights with performance that could not be replicated or were uncharacteristic, such as the two data points located below 14 minutes for both missions. These values were flights performed with *Battery A* and were uncharacteristically low for a LiPo battery with a capacity of 8000mAh. *Battery B* was identical and had consistent flight times of around 18 minutes. The poor performance was attributed to the age of the battery as it is expected for performance to drop with battery age and the number of charge and discharge cycles.

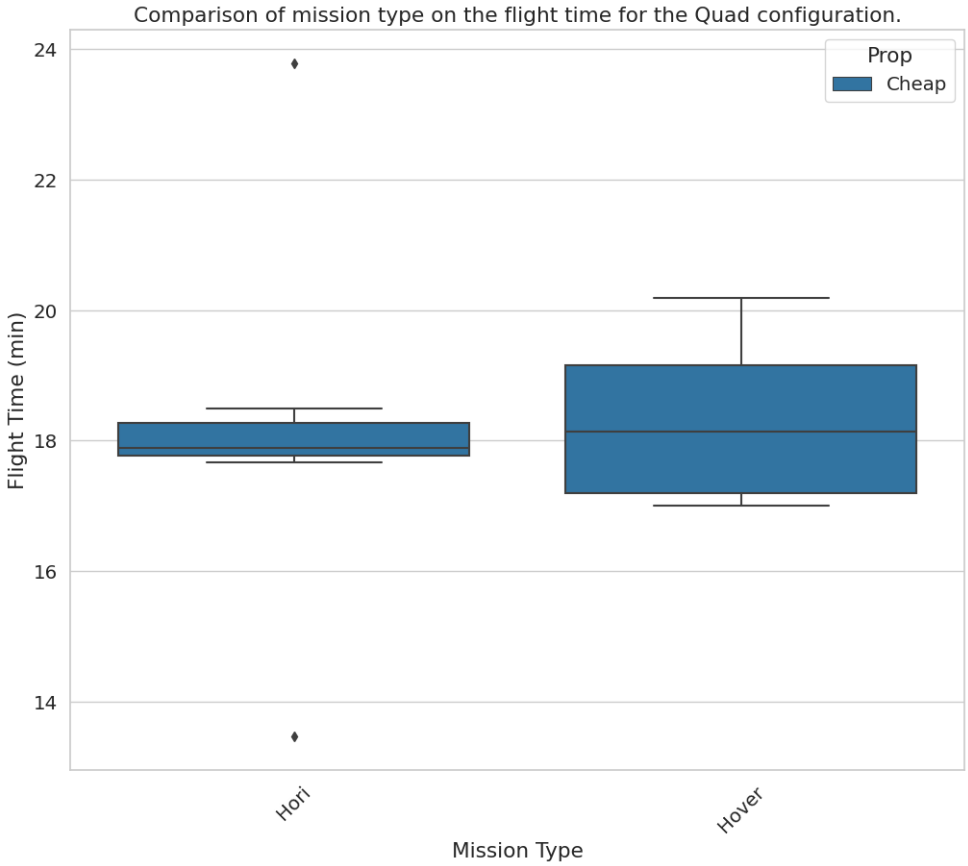

Figure 6.2: Quad flight time comparison for the two tested automated mission types.

Having presented the mission influence on performance for the Quad configuration, the influence on the Hex performance will now be presented for comparison.

Figure 6.3 depicts the current draw density distribution for the Hex whilst performing the two automated missions. The current draw density distributions of the Hex are similar between the hover and horizontal mission as they were for the Quad configuration. However, the difference for the Hex configuration is that the horizontal missions have a lower average current draw of 20.42A, 1.01A lower than the hover missions.

The major difference between the Quad and Hex automated mission tests was the number of tests performed, there were fourteen test repetitions, seven of each, for the Quad configuration and only seven for the Hex, 5 hover and 2 horizontal grids. When comparing a range of operating currents within one standard deviation of the mean it becomes clear that the operating ranges of the two missions overlap significantly and

the current demand is similar between the missions, Table 6.2 presents the operating current ranges for the Hex.

Table 6.2: Operating current ranges for the Hover and Horizontal tests in the Hex configuration.

Mission	No. Flights	Average Current	Standard Deviation (Sd)	Current Range
Static Hover	5	21.43A	3.51A	[17.93, 24.93]A
Horizontal Grid	2	20.42A	4.00A	[16.43, 24.42]A

The top end of the current range values in Table 6.2 are closely related with a difference of 0.51A. The horizontal grid had a slightly lower bottom of the range current value, however, this is a result of reduced current demand when flying at constant speed in a single direction.

The flight time comparison between the two mission types in the Hex configuration is presented in Figure 6.4. Given that the static hover mission had a higher average current it can be expected that it had a shortened flight time. The hover missions had an average flight time of 16.7, whereas the horizontal missions had an average flight time of 17.6 minutes. The respective standard deviations were 42 and 14 seconds, thus both missions had similar performance within expected error margins.

Two types of automated mission were considered to evaluate the performance of the HexaQuad under different flight manoeuvring conditions. For both the Quad and Hex configuration the flight time performance was similar within expected error margins for the two tested mission types. Galle et al's. [11] Hexacopter used to sample volcanic plumes reported similar behaviour for hover and horizontal movements. The difference between the operating currents for the two mission types was 3A with the horizontal movement achieving a lower value. Galle et al. [11] attributed this to the nature of horizontal flight, where a component of the horizontal thrust contributes to maintaining vertical position and thus reducing the overall power consumption. This trend of reduced current draw during horizontal flight began to become apparent in the Hex horizontal grid flights. However, the difference is not as pronounced likely due to the short distance between waypoints resulting in the HexaQuad moving at a slower speed with only a small horizontal thrust component.

With regards to the resulting flight time performance, the HexaQuad produced similar results to the sUASs used in Barbieri [10] atmospheric sensing studies. The fixed-wings and multirotor were expected to loiter and hover at predefined altitudes with a total flight time in the range of 14-16 minutes. Considering barbieri's [10] test specifications, the HexaQuad has performed sufficiently well and likely would have

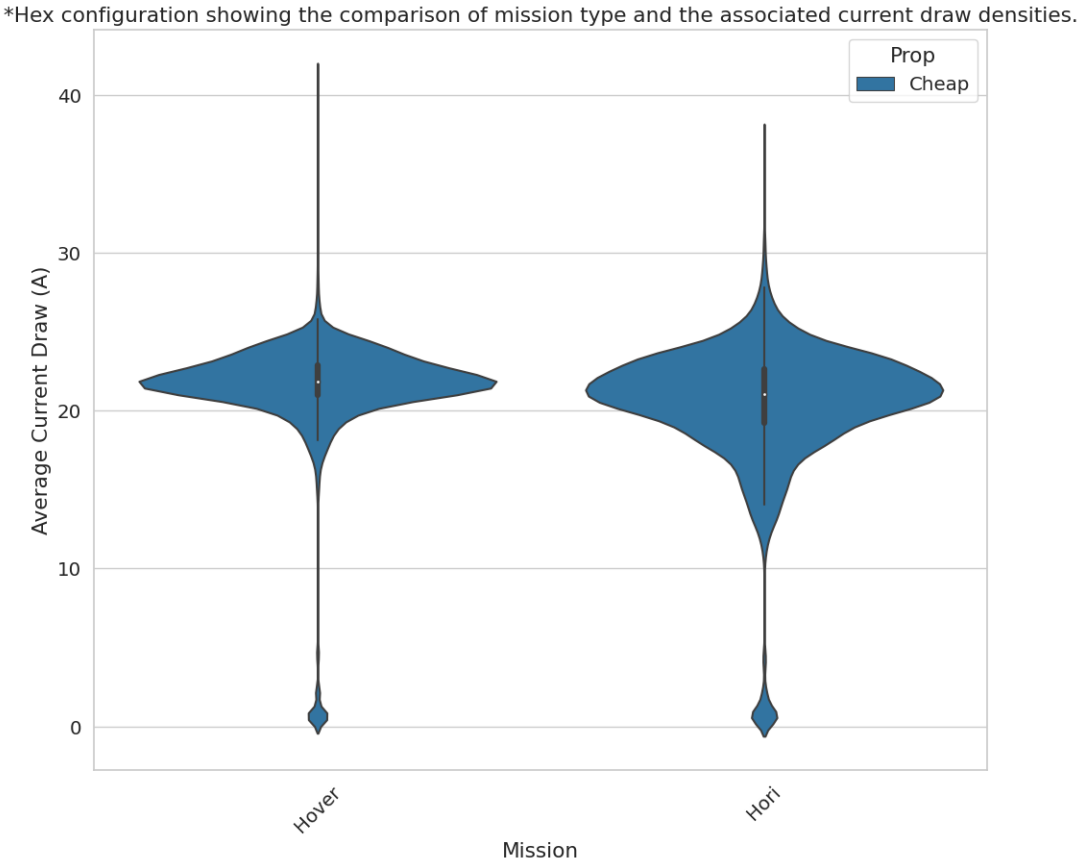

Figure 6.3: Comparison of the mission types and the associated current draw densities for the Hex configuration.

met the requirements to perform the same atmospheric test. The major difference between the tests conducted here and barbieri's was a single ascent and descent to 120 metres to loiter for 2 minutes. This is where the vertical grid survey tests would have been beneficial to define expected performance, however, it is believed, a single ascent and descent would not alter flight time massively. A summary of the flight performance for the different missions and configurations can be seen in Table 6.3.

Table 6.3: Average flight times with standard deviations for the two mission types and HexaQuad configurations. *Note: these times only compared the cheap propeller.*

Configuration	Static Hover (min)	Horizontal Grid (min)
Quad	18.3 ± 3	18.2 ± 3.3
Hex	16.7 ± 0.7	17.6 ± 0.23

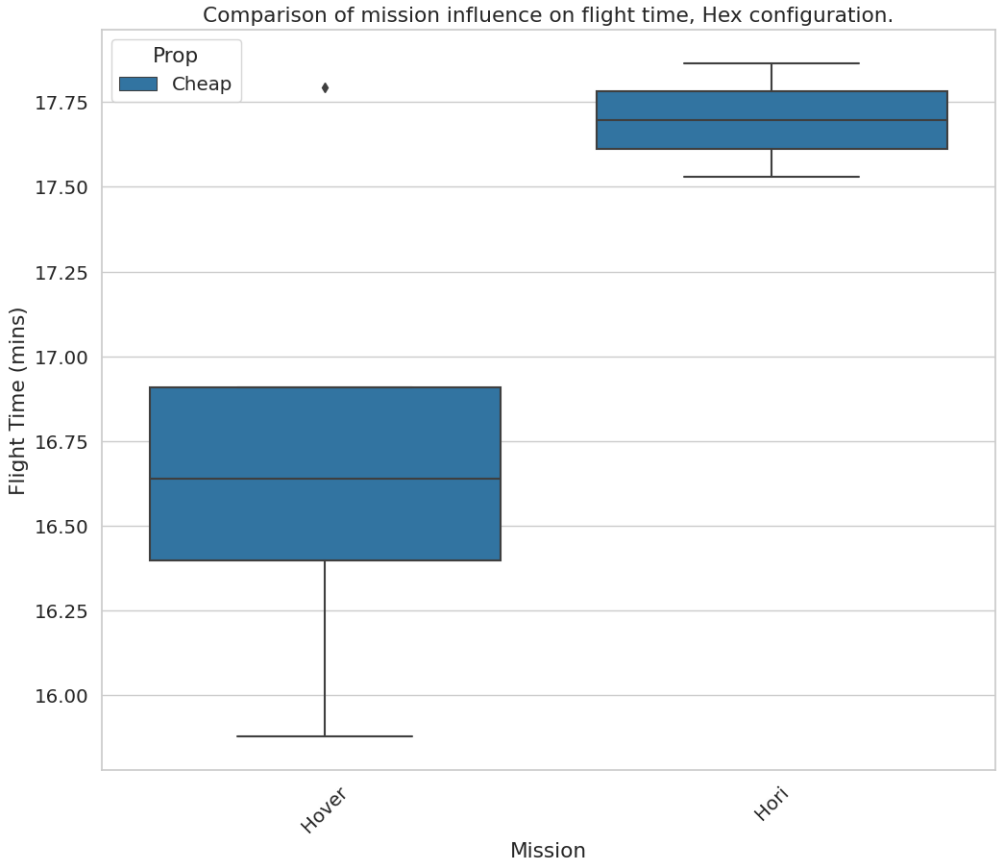

Figure 6.4: Comparison of the mission types and their influence on flight time for the Hex configuration.

6.2 Propeller and Battery Performance

During the automated missions, two sets of propellers were used in the horizontal grid missions, and are referred to as the cheap and expensive sets. The specifications of the two sets of propellers can be reviewed in Table 5.1. The two sets of propellers were compared to investigate if there was any practical flight time gain to support the increased cost. This section will present and compare the performance of the two sets of propellers by looking at two parameters of interest, the flight time and current demand during an automated flight. The influence of the propellers was only tested in a single mission type to reduce the number of repetitions.

Before proceeding it should be noted that during the Hex propeller comparison only four of the six propellers were of the expensive set. The only reason for this compromise was due to a pair of propellers being damaged in prior crashes, leaving only two usable sets. Referencing Figure 6.5, rotors one and two were equipped with

propellers from the cheap set.

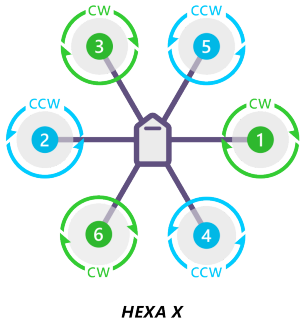

Figure 6.5: Hexacopter X configuration rotor layout to assist with distinguishing which propellers were replaced with the cheap set [25].

Furthermore, there is also a comparison of two different types of battery chemistry, LiPos and LiIons, which can also be referenced in Table 5.1. The two battery chemistries were compared to investigate the effect of the specific energy difference on flight endurance. The parameters of interest for this comparison were the flight time and current demand.

The section will first focus on the propeller comparison before moving to present the influence of the two battery types.

Figure 6.6 is a collection of the Quad horizontal grid test flights and displays the average current drawn as well as the flight time. Included, is an indication of the average wind speed in metres per second for each test flight. Immediately it is clear from Figure 6.6 that there is a performance benefit associated with the expensive propellers displayed in orange. For all flights using the expensive propellers, the average current values were below 16.3A and overall they had an effective average of 14.3A. The respective flight times were all in excess of 22 minutes with an average of 23.1 minutes. Comparatively, the flights that utilized the cheap propellers had an average current demand of 18.9A and an average flight time of 18.2 minutes Thus the expensive propellers had a reduction of 24.2% in average current demand and an increase of 27.1% in flight time. The performance improvement between the propellers is attributed to the higher quality and precision in manufacturing the expensive propellers. The precision of the leading edge, trailing edge, and blade tip of the propellers results in lower drag and torque to rotate the propellers, thus requiring less energy and improving efficiency.

There was a similar trend seen in the Hex propeller comparisons which is shown in Figure 6.7. The expensive propellers had an average current demand of 19.1A,

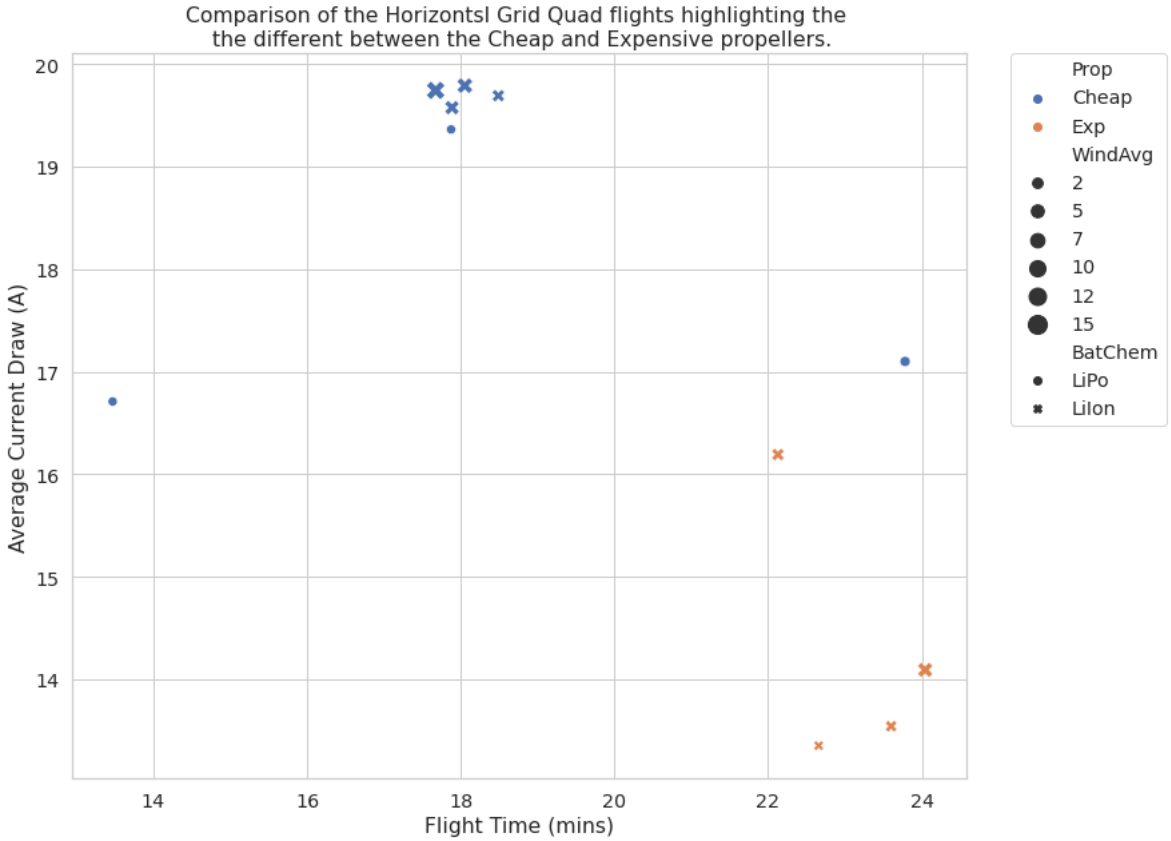

Figure 6.6: Influence of two propeller choices on Quad performance.

whereas the cheap propellers had a current demand of 20.42A. This resulted in flight time averages of 19.2 and 17.7 respectively. The improvements seen in the Hex comparison are not of the same scale as in the Quad tests. There was a reduction of 6.6% in average current demand and an increase of 8.2% in flight time. However, this reduced performance gain is attributed to the non-ideal use of a combination of cheap and expensive propellers for the Hex configuration.

Figure 6.7 also suggests that the Hex had improved performance with reduced power consumption and flight endurance in calmer wind conditions. This trend is not explicitly clear in Figure 6.6 for the Quad test flights. It can be seen that in slower wind conditions some average current values were lower, however, this did not translate to longer endurance in all cases as can be seen with the expensive propeller data points in Figure 6.6.

Moving to the influence of the battery chemistry and densities. It was expected

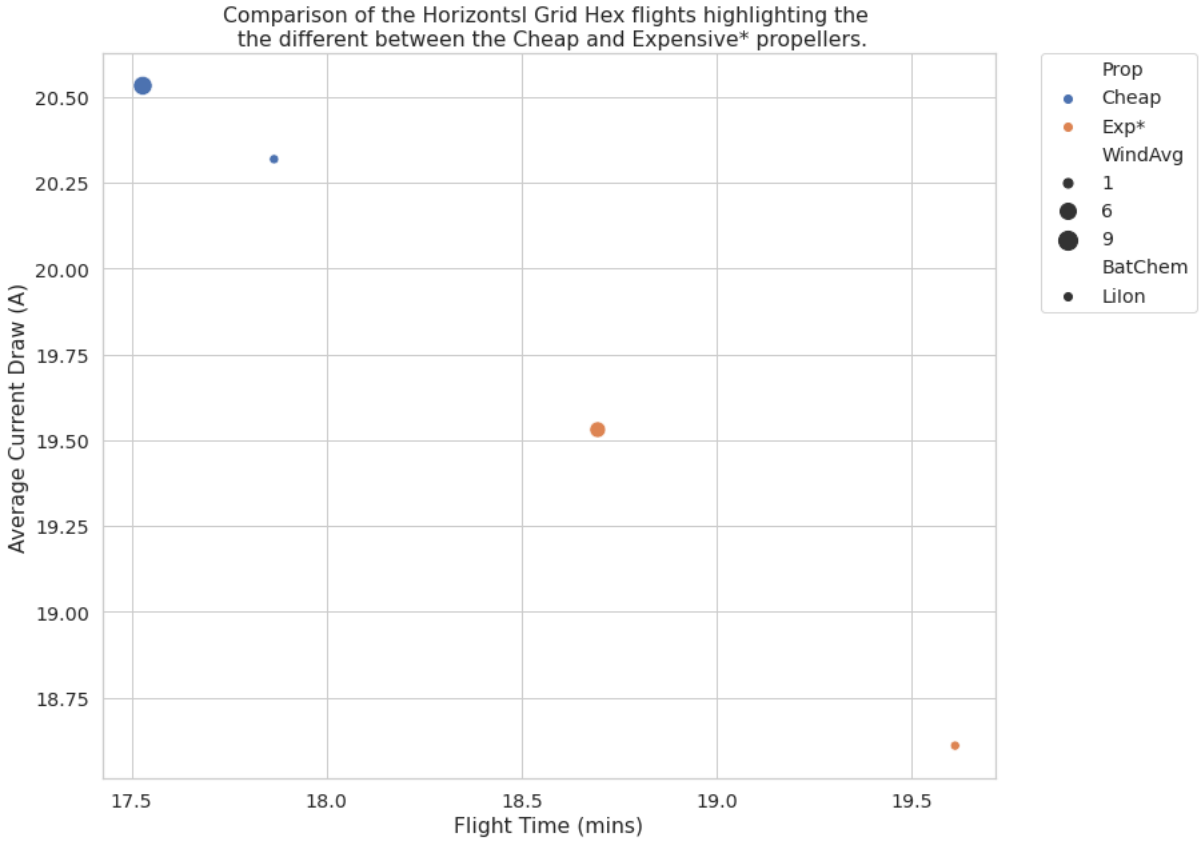

Figure 6.7: Influence of two propeller choice on Hex performance.

that the LiIons would outperform the LiPos in endurance due to their reduced weight but similar capacity. The LiIons had a capacity 5.0% higher than the LiPos and were 19.1% lighter. Figure 6.8 is a collection of all the flights, highlighting the battery chemistry, propeller and the effect on flight time.

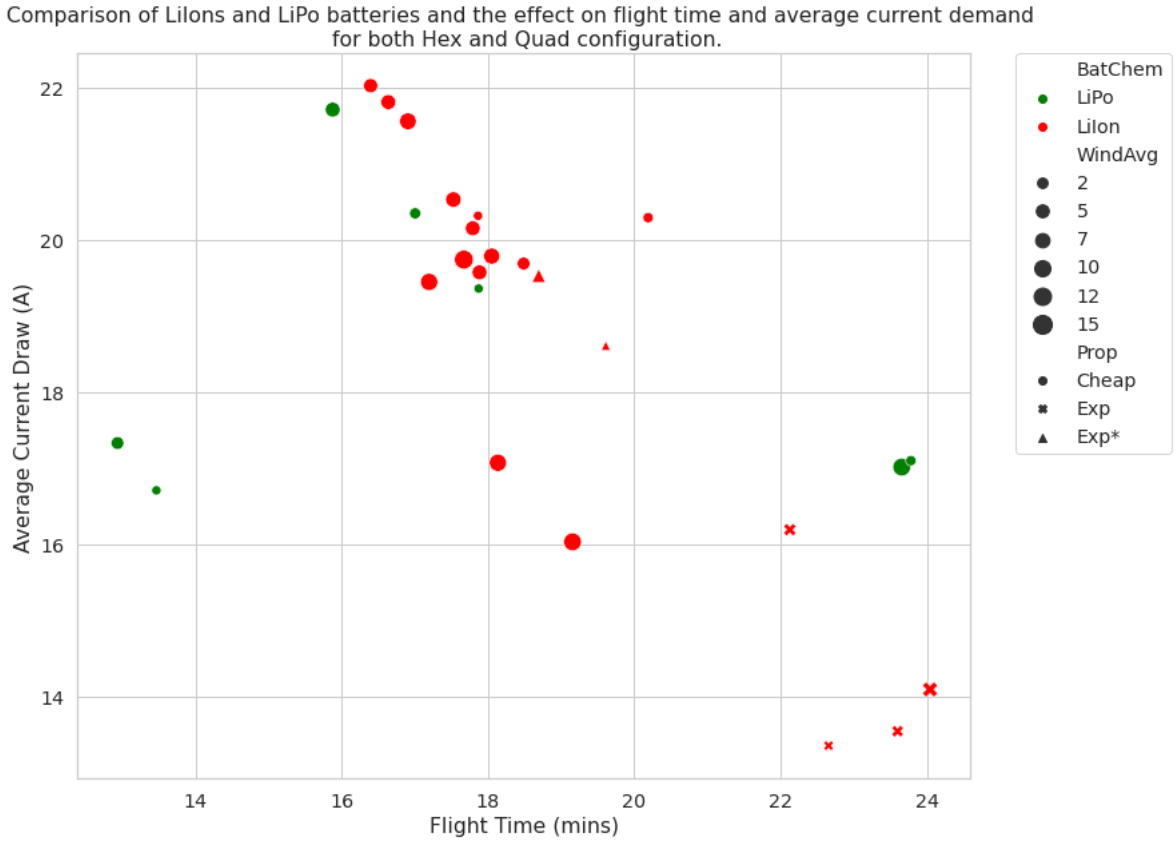

Figure 6.8: Comparison of LiIon and LiPo influence on flight performance for both Hex and Quad configuration.

There was no clear trend in the results that the LiIons reduced weight had a practical effect on endurance. The LiPos displayed similar performance under the same testing requirements as can be seen between current ranges of 19-22A. Considering all the test flights for the cheap propellers, the LiPos had an average current demand 3.1% higher relative to the LiIons. The average flight times were 5.2% shorter than the LiIons with values of 17.9 and 16.9 respectively. The LiIons did perform more consistently with close groupings of data points for the two separate propellers, this is beneficial for describing an expected performance. As can be seen from Figure 6.8, the LiPos had mixed performance with some flights exceeding 23 minutes and others not reaching 14 minutes. The 23 minute flights could not be repeated and likely occurred during optimal conditions. In the opposite case, the 14 minute flights represent the reduced performance as a result of multiple charge cycles and increasing battery age.

6.3 Specialised Test Performance

The specialised tests were set out to investigate the specific performance interest of the HexaQuad. The specialised tests that were conducted included the peak flight time and payload carrying capacity. The peak flight time test required the HexaQuad to be configured in a specific way, two major requirements were the use of two batteries for double capacity and the use of the more efficient expensive propellers. The payload carrying capacity was tested in two semi-manual modes, stabilise for a manual slow takeoff and loiter mode to hold the HexaQuad in a hover.

This section will first discuss the peak flight time performance and compare it to simulations and field results. Thereafter, the payload capacity testing results will be presented.

6.3.1 Peak Flight Time Performance Results

The peak flight time performance was conducted in the Hex configuration with a total of two test flights. Only two sets of expensive propellers were used, the remaining two missing propellers were supplemented with a cheap set. The LiIons were connected in parallel to double the capacity and extend the flight endurance. Thereafter all procedures were the same as for the automated horizontal grid test.

Table 6.4 presents a comparison of the average flight times between the single and double battery flights as well as a standard deviation. The double battery experimental test had a 59.7% increased flight time relative to the single battery tests. The expectation of improvement from the eCalc simulations was estimated at 36.8% increased flight.

Table 6.4: Comparison of peak performance flight time with two batteries relative to a single battery and simulated results.

Configuration	**Single Capacity**	**Two Batteries**(min)	**One Battery**(min)	**Improvement**
Hex	8400mAh	30.6 ± 0.18	19.2 ± 0.65	59.7%
eCalc Simulation [48]	10000mAh	25.3 ± 3.8	18.5 ± 2.8	36.8%

In comparison to the eCalc [48] simulated results the Hex exceeded expectations. With a double battery configuration, the Hex achieved an improvement of 20.3% over the respective simulation. It's worth noting that the single battery test also improved on the simulated results by a smaller margin of 3.5%. However, the initial simulation results made use of a larger battery capacity compared to that used in

the experimental tests and this would explain the lower improvement for the single battery comparison.

Considering earlier trends in flight time performance between the Hex and Quad, it is forecast that the Quad would have had a longer flight time in peak performance configuration. Unfortunately, there was not sufficient time to conduct these tests however, sample data from an unsuccessful flight was used to forecast performance. The Quad in peak performance configuration with a battery capacity of 16800mAh had an average current of 18.67A. Assuming this current level was maintained and the batteries were discharged to 75%, the result would have been a 40 minute flight. However, this is an estimation and should be compared to performance tests which are recommended for future work.

6.3.2 Payload Capacity Testing Results

With regards to lifting higher capacities, hexacopters would outperform quadcopters due to the additional thrust from the two extra motors. Thus the payload capacity test was run for the preferred Hex configuration to investigate whether it would meet the 5kg payload requirement.

The test was run in a semi-manual mode with user initiated takeoffs and landings in stabilise mode, while a steady hover was achieved via the GPS assisted loiter mode. There were five individual flights flown in Hex configuration equipped with the cheap propellers and a single LiPo battery. Each flight had a payload ranging from 1-5kg attached to the lower gimbals rails, the payload was increased in 1kg increments. The payload was attached via 3D printed snap on mounts and cable ties to secure the weights, this is illustrated in Figure 6.9.

During the test the Hex was held at a static hover to investigate the expected operating conditions, the flight times ranged between one to two minutes. On the day of testing, there were winds averaging 10km/h with 16km/h gusts, this would influence the current demand of the drone to remain static during the hover.

During the testing, the Hex successfully lifted all the payloads in the desired range and completed a static hover to acquire an estimated hover throttle percentage. Figure 6.10 presents the throttle output percentages to the motors for the duration of the flights. Included is a control 0kg payload flight which required an average of 12.5% throttle level to achieve a hover. The hover throttle levels steadily increased with payload and achieved a maximum of 31.4% average for the 5kg payload. The

Figure 6.9: Illustration of how the weights were mounted onto the HexaQuad gimbal rails for payload testing. A 3D print snap on mount supported the weights while zip ties were used to prevent the weights from shifting during the tests.

remaining 68.6% of the throttle range contributes to throttle overhead for manoeuvrability of the Hex and equates to a thrust-to-weight ratio of 3.2:1. The achieved thrust-to-weight ratio is thus higher than the initially designed ratio of 2:1 and can be linked to variance between simulation assumptions and practical performance.

The associated current demand for each individual payload flight can be seen in Figure 6.11 compared to a control 0kg automated flight. The average current demand ranged from 26.28A to 67.06A for the payload flights.

These current values were used to determine an estimated flight endurance for the different payloads. In the estimations, it was assumed the batteries would discharge 75% of their capacity to align with the fail-safe values set for the automated tests. The flight time estimates for two different battery capacities can be seen with a summary of the payload results in Table 6.5.

Upon review of the flight time estimates it is clear that the Hex can only lift a payload of 5kg for a short duration of 5.4 minutes if the 8000mAh LiPo were used. The

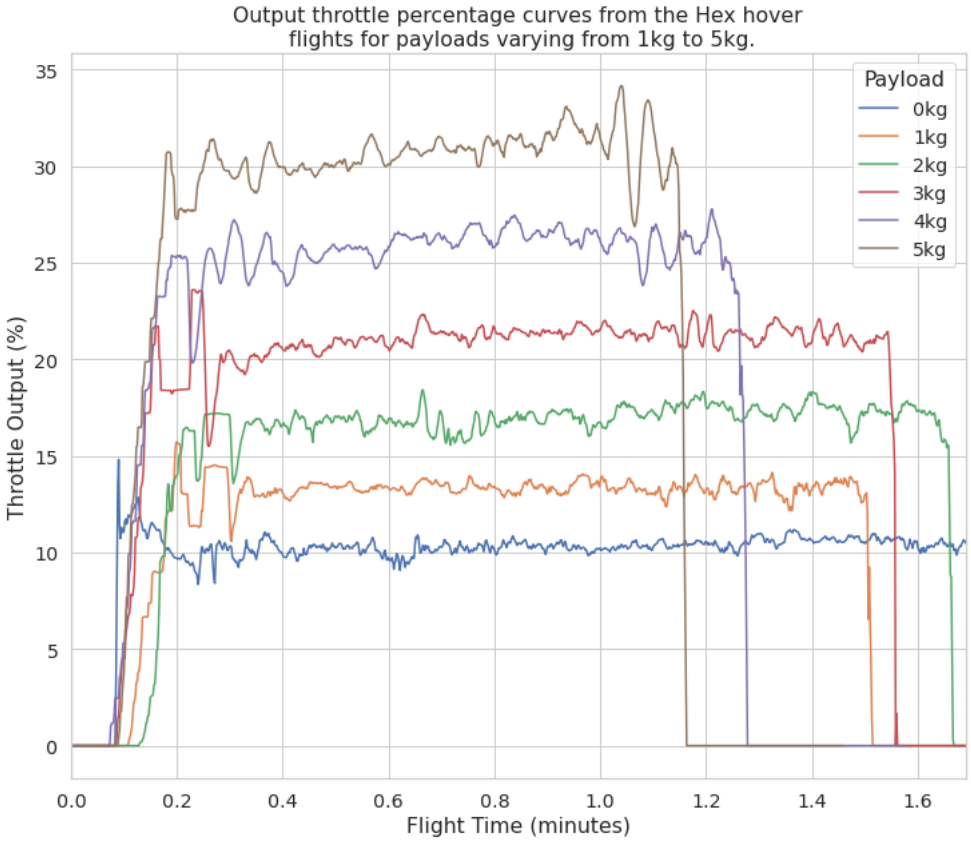

Figure 6.10: Comparison of the hover throttle output percentages for the payload tests and a control 0kg automated hover flight.

flight duration is expected to increase with increasing battery capacity, an estimate with double LiIon batteries meant the 5kg payload could fly for 11.3 minutes. With respect to simulations run during design, the Hex was expected to fly for 10.6 minutes with a 5kg payload and a 20000mAh battery. From the estimations in Table 6.5, the Hex is likely to match or improve on this value with an estimate of 11.3 minutes.

Table 6.5: Summary of payload test results showing hover throttle, average current and estimate flight times for two battery capacities.

Payload	**Hover Throttle (%)**	**Average Current (A)**	**8000mAh (min)**	**16800mAh (min)**
0kg	12.5%	21.78A	16.9	30.6
1kg	13.3%	26.28A	13.7	28.8
2kg	17.3%	34.73A	10.4	21.8
3kg	21.4A	44.83A	8.0	16.8
4kg	26.1A	54.64A	6.6	13.8
5kg	31.4%	67.06A	5.4	11.3

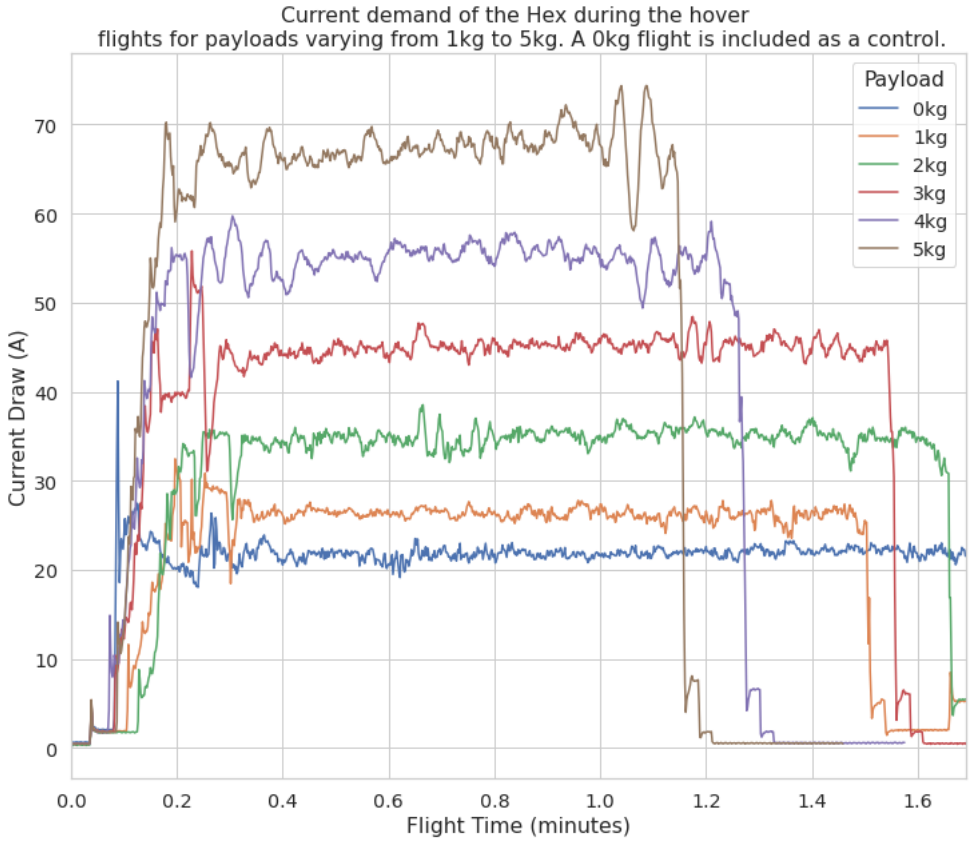

Figure 6.11: Comparison of the current demand from the static hover payload tests and a control 0kg automated hover flight.

The payload performance of the Hex again aligned with the performance of Galle et al's [11] volcanic investigation hexacopter. The volcanic scientific hexacopter was quoted to have a flight time of roughly 30 minutes with a 1kg payload attached and 20000mAh LiIon battery. In comparison with a smaller capacity battery, the HexaQuad performance estimation is expected to have a flight time only 1.2 minute shorter.

Under practical consideration of the HexaQuad and its estimated payload performance the overall system is best suited to fly payload weights in the range of 1-3kg if limited to the 16800 LiIon batteries used in this study. This effectively allows science studies a practically viable operation window between 16.8 - 28.8 minutes to collect sample data in situ. This payload range also allows the HexaQuad to meet the requirements to have an operation window between 15-20 minutes. Comparatively, the 4-5kg payload windows are significantly short and offer flight times between 11.3 -

13.8 minutes, effectively limiting the application use and forcing users to commence flights closer to the site of interest.

The flight times of the higher payloads can be increased with larger battery capacities as is done for the DJI Matrice 600 with a flight time of 16 minutes with a 6kg payload and a 34 200mAh battery [56,57]. However, there is an inflection point where additional capacity is nullified by the associated weight. Overall the payload performance achieves the requirement to support 5kg payloads, however, the applications of this payload range would be limited.

6.4 Summary of Results and Discussion

There were a number of individual tests and investigations carried out to evaluate the performance of the HexaQuad. A summary of the results and discussion are presented in this section

1. The static hover and horizontal grid missions displayed similar performance and were within the expected error margins for both configurations, the Quad flights differed by 9 seconds and by 58 seconds for the Hex. However, it is expected for the efficiency of the horizontal mission to improve over longer flight distances.

2. The expensive propeller significantly outperformed the cheaper counterpart due to the higher precision in the design of the leading and trailing edges thus improving efficiency. The expensive propeller had a 27.1% flight time improvement in the Quad configuration. Similar results were not seen for the Hex, however, this was attributed to the use of a combination of cheap and expensive propellers.

3. The LiIon battery had good consistency but did not have the expected superior endurance compared to the LiPo batteries. No certain conclusion was drawn from this study as it is suggested to perform more comparison tests to confirm the preliminary hypotheses of endurance gain.

4. Peak performance of Hex with no payload exceeded 30 minutes of flight with room for improvement if all propellers were expensive. This was a 59.7% improvement over the 19.2 minute single battery flights.

5. The Quad peak performance tests were not conducted due to time constraints, however, displayed a 23 minute flight time average on a single battery and was forecast to exceed 35 minutes with dual capacity.

6. Payload testing was only conducted with the Hex due to time constraints. The Hex was able to lift a 5kg payload at a throttle value of 31.4% indicating the potential to lift heavier payloads, however, with the batteries used in this study the maximum expected flight time was expected to be 11.3 minutes. This time could be extended with greater battery capacity, however, if limited to the batteries in this study it is recommended to operate within the payload range of 1 to 3kg with expected flight times of 16.8 to 28.8 minutes.

Chapter 7

Conclusion and Future Work

7.1 Conclusion

Data acquisition using small unmanned aircraft systems (sUAS) or drones for scientific research purposes continues to grow as a new norm across a wide spectrum of disciplines. Consumer sUAS often boast high quality stabilised video capture capabilities and easy-to-use platforms. However, given the need for stringent data provenance and rigour in scientific data capture processes, these platforms are often limiting for academic research purposes due to closed source firmware and communication links. Furthermore, where users attempt to capture data from custom or uncommon sensors these platforms fail to allow for advantageous tight integrations, leading to sensor and mechanical infrastructure duplication on deployed platforms.

This dissertation presented the LANDRS's HexaQuad, an open source, modular, and reconfigurable multirotor designed to allow users to integrate novel and uncommon sensors seamlessly, whilst further providing full access to all flight data. The HexaQuad was designed with accessibility and simplicity in mind, leading to the use of simple components and manufacturing techniques. The result is a simple to use design that can be recreated by users with no previous experience, requiring only access to standard shipping, a 3D printer and once off CNC routing. The use of 3D printing allowed for complex parts to be created, iterated and manufactured within hours. Furthermore, the HexaQuad can be configured into either a hexacopter or quadcopter to suit the payload, flight time, or budgetary requirements of an individual study.

The HexaQuad was designed to support a maximum payload of 2kg as a quadcopter and 5kg as a hexacopter, and have a flight time in the range of 15 to 20 minutes. Under testing, the hexacopter lifted payloads ranging from 1-5kg with a maximum hover throttle of 31.4% for the 5kg load, implying sufficient remaining throttle overhead to manoeuvre during flight or lift heavier payloads. However, the flight time of the 5kg payload was relatively short and is expected to last between 5.4 or 11.3

minutes when using an 8000mAh and 16800mAh battery respectively.

In contrast, the peak hex performance was conducted with two batteries connected in parallel, the expensive propellers and no payload. The 16800mAh capacity resulted in an average flight time of 30.6 minutes, a 59.7% improvement on the single battery flight time of 19.2 minutes Practically considering the requirements, the hex is more suitable for a payload range of 1-3kgs with expected flight times in the range of 16.8-28.8 minutes while using a 16800mAh battery.

Regarding the quad performance, there was not sufficient time to conduct all the same tests that were done for the hex, namely the payload and peak flight time performance. However, the quad did have a long single battery flight time averaging 23 minutes and was expected to continue on this trend in the peak flight time performance.

In order to cater to the science community, the HexaQuad operated two mission types to investigate the performance under anticipated operation. This investigation served to compare the performance between horizontal grid surveys and static hover missions to evaluate whether the drone was more suitable for a certain type of application. Considering the total 38 successful flights, the two mission types performed similarly within the expected error margins for both configurations, showing only minor differences in flight time of 9 seconds for the quad and 58 seconds for the hex. Limited time and weather conditions led to the removal of vertical grid surveys from the testing scheme.

Beyond the flight requirements, there were other investigations into design choices relating to battery chemistry and propeller quality. In comparison of the chemistry types, the LiIons were expected to outperform the LiPos due to their greater specific energy and potential for improved endurance. There was no significant endurance improvement identified with an increase of only 5.2% in flight time, however, there was greater consistency of flight times from the LiIon batteries. The comparison was limited by a low number of flights and the difference in age between the batteries, thus no definite conclusion was drawn.

Regarding the propeller consideration, a significant improvement in flight time and decreased current demand was seen with the use of the Expensive propellers, the T-Motor P18x6.1. The quad configuration saw improvements of 27.1% in flight time and a reduction of 24.2% in current demand. The hex did not see the same scale of improvements over the cheaper propellers, however, the decreased improvement was attributed to the non-ideal circumstances where 2 of the 6 propellers were from

the cheap set. The performance improvement was attributed to the higher precision associated with the trailing and leading edge of the expensive propellers making them more efficient. The final design is suggested to utilize the P18x6.1 propellers for maximum performance.

Overall, the HexaQuad presented in this dissertation suitably met the requirements to create an easy-to-use, open source, modular platform that allows for the versatile integration of novel sensors and caters to the high data provenance requirement of academic research. Furthermore, this design serves as a good entry point for researchers to begin using sUAS within novel studies and access the benefits associated with drone data capture.

7.2 Future Work and Recommendations

The work presented in this dissertation is intended as the first prototype of the LANDRS' Science Drone and measures have been put in place to assist with the continuation of the project.

File Access: Firstly, all the design files are accessible online in the form of a GitHub repository under a CERN open hardware license which encourages users to iterate on the design and simply reference the main work. To accompany the design files, a detailed set of documentation is also hosted on the repository to guide users through the building process along with simple tutorials associated with the assembly and use of the HexaQuad. Lastly, users are encouraged to submit pull requests and any other form of collaboration.

Git Hub Repository: https://github.com/landrs-toolkit/LANDRs-Science-Drone

Flight Pattern Testing: Notable future work would be to further test the HexaQuad in two areas, namely vertical survey grids and the efficiency gain of the rotoroboom lengths. The vertical survey grids will indicate the ability of the HexaQuad to ascend and descend, an operation that is expected to require more energy compared to horizontal and hover flights. In addition, under the completion of the vertical and horizontal flight pattern testing further analysis can be conducted on stability, control and accuracy of the system to ensure the performance of the HexaQuad is comparable under the identified flight applications.

Rotorboom Lengths: Since the rotorboom length performance was inferred from other work it is recommended to further investigate any efficiency gain and adjust the rotorboom length accordingly. The result may be a small reduction in

weight and improved portability of the drone if the efficiency gain is found to be unsatisfactory.

Quad Performance: There is further room to continue testing the quad configuration as this was limited due to time constraints, doing so would give incite into the maximum payload and flight time performance of the quad configuration.

Realistic Sensor Readings: Practical testing that could occur would be to completely integrate an external logging sensor, where the sensor data can then be compared to an associated ground truth to evaluate the performance. This operation would be the best comparison to a real world application of the HexaQuad.

Portability: With regards to recommended design considerations for prototype 2, a major impracticality of the large rotorbooms made the HexaQuad difficult to transport in a small vehicle. For the majority of the tests the HexaQuad was transported in a sedan where the quad could fit in the boot loading area, however, the hex did not fit into the boot opening with its larger dimensions. It is thus recommended to improve the portability of the HexaQuad by reviewing the rotorboom mounts to incorporate mechanisms to collapse the drone to a smaller form factor.

R/C Receiver: An additional design change recommendation would be to switch the current radio controller receiver to a 900MHz system. It was discovered late into the testing scheme that the communication link between the radio receiver and transmitter was poor, reaching critical status beyond 150m. It is believed that the poor performance was a result of numerous crashes potentially damaging the receiver. The 2.4GHz receiver is capable of operating in an unobstructed view of 2km, however, if the receiver is damaged it is recommended to replace it with a 900MHz receiver with greater range capability.

Aerodynamic Analysis: A further suggestion for future work on the HexaQuad project is a proposed aerodynamic investigation which will provide insight into the stability and efficiency of the design. This work will aid with further development and iteration of the design for improved performance.

Landing Gear Review: It was identified that designing the landing gear to act as a crumple zone could jeopardise any sensors attached below the drone. This is significant as sensing systems end up being the most expensive and fragile components of a drone. Thus it is suggested that future iterations review the landing gear connection points in an attempt to strength the structure and preserve any system housed below the battery bay. Alternatively, this could be solved by adding 'roll

cages' to high value sensors as desired.

Bibliography

[1] FAA, "Small unmanned aircraft systems (suas)," Jun 2016, (Advisory Circular: 107-2) ,(Accessed on 24/07/2021). [Online]. Available: https://www.faa.gov/documentlibrary/media/advisory_circular/ac_107-2.pdf

[2] M. Hassanalian and A. Abdelkefi, "Classifications, applications, and design challenges of drones: A review," *Progress in Aerospace Sciences*, vol. 91, no. November 2016, pp. 99–131, 2017.

[3] A. C. Watts, V. G. Ambrosia, and E. A. Hinkley, "Unmanned aircraft systems in remote sensing and scientific research: Classification and considerations of use," *Remote Sensing*, vol. 4, pp. 1671–1692, 2012.

[4] D. Giordan, M. S. Adams, I. Aicardi, M. Alicandro, P. Allasia, M. Baldo, P. D. Berardinis, D. Dominici, D. Godone, P. Hobbs, V. Lechner, T. Niedzielski, M. Piras, M. Rotilio, R. Salvini, V. Segor, B. Sotier, and F. Troilo, "The use of unmanned aerial vehicles (uavs) for engineering geology applications," *Bulletin of Engineering Geology and the Environment*, pp. 3437–3481, 2020. [Online]. Available: https://doi.org/10.1007/s10064-020-01766-2

[5] H. González-Jorge, J. Martínez-Sánchez, M. Bueno *et al.*, "Unmanned aerial systems for civil applications: A review," *Drones*, vol. 1, no. 1, p. 2, 2017.

[6] M. Dodson, "Beginners guide to fixed-wing drones," Apr 2022, (Accessed on 01/02/2023). [Online]. Available: https://www.droneblog.com/fixed-wing-drones/

[7] "Matrice 200 series v2 - dji," (Accessed on 10/07/2021). [Online]. Available: https://www.dji.com/matrice-200-series-v2?site=brandsite&from=landing_page

[8] C. Gaffey and A. Bhardwaj, "Applications of unmanned aerial vehicles in cryosphere: Latest advances and prospects," *Remote Sensing*, vol. 12, no. 6, p. 948, 2020.

[9] "Dji multispectral sensor for phantom 4," (Accessed on 10/07/2021). [Online]. Available: https://www.dji.com/p4-multispectral?site=brandsite&from=nav

[10] L. Barbieri, S. T. Kral, S. C. Bailey, A. E. Frazier, J. D. Jacob, J. Reuder, D. Brus, P. B. Chilson, C. Crick, C. Detweiler, A. Doddi, J. Elston, H. Foroutan, J. González-Rocha, B. R. Greene, M. I. Guzman, A. L. Houston, A. Islam, O. Kemppinen, D. Lawrence, E. A. Pillar-Little, S. D. Ross, M. P. Sama, D. G. Schmale, T. J. Schuyler, A. Shankar, S. W. Smith, S. Waugh, C. Dixon, S. Borenstein, and G. D. Boer, "Intercomparison of small unmanned aircraft system (suas) measurements for atmospheric science during the lapse-rate campaign," *Sensors (Switzerland)*, vol. 19, p. 2179, 5 2019. [Online]. Available: https://www.mdpi.com/1424-8220/19/9/2179/htmhttps://www.mdpi.com/1424-8220/19/9/2179

[11] B. Galle, S. Arellano, N. Bobrowski, V. Conde, T. P. Fischer, G. Gerdes, A. Gutmann, T. Hoffmann, I. Itikarai, T. Krejci, E. J. Liu, K. Mulina, S. Nowicki, T. Richardson, J. Rüdiger, K. Wood, and J. Xu, "A multi-purpose, multi-rotor drone system for long-range and high-altitude volcanic gas plume measurements," *Atmospheric Measurement Techniques*, vol. 14, pp. 4255–4277, 6 2021.

[12] J. Wyngaard, L. Barbieri, A. Thomer, J. Adams, D. Sullivan, C. Crosby, C. Parr, J. Klump, S. R. Shrestha, and T. Bell, "Emergent challenges for science suas data management: Fairness through community engagement and best practices development," *Remote Sensing*, vol. 11, p. 1797, 8 2019. [Online]. Available: www.mdpi.com/journal/remotesensing

[13] "Phantom 1 - dji." [Online]. Available: https://www.dji.com/phantom?site=brandsite&from=landing_page

[14] P. Lyons, "Modified dji phantom with hardware duplication," (Accessed on 01/02/2023). [Online]. Available: https://za.pinterest.com/pin/7459155606816665/

[15] J. M. Harris, J. A. Nelson, G. Rieucau, and W. P. Broussard, "Use of drones in fishery science," *Transactions of the American Fisheries Society*, vol. 148, pp. 687–697, 7 2019.

[16] W. Perryman, M. E. Goebel, N. Ash, D. Leroi, and S. Gardner, "Small unmanned aerial systems for estimating abundance of krill-dependent predators: a feasibility study with preliminary results," pp. 64–72, 2010, drones tested, old but useful. [Online]. Available: www.microdrones.com

[17] V. Pirotta, A. Smith, M. Ostrowski, D. Russell, I. D. Jonsen, A. Grech, and R. Harcourt, "An economical custom-built drone for assessing whale health," *Frontiers in Marine Science*, vol. 4, 12 2017. [Online]. Available: http://journal.frontiersin.org/article/10.3389/fmars.2017.00425/full

[18] F. H. Filho, W. B. Heldens, Z. Kong, and E. S. D. Lange, "Drones: Innovative technology for use in precision pest management," *Journal of Economic Entomology*, vol. 113, pp. 1–25, 2 2020. [Online]. Available: https://academic.oup.com/jee/article/113/1/1/5666881

[19] "Dji mavic 3m - specifications," (Accessed on 01/02/2023). [Online]. Available: https://ag.dji.com/mavic-3-m/specs

[20] Q. Systems, "Sanbs bloodwing project-behind the scenes," 2019. [Online]. Available: https://www.quantum-systems.com/tag/tron/

[21] E. Ackerman and M. Koziol, "The blood is here: Zipline's medical delivery drones are changing the game in rwanda," *IEEE Spectrum*, vol. 56, pp. 24–31, 5 2019.

[22] J. González-Rocha, C. A. Woolsey, C. Sultan, and S. F. D. Wekker, "Sensing wind from quadrotor motion," *Journal of Guidance, Control, and Dynamics*, vol. 42, pp. 836–852, 2019.

[23] J. Jeziorska, "Uas for wetland mapping and hydrological modeling," *Remote Sensing*, vol. 11, 2019.

[24] B. R. Jordan, "Collecting field data in volcanic landscapes using small uas (suas)/drones," *Journal of Volcanology and Geothermal Research*, vol. 385, 11 2019.

[25] Ardupilot, "Connect escs and motors." [Online]. Available: https://ardupilot.org/copter/docs/connect-escs-and-motors.html#connect-escs-and-motors

[26] A. Bondyra, S. Gardecki, P. Gasior, and W. Giernacki, "Performance of coaxial propulsion in design of multi-rotor uavs," *Advances in Intelligent Systems and Computing*, vol. 440, pp. 523–531, 2016.

[27] Y. Lei and M. Cheng, "Aerodynamic performance of a hex-rotor unmanned aerial vehicle with different rotor spacing," *Measurement and Control*, vol. 53, 3 2020.

[28] Y. Lei, Y. Huang, and H. Wang, "Aerodynamic performance of an octorotor suav with different rotor spacing in hover," *Processes*, vol. 8, p. 1364, 10 2020. [Online]. Available: https://www.mdpi.com/2227-9717/8/11/1364

[29] P. J. Burke, "A safe, open source, 4g connected self-flying plane with 1 hour flight time and all up weight (auw) ¡300 g: Towards a new class of internet enabled uavs," *IEEE Access*, vol. 7, pp. 67 833–67 855, 2019.

[30] E. Ebeid, M. Skriver, and J. Jin, "A survey on open-source flight control platforms of unmanned aerial vehicle." Institute of Electrical and Electronics Engineers Inc., 9 2017, pp. 396–402.

[31] E. Ebeid, M. Skriver, K. H. Terkildsen, K. Jensen, and U. P. Schultz, "A survey of open-source uav flight controllers and flight simulators," *Microprocessors and Microsystems*, vol. 61, pp. 11–20, 9 2018.

[32] Pixhawk, "Pixhawk series," Sep 2022, (Accessed on 21/11/2022). [Online]. Available: https://docs.px4.io/main/en/flight_controller/pixhawk_series.html

[33] C. P. Ltd., "Autopilot-on-module: Blue manufactured in usa: Blue assembled in usa: Pixhawk original team," (Accessed on 21/11/2022). [Online]. Available: https://www.cubepilot.com/#/carrier-board/features

[34] DroneCodeProject, "Qgc - qgroundcontrol - drone control," 2019, (Accessed on 24/11/2022). [Online]. Available: http://qgroundcontrol.com/

[35] M. Oborne, "Mission planner overview¶," 2021, (Accessed on 24/11/2022). [Online]. Available: https://ardupilot.org/planner/

[36] D. Project, "Introduction: Mavlink developer guide," (Accessed on 21/11/2022). [Online]. Available: https://mavlink.io/en/

[37] D. Bershadsky, S. Haviland, and E. N. Johnson, "Electric multirotor uav propulsion system sizing for performance prediction and design optimization." American Institute of Aeronautics and Astronautics, 1 2016. [Online]. Available: https://arc.aiaa.org/doi/10.2514/6.2016-0581

[38] M. N. Boukoberine, Z. Zhou, and M. Benbouzid, "A critical review on unmanned aerial vehicles power supply and energy management: Solutions, strategies, and prospects," *Applied Energy*, vol. 255, p. 113823, 12 2019.

[39] M. Cloud, "What is the energy density of a lithium-ion battery?" 2020, (Accessed on 23/11/2022). [Online]. Available: https://www.fluxpower.com/blog/what-is-the-energy-density-of-a-lithium-ion-battery

[40] U. of Washionton, "Lithium-ion battery," Sep 2020, (Accessed on 01/02/2023). [Online]. Available: https://www.cei.washington.edu/education/science-of-solar/battery-technology/

[41] T. Yao, Z. Deng, K. Zhang, and S. Li, "A method to predict the ultimate tensile strength of 3d printing polylactic acid (pla) materials with different printing orientations," *Composites Part B: Engineering*, vol. 163, pp. 393–402, 4 2019, this paper has the geometric model of the spcimen for uniaxial loading.

[42] G. A. Johnson and J. J. French, "Evaluation of infill effect on mechanical properties of consumer 3d printing materials," *Advances in Technology Innovation*, vol. 3, pp. 179–184, 2018.

[43] A. Internationals, "Standard test method for tensile properties of plastics 1. d638," 2014. [Online]. Available: http://www.ansi.org.

[44] J. Kiendl and C. Gao, "Controlling toughness and strength of fdm 3d-printed pla components through the raster layup," *Composites Part B: Engineering*, vol. 180, p. 107562, 1 2020.

[45] S. Nvss, B. Esakki, L.-J. Yang, C. Udayagiri, and K. S. Vepa, "Design and development of unibody quadcopter structure using optimization and additive manufacturing techniques," *Designs*, vol. 6, p. 8, 1 2022.

[46] D. Kotarski, P. Piljek, M. Pranjić, C. G. Grlj, and J. Kasać, "A modular multirotor unmanned aerial vehicle design approach for development of an engineering education platform," *Sensors*, vol. 21, p. 2737, 4 2021. [Online]. Available: https://pdfs.semanticscholar.org/0e96/fdb88a7edb0f3cc5d2809811a8cda20ab210.pdf?_ga=2.224819290.1178887376.1651149126-1924345320.1650651022

[47] K. R. I. Sanim, M. Kalaitzakis, B. Kosaraju, Z. Kitzhaber, C. English, N. Vitzilaios, M. Myrick, M. Hodgson, and T. Richardson, "Development of an aerial drone system for water analysis and sampling." IEEE, 6 2022, pp. 1601–1607.

[48] M. Müller, "ecalc - reliable electric drive simulations," 2004. [Online]. Available: https://www.ecalc.ch/

[49] "Turnigy plush-32 40a (2 6s) brushless speed controller w/bec (rev1.1.0)," (Accessed on 01/02/2023). [Online]. Available: https://hobbyking.com/en_us/turnigy-plush-32-40a-2-6s-brushless-speed-controller-w-bec-rev1-1-0.html

[50] H. N. America, "Xrotor pro 40a esc (dual pack)," (Accessed on 01/02/2023). [Online]. Available: https://www.hobbywingdirect.com/products/xrotor-pro-40a-esc?variant=1306506956

[51] "Pdb-hex, 12s," (Accessed on 01/02/2023). [Online]. Available: http://www.mateksys.com/?portfolio=pdb-hex

[52] D. S. S. Corporation, "Solidworks desktop 3d cad," 2021. [Online]. Available: https://www.solidworks.com/domain/design-engineering

[53] "Filament materials: Prusament," (Accessed on 01/02/2023). [Online]. Available: https://prusament.com/materials/

[54] SACAA, "Remotely piloted aircraft systems," 2021, (Accessed on 30/11/2022). [Online]. Available: https://www.caa.co.za/industry-information/rpas/

[55] SAMAA, "South african model aeronautical association," 2022, (Accessed on 30/11/2022). [Online]. Available: https://www.samaa.org.za/

[56] DJI, "Matrice 600 - product information - dji," (Accessed on 01/02/2023). [Online]. Available: https://www.dji.com/matrice600/info#downloads

[57] H. Madokoro, O. Kiguchi, T. Nagayoshi, T. Chiba, M. Inoue, S. Chiyonobu, S. Nix, H. Woo, and K. Sato, *Sensors*, vol. 21, 7 2021.

[58] C. Benson, "How to make a drone/uav," Aug 2019, (Accessed on 16/06/2021). [Online]. Available: https://www.robotshop.com/community/tutorials/show/how-to-make-a-drone-uav-lesson-1-terminology

[59] "Dji z30 - extreme zoom camera," (Accessed on 10/07/2021). [Online]. Available: https://www.dji.com/zenmuse-z30?site=brandsite&from=landing_page

[60] "Ndvi: Normalized difference vegetation index for agriculture," Apr 2021, (Accessed on 07/07/2021). [Online]. Available: https://eos.com/make-an-analysis/ndvi/

[61] M. Biczyski, R. Sehab, J. F. Whidborne, G. Krebs, and P. Luk, "Multirotor Sizing Methodology with Flight Time Estimation," *Journal of Advanced Transportation*, vol. 2020, 2020.